# Investigations on centrosomes, their function and regulation during immune synapse formation

## Dissertation

zur Erlangung des Doktorgrades (Dr. rer. nat.)

der Mathematisch-Naturwissenschaftlichen Fakultät

der Rheinischen Friedrich-Wilhelms-Universität Bonn

vorgelegt von

## Ann-Kathrin Weier

aus Kirchen

Bonn, October 2021

Angefertigt mit Genehmigung der
Mathematisch-Naturwissenschaftlichen Fakultät der
Rheinischen Friedrich-Wilhelms-Universität Bonn

1. Gutachter: Prof. Dr. Eva Kiermaier
2. Gutachter: PD Dr. Heike Weighardt

Tag der Promotion:18.01.2022
Erscheinungsjahr: 2022

# Contents

Content

# Preliminary remarks

I hereby declare that I wrote this dissertation without sources other than indicated in the main text and without help from third parties. I have designed and conducted all the experiments described in this thesis, except for EdU and pH3 stainings in dermal DCs, which were kindly provided by Prof. Dr. Eva Kiermaier and Stephanie Ebbinghaus. Data presented in Figure 3.18 d and 3.19 e was generated with student's help as indicated in the figure legends.

According to the common practice in English scientific writing, this dissertation is written using the first-person plural narrator.

Parts of this dissertation have been published on a preprint server:

**Weier, A.** and Homrich, M., et al. Amplified centrosomes in dendritic cells promote immune cell effector functions. 6 October 2020, PREPRINT (Version 1), available at Research Square DOI:10.21203/rs.3.rs-83155/v1

# Abbreviation list

| Abbreviation | Full name |
|---|---|
| **2N** | diploid |
| **2N2C** | diploid BMDCs with two centrioles |
| **2NCA** | diploid BMDCs with centrosome amplification |
| **3-S1P** | sphingosine 1-phosphate receptor 3 |
| **4N** | tetraploid |
| **ß-ME** | ß-mercaptoethanol |
| **γ-TuRCs** | γ-tubulin ring complexes |
| **ac-tubulin** | acetylated-tubulin |
| **ACKR4** | atypical chemokine receptor 4 |
| **ADAP** | adhesion and degranulation promoting adaptor protein |
| **ALR14** | ADP ribosylation factor-like protein 14 |
| **APC** | antigen presenting cell |
| **APC/C** | anaphase-promoting complex/cyclosome |
| **Arp2/3** | actin related protein 2/3 complex |
| **Arpc2** | actin related protein 2/3 Complex Subunit 2 |
| **ATP** | adenosine triphosphate |
| **Batf3** | basic leucine zipper transcriptional factor ATF-like 3 |
| **BMDC** | bone marrow-derived dendritic cell |
| **bp** | base pair |
| **BPDCN** | blastic plasmacytoid dendritic cell neoplasm |
| **BSA** | bovines serumalbumin |
| **CA** | centrosome amplification |
| **CCL** | C-C motif chemokine ligand |
| **CCL5** | C-C motif chemokine ligand 5 (RANTES) |
| **CCL17** | C-C motif chemokine ligand 17 (TARC) |
| **CCL22** | C-C motif chemokine ligand 22 (MDC) |
| **CCR** | C-C-chemokine receptor |
| **CD** | cluster of differentiation |
| **cDC** | conventional (classical) DCs |
| **cDC1** | conventional DC type 1 |
| **cDC2** | conventional DC type 2 |
| **Cdc42** | cell division control protein 42 homolog |
| **Cdk** | cyclin-dependent kinases |
| **CDK5RAP2** | CDK5 regulatory subunit associated protein 2 |
| **CDP** | common DC progenitor |
| **Cdt1** | chromatin licensing and DNA replication factor 1 |
| **CEP** | centrosomal protein |
| **CETN** | centrin |
| **CETN2-GFP** | centrin2-green fluorescent protein |
| **CFSE** | carboxyfluoresceinsuccinimidylester |
| **CIP4** | cdc42-interacting protein 4 |
| **CMP** | common myeloid progenitors |
| **CLIP** | class II-associated invariant chain peptide |
| **CLP** | common lymphoid progenitors |
| **CLRS** | C-type lectin receptors |
| **CoM** | center of mass |
| **CPAP** | centrosomal P4.1-associated protein |
| **CRAC** | $Ca^{2+}$ release-activated $Ca^{2+}$ channels |
| **CSF-1R** | colony-stimulating factor 1 receptor |
| **cSMAC** | central SMAC |

Abbreviation list

| | |
|---|---|
| **Ct** | threshold cycle value |
| **CTL** | cytotoxic T lymphocyte |
| **CTLA-4** | cytotoxic T-lymphocyte-associated protein 4 |
| **CXCL** | C-X-C motif chemokine ligand |
| **CXCR** | C-X-C motif chemokine receptor |
| **DC** | dendritic cell |
| **DAPI** | 4',6-diamidino-2-phenylindole |
| **DAG** | diacylglycerol |
| **ddH2O** | double-distilled water |
| **DMEM** | Dulbecco's Modified Eagle Medium |
| **DMSO** | dimethylsulfoxid |
| **DNA** | deoxyribonucleic acid |
| **DNase** | deoxyribonuclease |
| **dSMAC** | distal SMAC |
| **EB1** | plus-end-binding protein 1 |
| *E. coli* | *Escherichia coli* |
| **e.g.** | *exempli gratia* (for example) |
| **ECASP** | extra centrosome-associated secretory pathway |
| **EdU** | 5-ethynyl-2'-deoxyuridine |
| **EDTA** | ethylenediaminetetraacetic acid |
| **ELISA** | enzyme-linked immunosorbent assay |
| **ER** | endoplasmic reticulum |
| **ERAP1** | ER-associated aminopeptidase 1 |
| *et al.* | *et alia* (and others) |
| **F-actin** | filamentous actin |
| **FACS** | fluorescence-activated cell sorting |
| **FBS** | fetal calf serum |
| **Fbxw7** | the F-box protein F-box/WD repeat-containing protein 7 |
| **FLT3** | fms-like tyrosine kinase 3 (CD135) |
| **FRC** | fibroblastic reticular cells |
| **Fucci** | fluorescent, ubiquitination-based cell cycle indicator |
| **GEF** | GTPase exchange factor |
| **GM-CSF** | granulocyte-macrophage colony-stimulating factor |
| **GSK3** | glycogen synthase kinase-3 |
| **GTP** | nucleotide guanosine triphosphate |
| **HEK T293 cells** | human embryonic kidney cells |
| **HEL** | hen egg lysozyme |
| **HEV** | high endothelial venule |
| **HRP** | horse-radish peroxidase |
| **HSCs** | hematopoietic stem cells |
| **ICAM** | intercellular adhesion molecule |
| **Id2** | inhibitor of DNA binding2 |
| **Ii** | invariant chain |
| **IL** | interleukin |
| **im** | immature |
| **INF** | interferon |
| **IP$_3$** | inositol-1,4,5-trishosphat |
| **IQGAP1** | IQ motif containing GTPase activating protein 1 |
| **IS** | immune synapse |
| **IRAP** | insulin-responsive aminopeptidase |
| **IRF** | interferon regulatory factor |
| **ITAM** | immunoreceptor tyrosine-based activation motifs |
| **kb** | kilo baispairs |
| **kDa** | kilo daltons |
| **KLF4** | kruppel-like factor 4 |

| | |
|---|---|
| **KO** | knockout |
| **LAT** | linker for activation of T cells |
| **LB** | lysogeny broth |
| **LFA-1** | lymphocyte function-associated antigen 1 |
| **LC** | Langerhans cell |
| **LCK** | protein tyrosine kinase |
| **LEC** | lymphatic endothelial cells |
| **LN** | lymph node |
| **LPS** | lipopolysaccharide |
| **m** | mature |
| **MIIC** | MHC class II containing compartments |
| **MAP4** | microtubule-associated protein 4 |
| **MAPK** | mitogen-activated protein kinase |
| **MFI** | mean fluorescence intensity |
| **MHC** | major histocompatibility complex |
| **MHCI** | major histocompatibility complex class I |
| **MHCII** | major histocompatibility complex class II |
| **miR-9** | micro RNA-9 |
| **miRNA** | micro RNA |
| **MPP** | multipotent progenitor |
| **mRNA** | messenger RNA |
| **MT** | microtubule |
| **MTOC** | microtubule organizing center |
| **NF-κB** | nuclear factor-κB |
| **NFAT** | nuclear factor of activated T-cells |
| **Nfil3** | nuclear factor, interleukin 3 regulated |
| **NK** | natural killer cells |
| **Notch2** | neurogenic locus notch homolog protein 2 |
| **NOX2** | NADPH oxidase 2 |
| **NPM1** | nucleolar protein nucleophosmin 1 |
| **NRL** | Nod-like receptors |
| **ova$_{(323-339)}$** | ovalbumin peptide$_{(323-339)}$ |
| **p-MHC** | peptide-MHC |
| **PBS** | phosphate buffered saline |
| **PCM** | pericentriolar material |
| **PCR** | polymerase chain reaction |
| **pDC** | plasmacytoid DC |
| **PDMS** | polydimethylsiloxane |
| **PFA** | paraformaldehyde |
| **pH3** | phospho Histone H3 |
| **PI** | propidium iodide |
| **PI3K** | phosphoinositide 3-kinase |
| **PIP$_2$** | phosphatidylinositol-4,5-bishosphat |
| **PIP$_3$** | phosphatidylinositol-3,4,5-triphosphat |
| **PKC-θ** | protein kinase C-θ |
| **PLC-γ** | phospholipase C-γ |
| **Plk** | polo like kinases |
| **rpm** | rounds per minute |
| **RPMI medium** | Rosswell Park Memorial Institute Medium |
| **PRR** | pattern recognition receptors |
| **pSMAC** | peripheral SMAC |
| **R10** | full medium |
| **Rab** | Ras-related in brain |
| **RIG-1** | retinoic acid inducible gene 1 |
| **RLR** | Rig-like receptors |

Abbreviation list

| | |
|---|---|
| **RNA** | ribonucleic acid |
| **ROS** | reactive oxygen species |
| **RT** | room temperature |
| **s.d.** | standard deviation |
| **S1PR1** | sphingosine-1-Phosphate Receptor 1 |
| **SAS6** | spindle assembly abnormal protein 6 homolog |
| **sc** | scramble |
| **SCF** | SKP1-CUL1-F-box protein complex |
| **SCS** | subcapsular sinus |
| **SDS-PAGE** | sodium dodecyl sulfate polyacrylamide gel electrophoresis |
| **sgRNA** | single guide ribonucleic acid |
| **SLP-76** | SH2 domain containing leukocyte protein 76 |
| **Slp3** | synaptotagmin like 3 |
| **SMAC** | supramolecular activation clusters |
| **SNARE** | soluble N-ethylmaleimide-sensitive-factor attachment receptor |
| **STIL** | SCL-interrupting locus protein |
| **T regs** | regulatory T cells |
| **T-bet** | T-box transcription factor TBX21 |
| **TAE** | Tris-acetat-EDTA-buffer |
| **TAP** | transporter associated with antigen processing |
| **TBP** | TATA-binding protein |
| **TBS** | Tris-buffer-saline |
| **TBS-T** | TBS-Tween |
| **Tcf4** | transcription factor 4 (E2-2) |
| **TCR** | T cell receptor |
| **TGS** | Tris-glycine-SDS buffer |
| **Th** | T helper cell |
| **TLR** | Toll-like receptor |
| **VAMP** | vesicle-associated membrane protein |
| **VAV1** | vav guanine nucleotide exchange factor 1 |
| **VEGF- α** | cytokine vascular endothelial growth factor α |
| **WT** | wildtype |
| **XCR1** | XC-chemokine receptor 1 |
| **ZAP-70** | zeta-chain-associated protein kinase 70 |
| **Zbtb46** | zinc finger and BTB domain containing 46 |
| **Zeb2** | zinc finger E-box-binding homeobox 2 |

# Summary

The centrosome is a cellular organelle well known for its function during cell division. It consists of two centrioles that are formed by microtubules and surrounded by a multiprotein matrix the so-called pericentriolar material. In G1 phase of the cell cycle one centrosome is present, which is duplicated in parallel to the DNA once the cell starts progressing through the cell cycle, leading to two centrosomes in S/G2 phase and mitosis. This duplication process is tightly controlled, ensuring correct numbers of centrosomes in each phase of the cell cycle. By nucleating microtubules, the centrosome overtakes the task of a microtubule organizing center and thus plays an important function for various interphase specific processes such as antigen presentation, migration and immune synapse formation. The immunological synapse represents a cell-cell contact zone between an antigen-presenting cell and a T cell, which is a highly specialized structure made of signaling transduction molecules and cytoskeletal components. Downstream of the immune synapse, reorientation of the centrosome takes place, once a cell-conjugate is formed. However, on the antigen-presenting cell side of the immune synapse centrosome dynamics are insufficiently understood. Therefore, we aimed to clarify microtubule organizing center conformation and how this affects immune responses. By doing so, we identified a previously unrecognized phenomenon of extra centrosomes within arrested dendritic cells. These extra centrosomes arise during the process of cell maturation after stimulation with the Toll-like receptor 4 agonist lipopolysaccharide. The phenomenon of having amplified centrosomes is a well-described characteristic of cancer cells, therefore often associated with malignancy. Only recently, cycling progenitors of olfactory sensory neurons have been identified to contain amplified centrosomes as part of normal cell development. As dendritic cells represent a critical linker between innate and adaptive immunity, we sought to investigate the physiological function of extra centrosomes in dendritic cells during immune responses.

As a result, we identified two mechanisms how extra centrosomes arise: either through centriole overduplication or by an aborted cell division. Additionally, we observed a strong upregulation of polo-like kinase 2 upon maturation of dendritic cells. This protein is a central element in controlling regular centriole duplication. In polo-like kinase 2 deficient cells, centrosome numbers were significantly reduced, indicating that polo-like kinase 2 is a major driver of extra centrosome generation in dendritic cells.

In the next step, we evaluated the capacity of extra centrosomes in nucleating microtubules and observed excess microtubule numbers emanating from amplified centrosomes during immune synapse formation. Furthermore, we were able to separate dendritic cells based on their centrosomal content and demonstrate that in co-culture experiments of antigen loaded dendritic cells with CD4$^+$ T cells, T cells were activated more efficiently when primed with

dendritic cells carrying extra centrosomes. Secretome analysis revealed higher amounts of immune cell attracting and activating cytokines released by dendritic cells with amplified centrosomes providing a possible explanation for the observed optimized T cell response. During immune synapse formation, the centrosome(s) in dendritic cells is positioned centrally with extra centrosomes clustering in close proximity to each other. This seems to be the favoured centrosome conformation for dendritic cells, however the impact on T cell activation still needs to be clarified.

In summary, we provide evidence for a beneficial physiological function of extra centrosomes within the immune compartment and further strengthen our understanding on how the immune system operates on a molecular level. Our studies provide valuable results for distinct research fields such as Cell biology, Immunology and Cancer Biology and are therefore of great value for a large scientific community.

# 1. Introduction

## 1.1.    Dendritic cells

Dendritic cells (DCs) function as critical linker between innate and adaptive immunity. They are professional antigen presenting cells (APCs), which are specialized in antigen processing, migrating to the lymph node (LN) and antigen presentation to T lymphocytes [1]. Thereby, DCs represent a functional diverse class of cells, which differ depending on the developmental path, phenotype, localization and species. In brief, DCs can be separated into two main functional subgroups: conventional (also called classical) DCs (cDCs) and plasmacytoid DCs (pDCs). Whereby cDCs are further divided into type 1 (cDC1) and type 2 (cDC2), based on the phenotypic markers and specialization in detecting pathogens, producing cytokines and presenting antigens for proper T cell response [2,3]. pDCs in contrast, overtake mainly innate immune functions, detecting viral infections and the production of type I interferon (INF) [4].

### 1.1.1. Development and lineage ontogeny

Over the past decades, much knowledge has been gained on DC ontogeny (Figure 1.1). Hematopoietic stem cell (HSC) derived precursor and progenitors develop into DCs within the bone marrow [3]. First HSCs give rise to multipotent progenitors (MPPs), which themselves undergo stages of differentiation, generating restricted progenitors of myeloid- or lymphoid lineage: so-called common myeloid progenitors (CMPs) and common lymphoid progenitors (CLPs). DCs together with granulocytes, macrophages and monocytes belong to the myeloid lineage, but lineage development pursues from this stage on differently. The common DC progenitor (CDP) represents the first progenitor, which exclusively gives rise to DCs [5–9]. Characteristic for CDPs is the high expression of fms-like tyrosine kinase 3 (FLT3, CD135) and colony-stimulating factor 1 receptor (CSF-1R) [10]. The transcription factor interferon regulatory factor (IRF) 8 is critically important for the CDP survival and development towards the cDC1 lineage [11]. This precursor matures into heterogeneous pre-cDCs, which are either cDC1 or cDC2 specific progenitors [8]. The pre-cDCs and cDCs can be distinguished amongst others based on their transcription factor profile and surface marker expression. For cDC1 development *Irf8* [12,13] *basic leucine zipper transcriptional factor ATF-like 3* (*Batf3*) [14–16], *inhibitor of DNA binding2* (*Id2*) [13,17] and *nuclear factor, interleukin 3 regulated* (*Nfil3*) [18] are required. In addition, the transcription factor *zinc finger and BTB domain containing 46* (*Zbtb46*) is characteristic for cDC1 as well as cDC2 development [19]. High expression levels of IRF4 are necessary for cDC2 progression [20]. Further branching of the cDC2 subsets depends on the expression of transcription factor neurogenic locus notch homolog protein 2 (Notch2), kruppel-like factor 4 (Klf4) and T-box transcription factor TBX21 (T-bet) [21–23]. After pre-cDC1 and pre-cDC2 have developed, both cell types leave the bone marrow and migrate to

peripheral organs where they may go through additional rounds of cell division. Under the influence of organ-specific microenvironment, these cell types then evolve into cDC1 and cDC2 [3,24,25]. Apart from pre-cDCs, pre-pDCs arise from CDPs as well. The latter cell type is believed to not only rise from CDPs but also to originate from CLPs [26,27]. pDC development depends on the transcription factor *Irf8*, *transcription factor 4* (*Tcf4, E2-2*) and *zinc finger E-box-binding homeobox 2* (*Zeb2*). [11,28–31] Unlike cDCs, pDCs leave the bone marrow fully generated, terminal differentiated and only then colonize into peripheral organs [5,32,33].
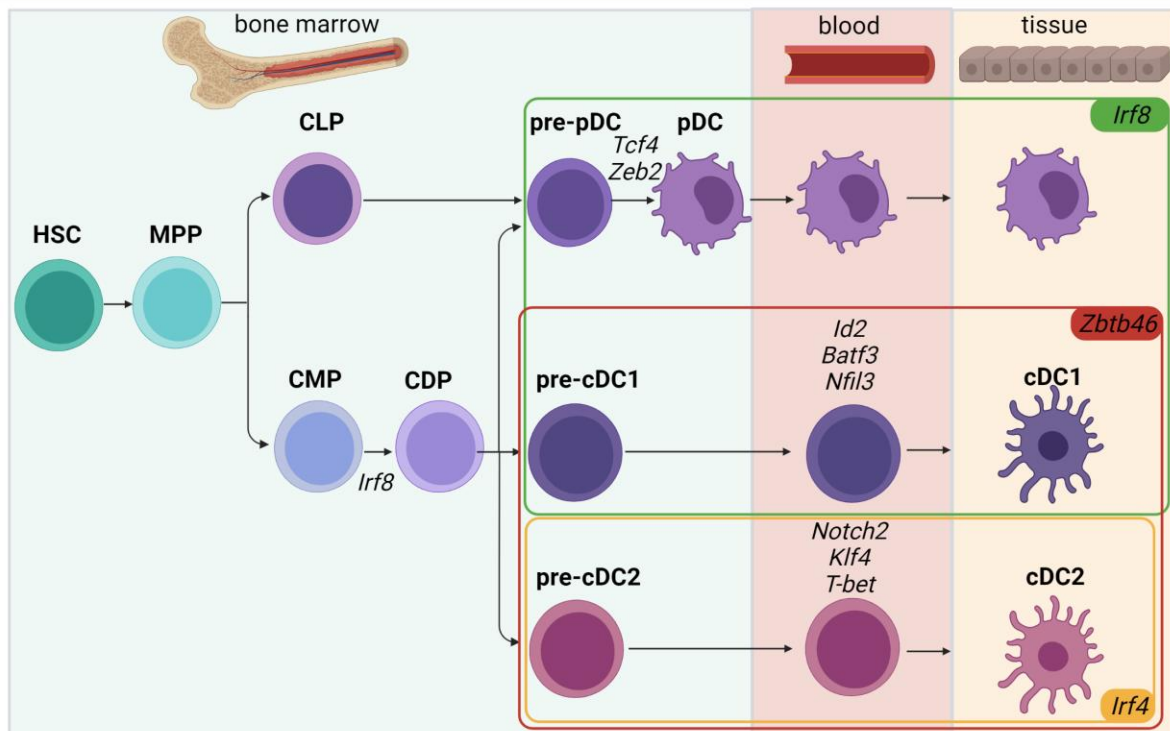


**Figure 1.1** Schematic overview of the dendritic cell (DC) ontogeny.

In the bone marrow, hematopoietic stem cells (HSCs) develop into multipotent progenitors (MPPs), which differentiate into common lymphoid progenitors (CLPs) and common myeloid progenitors (CMPs). CLPs give rise to pre-pDCs, whereas CMPs generate to the common DC precursor (CDP). CDPs mature into plasmacytoid DCs (pDCs) and conventional DCs (cDCs) type 1 (cDC1) and 2 (cDC2) via their respective pre-DC precursors. pDCs leave the bone marrow fully developed, whereas pre-cDCs differentiate into cDCs within the tissue. Transcription factors which are important for specific DC subsets generation are displayed: *Interferon regulatory factor 8 (Irf8), transcription factor 4 (Tcf4), Zinc finger E-box-binding homeobox 2 (Zeb2), zinc finger and BTB domain containing 46 (Zbtb46), inhibitor of DNA binding2 (Id2), basic leucine zipper transcriptional factor ATF-like 3 (Batf3), nuclear factor, interleukin 3 regulated (Nfil3), interferon regulatory factor 4 (Irf4), neurogenic locus notch homolog protein 2 (Notch2), kruppel-like factor 4 (Klf4) and T-box transcription factor TBX21 (T-bet).* Image adapted from Anderson et al.,2021.

### 1.1.2. Functional differences of dendritic cell subsets

The focus of this work lies on cDC1 and cDC2 subsets of DCs, which are transcriptionally and functionally closer to each other than to pDCs [3]. Both are crucially important for inducing adaptive immune responses by activating T cells, leading to their differentiation into effector and memory cells [34]. Both subsets represent a minor cell population, as cDC1 frequency ranges from less than 0.01% to 0.1% of CD45^{+} lymphocytes and cDC2 frequency ranges from 0.1% to 1% of CD45^{+} lymphocytes, depending on the tissue site [35]. Due to small cell numbers, bone marrow-derived dendritic cells (BMDCs) have been used for the major part of this study [36,37].

cDC subsets can be distinguished based on their unique cell surface marker composition. The integrin cluster of differentiation 11c (CD11c) and the major histocompatibility complex class II (MHCII) are expressed on both subsets. The expression of the latter depends on the functional task. Migratory cDCs express higher levels of MHC class II compared to resident cDCs [38]. Besides their functional differences, the localization also influences the marker composition. Resident cDC1 within lymphoid tissue, such as the LN and spleen, express CD8α whereas migratory cDC1 in non-lymphoid tissue, such as the barrier organs, skin and lung, express CD103 [2,39,40]. When migrating to the LNs, they still express the same set of markers. Independent of their localization, cDC1 express CD24 and the XC-chemokine receptor 1 (XCR1) [39]. Characteristic for cDC2s is the expression of CD11b and CD172α (SIRPα) [39,41,42]. pDCs, which are positive for CD11c and MHCII as well, can be separated from cDCs by means of their surface markers B220 and Siglec-H [43]. Recent transcriptome data revealed a common early progenitor shared by pDCs and B cells, indicating the major developmental path relies on the lymphoid lineage leading to a further separation from the cDCs [26,27,44].

cDC1 are superior inducers of CD8^{+} cytotoxic T lymphocyte (CTL) response, by a process termed cross presentation or cross-priming. Thereby, cell-associated antigens from intracellular pathogens or cancer cells are processed into peptides, loaded onto MHC class I molecules, and presented to CD8^{+} T cells [45–49]. Furthermore, these cells release high amounts of interleukin (IL) -12 causing the generation of CD4^{+} T helper (Th) cell subset 1 (Th1) [50]. In addition, cDC1 overtake important functions during innate immune response by the unique expression of Toll-like receptor (TLR) 3 and TLR11, favoring anti-viral responses [51–53]. By rapidly attracting innate immune cells to the site of infection through local cytokine release, innate immune processes get amplified [54]. Ginhoux and colleagues showed that increased neutrophil recruitment into inflamed skin depends on cDC1-mediated release of the cytokine vascular endothelial growth factor α (VEGF- α) [55].

cDC2 are more potent in activating CD4^{+} T helper cells and CD4^{+} regulatory T cells (T regs). In this process, they mainly present peptides of soluble antigens on MHC class II molecules to CD4^{+} T cells. [56] Thereby they favor the polarization of T helper cells into Th2 and Th17 subsets [22,57,58]. DC specific delivery of the cytokines C-C motif chemokine ligand 17 (CCL17) and C-C motif chemokine ligand 22 (CCL22) supports the attraction of CD4^{+} T cells [59–63]. Due to the extensive bearing of pattern recognition receptors (PRRs) such as TLR 5, 6, 7, 9, 13 and retinoic acid inducible gene 1 (RIG-1) they [64] overtake important roles in the defense of extracellular pathogens, parasites and allergens [59,65–68].

## 1.2. Antigen uptake, processing and presentation

Almost all cells can present intracellular antigens from bacteria, parasites, viruses or tumors after peptide breakdown via cytoplasmic proteolysis. Within the endoplasmic reticulum (ER) these peptides are trimmed by aminopeptidases, loaded onto MHC class I molecules and presented to CD8^{+} T cells: a process called classic MHCI pathway [69]. Nevertheless, before an immune response can be triggered by these events, CD8^{+} T cells need to be stimulated by professional APCs. This group of professional APCs comprises DCs, macrophages, B lymphocytes and under special inflammatory conditions endothelial and epithelial cells [70]. DCs represent the most potent APCs [71,72]. By studying the underlying mechanisms of antigen presentation, two varying pathways have been discovered. The classic MHCII pathway and a MHCI based cross-presentation pathway, which can depend on either endosome-to-cytosol antigen processing or vacuolar antigen processing [73–77].

Before an immune response translates into action, APCs need to sense the antigen in form of pathogen-associated molecular patterns and danger associated molecular patterns via the PRRs. Therefore, these receptors are located on various position within the cell: in the cytosol, within the plasma- or endosomal membranes or inside the nucleus. The PRR family consists of Rig-like receptors (RLRs), TLRs, C-type lectin receptors (CLRS), Nod-like receptors (NRLs) and DNA/RNA sensors [78–81]. Depending on the receptor and the adaptor molecules involved, varying signaling pathways are induced. During the antigen internalization and processing DCs mature, introducing morphological changes such as formation of dendrites, upregulation of MHC class II and co-stimulatory molecules like CD40, CD70, CD80, CD86. Enhanced migratory capacities and release of various cytokines are other important aspects. All of them are required to ultimately activate T cells [82–87].

### 1.2.1. Classic MHC class II pathway

MHC class II molecules present exogenous antigens and self-antigens degraded within the endocytic pathway to CD4+ T cells (Figure 1.3 a). In contrast to MHC class I molecules, MHC class II molecules are only expressed by APCs. Within mice, two polymorphic genes encode for MHC class II (I-A and I-E) and in human three (HLA-DP, HLA-DQ and HLA-DR). Inside the ER two integral membrane chains, α and β are synthesized and assembled to one MHC class II heterodimer. For stabilization of the heterodimer, the invariant chain (Ii) protein associates within the peptide-binding groove of the MHCII, acting as a pseudo peptide. This complex is transported from the ER to endo/lysosomal compartments. There, lysosomal proteases degrade the Ii, leading to binding of a 24 amino acid small peptide fragment (class II-associated invariant chain peptide, CLIP). Finally, CLIP is replaced by specific antigen-derived peptides with the help of the peptide exchange factor H2-M (mice) or HLA-DM (human). These chaperons have restricted activity to more acidic compartments [69,88,89].

Prior to the MHCII loading with specific antigen-derived peptides, the antigens need to be sensed and internalized (Figure 1.2). Therefore, DCs can apply distinct endocytic mechanisms such as receptor-mediated endocytosis [90], macropinocytosis [91,92], phagocytosis [93] or autophagy [69,94,95].

Receptor-mediated endocytosis is a highly specific, evolutionary conserved and very efficient process. Several cell surface receptors sense soluble material in the extracellular milieu at very low concentrations and enter the cell through clathrin-coated vesicles. This process includes more than 50 proteins and results in vesicle internalization forming early endosomes, subsequently evolving into multivesicular late endosomal-lysosomal antigen-processing compartments [96,97].

During macropinocytosis, high concentrations of exogenous antigens are detected in a non-specific way in the extracellular milieu. It is an actin-dependent endocytic process, in which the plasma membrane extends by forming ruffles, which seal at their distal tips, thereby, enclosing the soluble antigens. Once internalized, the macropinosomes fuse with endocytic compartments, eventually owning an acidic pH and degradative environment within the macropino-lysosome [69,98].

Phagocytosis, similar as macropinocytosis, is an actin-dependent mechanism, but in contrast to macropinocytosis internalizes a wide-variety of specific antigens. These are large, insoluble antigens and apoptotic cells. Recognition of these opsonized particles activates a signaling cascade, which directs their internalization into membrane-derived phagosomes. Phagocytosed antigens in DCs are then processed for cross presentation on MHC class I molecules to CD8+ T cells or the phagosome can fuse with lysosomes, forming phagolysosomes, subsequently leading to a MHC class II dependent antigen presentation

[96,99]. Besides exogenous antigens, endogenous antigens are presented by MHC class II molecules. Therefore, the process of autophagy overtakes an important role. During this process, membranes wrap up cytosolic antigens building so-called autophagosomes. When fusing with lysosomes, autophagolysosomes are generated. Cytosolic and nuclear proteins make up 20 to 30% of peptides that are presented by MHC class II to T cells. Thus, autophagy is an important mechanism how self and foreign antigens are presented [94,96,100].
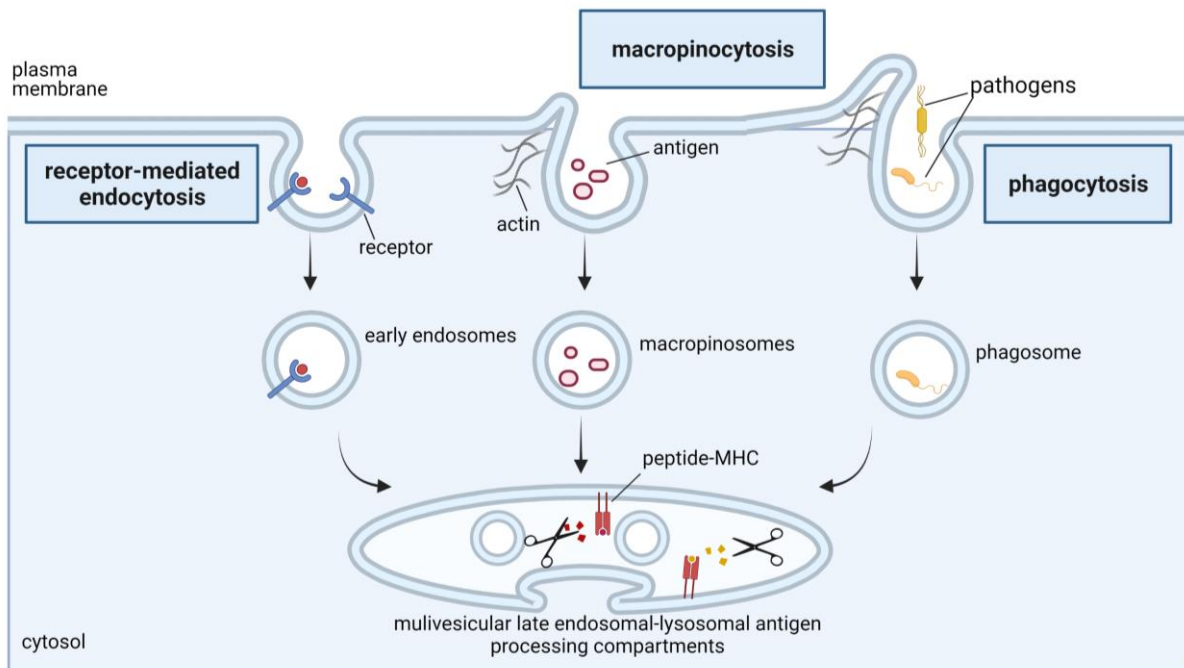


**Figure 1.2** Internalization of extracellular antigens by endocytic pathways.
Antigens can be taken up by differing mechanisms, such as receptor-mediated endocytosis, macropinocytosis or phagocytosis. Ultimately, the antigens are processed (depicted as scissors) in multivesicular late endosomal-lysosomal compartments and peptides are loaded onto major histocompatibility complex (MCH) molecules. Image adapted from Roche and Furuta, 2015.

All the described antigen-related mechanisms, lead to multivesicular late endosomal-lysosomal antigen-processing compartments. These compartments have a highly acidic and proteolytic nature [101]. Adenosine triphosphate (ATP) -dependent vacuolar proton pumps are responsible for establishing and maintaining the low pH. Asparaginyl endopeptidase and cathepsin S, for instance, are proteases required for antigen degradation into smaller peptides thus generating various epitopes. Here, antigenic protein proteolysis and proteolytic destruction is important to be in balance. Thereafter, antigen-peptide can be loaded onto MHC class II molecules and transported via microtubules (MTs) and their associated motor proteins to the cell surface where CD4+ T cells encounter the cognate peptide-MHCII complex (p-MHCII) [69].

### 1.2.1.1. Peptide-MHC class II transport

The multivesicular late endosomal-lysosomal antigen-processing compartments are regularly referred to as MHC class II containing compartments (MIIC). MIIC form into elongated vesicles/tubules and deliver p-MHCII to the plasma membrane where the immunological synapse is formed. These vesicles move along MTs in a `stop and go' manner [102–104]. MTs are built of α- and β- tubulin heterodimers in a cylindrical form, most often consisting of 13 parallel protofilaments. These filaments assemble and disassemble in a process termed dynamic instability, whereby the α-tubulin is exposed at the slower growing minus end and β- tubulin terminates the fast growing plus end [105,106]. For the MT-dependent vesicle transport, the motor proteins dynein and kinesin are important. Dynein affects the inward transport along MTs to the minus end and kinesin (kinesin-1 and kinesin-2) the outward transport to the MT plus ends [107,108]. In addition, several components including cholesterol, kinases and GTPases have been described to regulate p-MHCII movement. Rab7, a GTPase of the Rab (Ras-related in brain) family, decorates the membrane of MIIC and functions in recruiting dynein [109]. The GTPase ADP ribosylation factor-like protein 14 (ALR14, or also ARF7) and myosin 1E have been brought into context with actin-based movement. After all, p-MHCII transport remains an active area of investigation [96,104].

### 1.2.2. Cross-presentation

Cross-presentation describes the pathway of exogenous antigens, which are presented, on MHCI after internalization. In mice and humans, three genes encode for classical MHC class I molecules (H2-D, H2-K, H2-L and HLA-A, HLA-B, HLA-C, respectively). The two proteins heavy chain α and β2-microglobulin form the MHCI molecule. Within the peptide binding groove, molecules of 8-11 amino acids (in comparison, MHCII can bind 10-30 amino acid residues) can be loaded [110]. In recent years, much knowledge about the cross-presentation pathway has been gathered, but yet the molecular mechanisms are not fully understood and partly controversial data exists. The two major pathways are the endosome-to-cytosol pathway and the vacuolar pathway (Figure 1.3 b).

Endosome-to-cytosol pathway: After the internalization of exogenous antigen, these are transported from the endosomal compartments to the cytosol. Within the cytosol, proteasomes overtake the task off peptide degradation. Following, the peptides are transported through the protein transporter, transporter associated with antigen processing (TAP) to the ER or back to endosomes [111–115]. Subsequently trimming of the peptides occurs within these compartments. In the ER the peptidase ER-associated aminopeptidase 1 (ERAP1) fulfills this duty and in the endosome the peptidase insulin-responsive aminopeptidase (IRAP) [115–117]. The trimmed peptides are then loaded onto MHCI and translocated to the cell surface. The MHC class I

molecules can enter the loading compartments via two different recruiting routs. They are either transported from the plasma membrane via endocytosis to endosomes or they are synthesized newly in the ER and brought to the endosome [118–120].

Vacuolar pathway: This alternative cross presentation pathway is independent of TAP and does not seem to involve the proteasome. Antigens are internalized and degraded by cathepsin S and other phagosomal/endosomal/lysosomal proteases. Afterwards the antigen-derived peptides are loaded onto MHCI and presented to cytotoxic CD8$^+$ T cells [121,122].

Several mechanisms of the cross-presentation pathways have shown to be critical. One of these mechanisms is the antigen stability within phagosomes and endosomes. A limited acidification prevents proteolytic degradation causing the preservation of varying epitopes which can be loaded onto MHCI [122]. Rapid lysosomal antigen degradation thereby can be prevented actively by lower levels of lysosomal proteases [123,124], expression of endocytosis receptors that lead to internalization of the antigen to non-degradative endosomal compartments [125] or an active alkalization. The latter can be achieved through reduced V-ATPase activity [126]. V-ATPase transports protons into the luminal space of the lysosome during maturation generating an acidic pH. Another aspect of endosome alkalization is the recruitment of NADPH oxidase complex NADPH oxidase 2 (NOX2). This complex promotes the formation of reactive oxygen species (ROS), which themselves trap protons to assemble hydrogen peroxide, causing alkalization. In a more alkaline environment, proteases relying on acidic pH are not active and therefore different antigen-epitopes as in the classical MHCII pathways are generated [124,127,128]. Equally to the results of MHCII pathway also peptides presented via cross presentation on DCs need to get in spatial proximity with their interaction partner. For this purpose, DCs migrate to the draining LN.
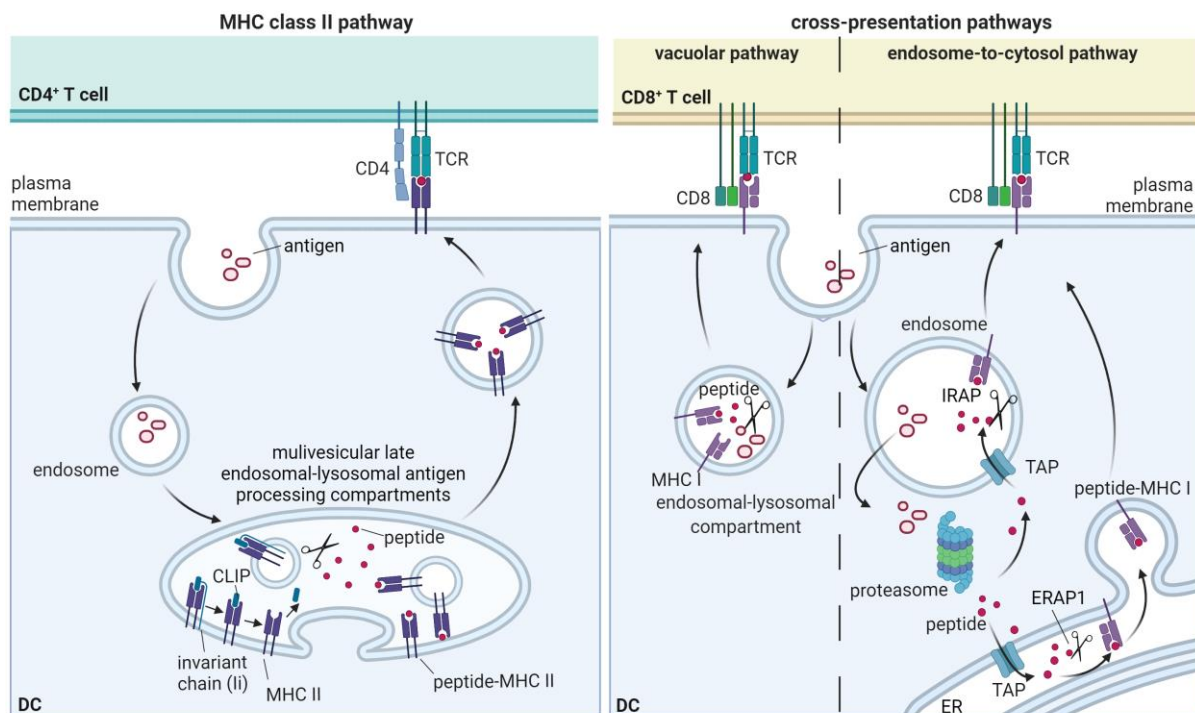
**Figure 1.3** Schematic overview of antigen presentation mechanisms.

(**a**) Major histocompatibility complex (MHC) class II pathway: internalized antigens proceed through endosome into late endosomal/lysosomal compartments, where they are degraded into peptides. Afterwards, peptides are loaded onto MHCII. Before MCHII can be loaded with peptide, invariant chain (Ii) and class II-associated invariant chain peptide (CLIP) are removed. Peptide loaded MHCII complex is transported to the cell surface and recognized through the T cell receptor (TCR) associated with co-receptor CD4 of T helper cells. (**b**) The cross-presentation pathway is separated into two mechanisms. Left panel: vacuolar pathway: internalized antigens are degraded into peptides and loaded onto MHCI with in endosomal-lysosomal compartment. Right panel: antigens are transported from endosomes to the cytosol for proteasomal degradation. From here peptides can either be transported via transporter associated with antigen processing (TAP) into the endoplasmic reticulum (ER) or back to the endosome. In both compartments the peptides are trimmed, either through ER-associated aminopeptidase 1 (ERAP1) or insulin-responsive aminopeptidase (IRAP), respectively. Thereafter, peptides are loaded onto MHCI. At the end of both pathways, peptide-MHCI complex is transported to the cell surface and recognized through the TCR associated with co-receptor CD8 of cytotoxic T cells. Images adapted from Roche and Furuta, 2015 and Embgenbroich and Burgdorf, 2018.

### 1.2.3. Homing of dendritic cells

Immature DCs in the tissue search their surrounding for damage or danger signals. Upon antigen encounter DCs get activated and mature. They migrate to the draining LN via afferent lymphatic vessels to transfer activating signals to cognate T cells (Figure 1.4). The strategic localization of LNs results in draining to nearly all tissues, including the skin [129,130]. The LN consists of different departments such as the subcapsular sinus (SCS), where migratory DCs arrive. The SCS is located between the LN capsule and the cortex. From here, DCs pass through the SCS floor to the T cell rich area of LN parenchyma in an integrin independent manner [131,132]. Besides migratory DCs, also LN resident DCs are present in the T cell area. These cells also sample their environment for antigens, but here the antigens arrive directly in the LN via so called lymph node conduits formed of fibroblastic reticular cells (FRC) [133]. Alternatively, resident DCs can also capture antigens through transmission from migratory DCs [38]. Resident DCs populate the LN by means of pre-cDCs in the bloodstream, entering the LN through high endothelial venules (HEVs) like naïve T cells [24,134,135]. Within the FRC network of the T cell area, naive T cells crawl in an random pattern, moving with a three-dimensional velocity of ~15 µm per minute [136]. The T cell area can be separated into two regions, the deep paracortex and the interfollicular regions. The follicles are the compartments where B cells are organized in. Naïve B cells reside in the LN for approximately 24 hours, naïve CD8$^+$ T cells for roughly 20 hours and CD4$^+$ T cells for about 12 hours [137,138]. Within the T cell areas, cDCs are separately distributed. cDC1 are found within the deep paracortex whereas cDC2 are mainly present in the interfollicular regions, accompanying with their specific T cell interaction partner [34].

Various aspects regulate DC mobilization and positioning; the most important regulator is the CC-chemokine receptor (CCR) 7 [139,140]. DCs are guided in a CCR7-dependent manner during homeostatic and inflammatory conditions by a process called haptotaxis. Here, directional motility is based on gradients of immobilized chemoattractant on cells or elements of the extracellular matrix. The ligands of CCR7 are the CC-chemokines CCL21 and CCL19. Gradient formation of immobile CCL21 overtakes a significant role during migration while soluble CCL19 plays a minor role in establishing immobilized gradients [141]. CCL21 is expressed by lymphatic endothelial cells (LECs) of the lymph vessels. The highest expression is found at the side where DCs enter lymphatic vessels, indicating CCL21-mediated regulation of lymphatic vessel entry. CCL21 relevance was also shown for enhanced DC migration within the lymphatic vessels [142–145]. Lymphatic vessels are terminal blind-ended three-dimensional tubes and consist of a discontinuous basement membrane streaked with flap valves, through which DCs enter. When reaching the LN, DCs follow the chemotactic gradient of CCL21 through the floor of SCS to the LN parenchyma. This gradient is established since LECs lining

the ceiling of SCS express the atypical chemokine receptor 4 (ACKR4) that scavenges CCL21 and CCL19 [146].

Besides CCR7 and its ligands, other mediators influence DC movement. In CCR7-deficient mice, it was laid out that C-X-C motif chemokine receptor (CXCR) 4- C-X-C motif chemokine ligand (CXCL)12 [147], CCR8-CCL1 [148] and Sphingosine-1-Phosphate Receptor 1 (S1PR1)/ Sphingosine 1-Phosphate Receptor 3 (3-S1P) [149] overtake complementary tasks [150]. The latter is also responsible for lymphocyte egress [151], whereas DCs do not leave the LN and die after 1 to 3 days of antigen presentation [152,153].

Besides studying DC mobilization and positioning aspects, extensive attempts have been made to analyze the complex cell intrinsic migratory machinery. These studies have resulted in major achievements: in general, DCs adjust their migratory mode, depending on the environment. They can move in an amoeboid like fashion without adhesion to the substrate. In this process, the cell shape frequently changes, relying on actin-rich protrusions at the front and acto-myosin depended retraction at the cells back [131]. They favor the direction of least resistance and the microtubule organizing center (MTOC) overtakes necessary tasks by nucleating dynamic MTs which are needed for the local retraction of protrusions [154–156]. Actin and MTs are part of the cell's cytoskeleton, which are not only required for DC migration but also important during immune synapse (IS) formation.

### 1.2.4. T cell activation

Once the antigen loaded DC reaches the T cell zone of the LN, a signaling cascade is triggered when the p-MHC is recognized by a cognate T cell via its T cell receptor (TCR). A specialized membrane structure is formed: the immunological synapse [1,157,158]. During IS formation and maturation various molecules besides the TCR are involved in signal transduction, such as integrins, co-stimulatory molecules, cytokines and parts of the cytoskeleton, causing spatio-temporally controlled activation and proliferation of naïve T cells and their differentiation into short-lived effector cells and long-lived memory cells. Effector cells promote either an immune response towards the elimination of pathogens themselves or they communicate with further cells for a proper immune defence, whereas memory cells are responsible for the quick reaction after a second encounter with the same antigen [159–161].
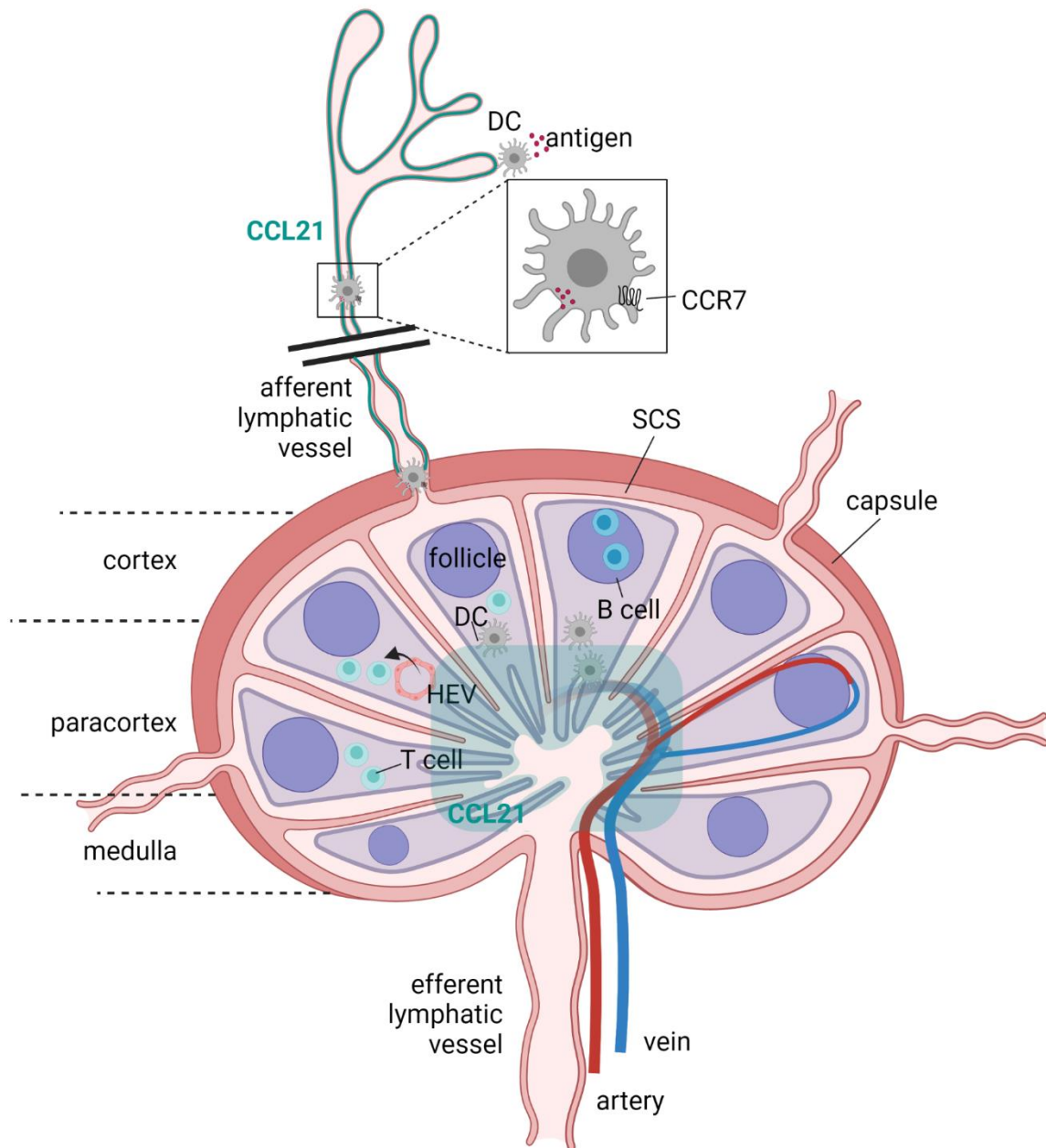
**Figure 1.4** Dendritic cell (DC) homing to lymph node.

DCs sense antigens in the periphery and migrate through afferent lymphatic vessels in a CCR7-CCL21 dependent manner to the lymph node. The lymph node consists of three main regions: cortex, paracortex and medulla. B cells are located within follicles, whereas T cells are present in the T cell zone of the paracortex. Lymphocytes enter the lymph node via high endothelial venules (HEVs) or afferent lymphatic vessels. When migratory DCs reach the lymph node, they pass through the subcapsular sinus (SCS) floor into the T cell rich area. Image adapted from Girard et al., 2012.

## 1.3.     Immune synapse

The IS represents a tight cellular contact zone between two cell types conducting the activation of intracellular signaling, cytoskeleton reorganization and altered membrane trafficking on both cell sides. APCs such as B cells and DCs that interact with their effector cell such as T cells, belong to the group of primary synapses. Secondary synapses refer to cell-cell contacts that are formed after initial priming of activated T cells. For example, the synapse formation between CTLs or natural killer cells (NK) and their target cell during which lytic granules for cell killing are untied [162]. These highly organized subcellular structures vary between immunological synapses, deepening on the cell types involved, antigen presented, or duration of contact. The B cell, NK and T cell side of the IS are well understood, but less is known about the molecular behavior on the DCs side [163].

### 1.3.1. Structure of the immunological synapse

First, in the 1990s Kufper's group described the IS to form a `bulls eye´, which represents a highly supramolecular organized structure of a monocentric synapse (Figure 1.5). For these analysis, cell-cell interaction as well as planar model membranes like lipid bilayers were used. The contact zone revealed a series of at least three supramolecular activation clusters (SMAC) containing signaling receptors, integrins, co-stimulatory molecules and actin [158,164,165]. The SMACs are organized in radial symmetric zones leading to a polarization towards the contact cell. The central SMAC (cSMAC) is responsible for proximal signaling events and active secretion [166,167]. The cSMAC is surrounded by a ß2-integrin rich peripheral SMAC (pSMAC). Lymphocyte function-associated antigen 1 (LFA-1) and intercellular adhesion molecule (ICAM) belong to the group of these integrins and function as adhesion molecules connecting the engaged cell types. A distal SMAC (dSMAC) encloses the former one, functionally overtaking the task of applying mechanical forces through filamentous actin (F-actin) [160]. For the past years many studies have focused on TCR signaling and thereby modified the original view [168,169]. TCRs are present in microclusters together with co-stimulatory molecules such as CD28, signaling adaptor molecules, and molecules that relate to the cytoskeleton [170,171]. These microclusters establish at the dSMAC, move through the pSMAC, reaching the cSMAC upon TCR stimulation. This translocation depends first on actin filaments and eventually on dynein. Dynein is a motor protein that moves along MTs and plays a major role during centrosome

relocalization towards the IS. Within the cSMAC signaling-incompetent TCRs are removed, rather than being activated within the cSMAC, which was believed beforehand [161,163,172].

**immune synapse of monocentric structure**

**multi-conjucated immune synapses of multicentric structure**
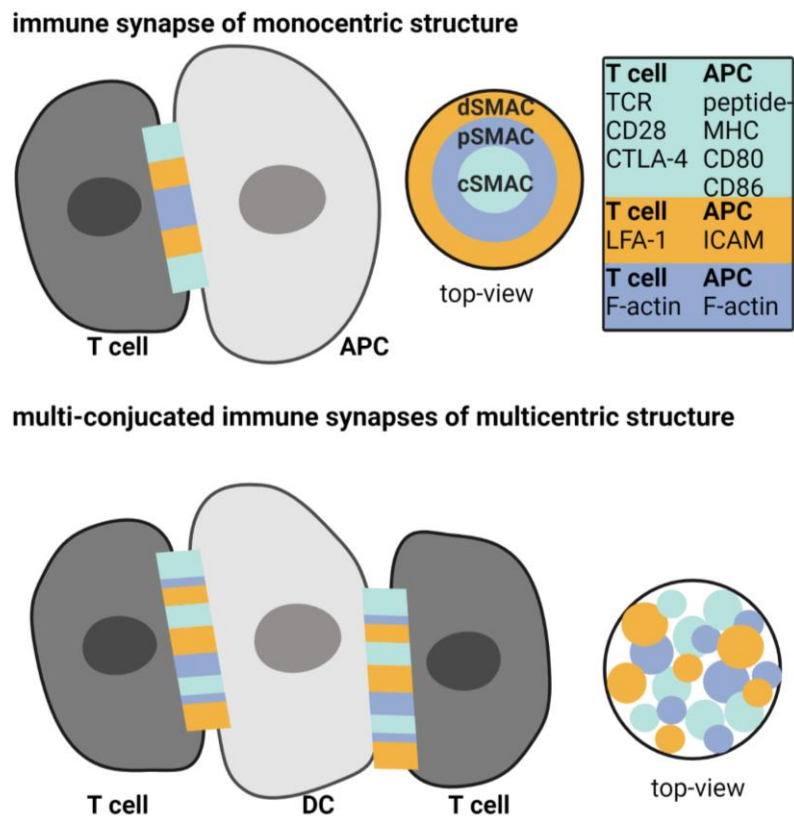
**Figure 1.5** Schematic illustration of immune synapse (IS) structures.
A monocentric IS is organized in at least three supramolecular activation clusters (SMAC): central (cSMAC), peripheral (pSMAC) and distal (dSMAC). Each structure consists of special signaling molecules. A multicentric IS, which is formed by DCs, shows an altered pattern of signaling molecules. Additionally, DCs are well known for their capacity to form multi-conjugated ISs, thus interacting with several T cells at once. Image adapted from Thauland and Parker, 2010.

### 1.3.2. Multicentric synapses between DCs and T cells

Over the last decades, many studies in explanted LNs with multiphoton imaging and intravital imaging of live mice have focused on T cell priming by DCs [173–177]. When comparing these results with the described monocentric synapse, differences have been observed. A non-classical multicentric synapse is formed (Figure 1.5) [178–180]. The classical structure of a `bulls eye´ does not apply, even though the main players are similar: TCR, p-MHCII, co-receptors and adhesion molecules ensemble in multiple small clusters [180]. Thereby one DC can interact with several T cells, thus forming multi-conjugated ISs. The contact time of cellular engagement relies on the cells involved and varies between seconds to several hours [162,174]. The IS contact of DCs and T cells can be separated into different periods. When a migrating T cell interacts with an unloaded DCs, this contact is no longer than 3 minutes [175]. However, when DCs are presenting a cognate antigen, T cells contact multiple DCs with a somewhat

prolonged contact time, still in the range of minutes. Within a few hours after the initial first phase, a second phase of T cell priming follows. Long-lasting stable synapses between one DC and multiple T cells are generated concurrently. The secretion of IL-2 and INF-γ begins. Finally yet importantly, a third phase takes places, when T cells start proliferating and differentiating [34,163,174–176]. Evidence exists, that short and sequential cellular contacts are satisfactory to activate T cells [159,162,178], whereby the inflammatory context and the antigen density are essential factors that need to be considered.

### 1.3.3. Immune synapse signaling

Once the TCR in cooperation with CD4 or CD8 co-receptors recognized the cognate p-MHC, a signaling cascade is orchestrated. Depending on the magnitude of these signals, different effector lineages are pursued. For activation, immunoreceptor tyrosine-based activation motifs (ITAMs) are phosphorylated by protein tyrosine kinases (PTKs). ITAMs are present on the TCR-CD3 protein complex. The TCR itself consists of an α- and a β chain that make up the antigen-recognition side and ζ-chain homodimer, functioning as signaling motive containing two ITAMs. The TCR is coupled to four chains of CD3, holding additional ITAMs [161,181]. After p-MHC recognition, lymphocyte-specific protein tyrosine kinase (LCK) phosphorylates the TCR-CD3 complex [182]. Through the activation, the recruitment of zeta-chain-associated protein kinase 70 (ZAP-70) follows, which in turn is phosphorylated by LCK. Next, the linker for activation of T cells (LAT) is recruited through ZAP-70 [183]. LAT functions as docking side for further molecules, including SH2 domain containing leukocyte protein 76 (SLP-76), phosphoinositide 3-kinase (PI3K), the Rho-family GTPase exchange factor (GEFs) VAV1 and phospholipase C-γ (PLC-γ) [184–187]. From here on, PLC-γ activates the protein kinase C-θ (PKC-θ) by releasing diacylglycerol (DAG). DAG is released by the hydrolysis of phosphatidylinositol-4,5-bishosphat ($PIP_2$) to DAG and inositol-1,4,5-trishosphat ($IP_3$). This signaling cascade eventually causes the transcription of the cytokine IL-2, receptor CD69 and others. Besides this signaling axis, PI3K induces another one by production of phosphatidylinositol-3,4,5-triphosphat ($PIP_3$). $PIP_3$ recruits actin associated proteins causing actin cytoskeletal rearrangements [188].

Another important aspect during TCR signaling is the function of calcium as a second messenger via the $IP_3$-$Ca^{2+}$-nuclear factor of activated T-cells (NFAT) pathway. By interaction of $IP_3$ to the $Ca^{2+}$ permeable ion channel receptor $IP_3R$ in the ER membrane, $Ca^{2+}$ is distributed from the ER to the cytoplasm. Reduction of $Ca^{2+}$ levels in the ER leads to an extracellular $Ca^{2+}$ influx via plasma membrane $Ca^{2+}$ release-activated $Ca^{2+}$ channels (CRAC) [189,190]. The elevation of cytosolic $Ca^{2+}$ concentration eventually triggers the translocation of transcription factors to the nucleus [191,192].

Besides signaling transduction upon TCR ligation, additional mechanisms are essential for a

T cell response. These include, as mentioned above, integrins, cytokines and co-stimulatory factors, which regulate the threshold needed for activation. There are positive co-stimulatory factors available as well as inhibitory factors, such as CD28 and CTLA-4, respectively. Both proteins interact with the co-stimulatory molecules CD80 and CD86 on the APC, thereby ensuring tight control of T cell responses (Sansom, 2000; O'Neill and Cao, 2019). The process of T cell activation includes a dynamic regulation of the actin and MT cytoskeleton. For actin, this is achieved throughout multiple signaling pathways, incorporating downstream routs of TCR, CD28 and LFA1 [186,193]. Thereby the activation of VAV1 and other GEFs trigger the small GTPases cell division control protein 42 homolog (Cdc42) and Ras-related C3 botulinum toxin substrate (Rac) 1. These in turn select and stimulate nucleation promoting factors WAVE2, WASp and HS1. Lastly, these factors coordinate polymerization of branched actin filaments via the actin related protein 2/3 complex (Arp2/3) [193–195]. Only recently, a study was published on actin significance during multicentric synapse formation on the DCs side. Leithner and colleagues found out that dynamic F-actin is important for the structural organization of multicentric synapses and thus increased turnover rates of T cells are achieved rather than stable contacts. Higher numbers of contact partners in turn led to increased activation and proliferation of the effector cells [196].

### 1.3.4. MTOC function during immune synapse signaling

T cell activation depends on a dynamic actin and MT cytoskeleton. The MTOC overtakes the function as MT nucleation side. In leukocytes the MTOC is represented by the centrosome. Upon IS formation it relocalizes towards the contact zone in certain immune cells such as T and B cells as well as in NK cells. Meanwhile it is associated to the Golgi Apparatus and is a key player orchestrating vesicle trafficking and polarized secretion of lytic granules or cytokines [197,198]. The underlying mechanisms of centrosome displacement rely on MTs anchoring to the cell cortex [199–201].

### 1.3.5. MTOC reorientation

Once MTs reach the contact zone, bending of the tubules was observed, indicating their interaction with motor proteins at the inner cell membrane. Within the pSMAC the cytoskeletal adaptor proteins IQ motif containing GTPase activating protein 1 (IQGAP1) and Cdc42-interacting protein 4 (CIP4) overtake the function of allies [166], causing to MTOC positioning to the contact zone. Destabilization of MTs impairs MTOC translocation, highlighting a crucial role of dynamic MT filaments for MTOC relocalization [202]. MT destabilization can be induced via deacetylation of tubulin or depletion of formins and microtubule-associated protein 4 (MAP4) [202–204]. In addition to MT stability, also their polymerisation of the plus-ends is a key aspect of their dynamic behaviour. In the course of this, the precise work of plus-end-binding

protein 1 (EB1) is needed [205–207]. EB1 recruits dynein to the plus-end of MTs. Dynein is a minus-end directed motor protein and part of the cytoplasmic dynein complex. The protein has also been linked to MTOC translocation. More precisely, dynein has been the focus of interest in many studies, resulting in functional distinct pathways: one is the "cortical sliding mechanism", where dynein at the cell cortex stays in this position and walks simultaneously to the minus-end of the MT, which are anchored at the centrosome, leading to a pulling event of the centrosome to the IS [200]. The second pathway is referred to as "capture-shrinkage mechanism". Here, MT dynamic instability overtakes the major aspect. Dynein attaches the depolymerizing MTs at the plus end via EB1 to the cell cortex. MT shortening also induces force generation and MTOC repositioning [201].

Independent of the model, the outcome is similar: once MTs are attached to the cell cortex, the MTOC is positioned to the contact zone via a dynein-mediated force [156,208].

For dynein to become trapped at the cell cortex, the association with adhesion and degranulation promoting adaptor protein (ADAP) [200] has been reported to play an important role as well as the recruiting partner DAG that needs to be present at the plasma membrane [209]. DAG production is induced by TCR activation, linking fast reorientation of the MTOC to the initial steps of T cell activation. Another facet of quick MTOC relocalization is the "search and capture" model, which was established to determine the MT capture time. The model was originally introduced in the context of cell proliferation where MTs attach to the chromosomes [210,211]. Later on, a mathematical model was established to calculate the search and capture times of MTs to attach to the plasma membrane underneath the IS. "Searching" refers to the process of MTs growing and shrinking from the MTOC to periphery is meant, and "capture" refers to the dynein-based MT anchoring to the cortex. In this model, cell size, number of nucleating MTs, nucleus and MTOC positioning within the cell are important parameters. Sarkar and colleagues conclude that the search time is minimal when the IS is formed at the closes or most distant position of the perinuclear MTOC [212].

The studies described above refer to the T cell side of the IS. Focusing on the DC side, only little is known about MTOC positioning behavior. One study reports MTOC reorientation, which depends on Cdc42, in a minor fraction of DCs under certain antigen conditions [213], whereas other studies, under experimentally different conditions, do not observe MTOC translocation within the DC side of the IS [214,215]. Nevertheless, the function of the MTOC in nucleating MTs has been highlighted on both sides of the IS.

### 1.3.6. Microtubule dependent trafficking

Many processes of MT-dependent trafficking during IS signaling exist. Most of these events are well characterized in T helper or cytotoxic T cells. The latter are specialized in the release

of cytotoxic granules containing granzymes, cathepsins and perforins towards the target cell. First, these vesicles are delivered in a dynein minus-end-mediated MT transport to the polarized MTOC [216]. From here, a plus-end mediated transport moves the secretory vesicles along MT filaments. This plus end-mediated transport to the cSMAC is based on a complex of kinesin-1, synaptotagmin like 3 (Slp3) and Rab27 [217,218]. At the plasma membrane, vesicle-associated membrane protein (VAMP) 2 drives the final membrane fusion step, in a way that has been recognized to be similar to neurotransmitter release [219]. Moreover, MTs are essential for vesicle transport within CD4^{+} T cells, for instance in directing cytokines into the IS [208,220,221].

For an intact IS formation in both T cell types, the TCR needs to be constantly restored after the prior ones were downregulated once engaged. Therefore, one mechanism to restore TCR to the cell surface is its recycling from the endosomal pool. This recycling can depend on two mechanisms, one is MT-independent, and the other one is MT-dependent. In the latter one, Rab5^{+}-Rab11^{+} recycling endosomes containing TCRs are delivered to the plasma membrane via docking to GTPase Rab8^{+} and soluble N-ethylmaleimide-sensitive-factor attachment receptor (SNARE) protein VAMP3^{+} vesicles [222]. This movement relies on dynein, its recruiter EB1 and their interaction to TCR-complex component CD3ζ [207,208,222].

Next to the recycling of TCR, Lck and LAT also link to endosomal compartments and subordinate on MT transport [223,224]. Besides MT-dependent transport of recycling endosomes, the transport also relies on actin, linking both cytoskeletal components to each other. Actin related protein 2/3 complex subunit 2 (Arpc2), a protein of the Arp2/3 complex, interacts with TCR[+] endosomes and promotes actin polymerization from these vesicles. In addition, WASH has also been recognized for this interaction with tubulin linking the MT and actin cytoskeleton for endosome relocation [225].

MT-dependent transport is not only crucial during signal transduction on the receiver side but also on the side of the sender. As described, MIIC tubulation and trafficking depends on MTs, whereby p-MHC is delivered to the IS at the DCs side [103,226–228]. Together with p-MHC, ICAM-1 and CD70 also reside in these compartments possibly sharing the intracellular trafficking pathway [229,230]. Next to MIIC, further vesicle trafficking is based on MT interaction. Molecules that are delivered in such a way are the co-stimulatory molecule CD86 and the cytokine IL-12 [163,213,231].

Altogether, IS formation represents a very complex network of signal transduction and overtakes indispensable functions during many immune responses. Here the focus lies on T cells and DCs, whereas a much deeper understanding of the T cell side is present. To obtain a similar state of knowledge for the DCs side, one focus needs to concentrate on the centrosome and one on its function as vesicle trafficking organizer.

## 1.4. Centrosomes

The centrosome overtakes the function of MT organization, by nucleating and forming MT filaments. Besides the centrosome, other organelles depending on the organism and cell type can overtake the function of an MTOC. For example in epithelial cells [232], muscle cells [233], pancreatic ß cells [234] and neurons [235] the Golgi apparatus can be the source of MT nucleation capacity. Within most animal cells, the centrosome functions as the main MTOC, being responsible for the organization of MT structure dependent processes, like motility and cell signaling, in the interphase. During meiosis and mitosis the centrosomes are the center of the spindle apparatus and therefore responsible for proper cell division [236]. The centrosome consists of a centrally located pair of centrioles. The pericentriolar material (PCM), a well-structured multiprotein complex, surrounds the centrioles. This membrane-less structure occupies 1-2 µm$^3$ of the cell volume. During interphase, a single centrosome containing one centriole pair is present. This pair of centrioles is made of one parentcentriole connected to one procentriole and is localized in the center of the cell in close relationship to the nuclear envelope. Once the cell starts to duplicate, the centrosome itself is duplicated in parallel, eventually leading to two centrosomes each at the opposite side of the cell forming the spindle poles and defining the axis for cell proliferation [237].

### 1.4.1. Molecular composition and structure of the centrosome

The centrosome is a compartment that is well conserved between species, consisting of a multiprotein complex that shows high homology. One centriole pair forms the core of the centrosome (Figure 1.6 a). The evolutionarily preserved cylindrical structure that is formed by the centriole is made of a radial nine-fold symmetry, thereby consisting of nine triplets. The size of a centriole is about 450-500 nm in length and 200-250 nm in diameter MTs [238,239]. A mature parentcentriole (which is also called mature mother centriole) is not only associated to the centrosome but also functions as basal body for the generation of cilia or flagella. A characteristic feature of a mature centriole is the presence of subdistal and distal appendages. These structures are responsible for anchoring astral MTs to the cell membrane during ciliogenesis and cell division [240,241]. The appendages are only present on the mature centriole, thereby allowing to be distinguished from the procentriole. Within the distal lumen of full-length centrioles, centrin (CETN) proteins arrange [242]. A property that is linked to the procentriole is the cartwheel; this structure serves as scaffold for forming the centriolar MT wall during the generation of the procentriole. Thereby the cartwheel is located at the proximal end, connected to the parentcentriole and marks one of the first steps during centriole duplication [243,244].

The centrioles are surrounded by a highly organized protein matrix, the PCM, which consists of ~ 200-300 proteins organized in distinct radial layers with some of these proteins being

permanently exchanged [245,246]. The mechanisms on how the PCM assembles is not yet fully understood. A self-assemble organization of large proteins via multimerization into microscale structures as well as a model based on phase separation from liquid-to-condensate are currently under investigation [247–250]. Part of the PCM proteins overtake the task of MT nucleation whereas others function in regulating the cell cycle and its checkpoints [251]. It was first described for centrosomes of *Drosophila melanogaster*, that γ-tubulin ring complexes (γ-TuRCs) of 25-30 nm diameter were present [252] which were later identified to induce MT nucleation from the minus end [253]. Over the last years, more and more details on the structure and organization of PCM components have become available. Some of the most prominent proteins localized to centrosomes are pericentrin, centrosomal protein (CEP) 192, CDK5 regulatory subunit associated protein 2 (CDK5RAP2), CEP152 and polo like kinases (Plks) [236].

### 1.4.2. Duplication cycle

Being responsible for many different aspects during cellular processes, centriole numbers need to be supervised closely. If centriole numbers are altered, this can have a huge impact by transforming physiological functions into pathological conditions [236]. Within G1 phase of cycling cells, one pair of centrioles is typically present (Figure 1.6 b). Here a fully mature parentcentriole is tethered to its procentriole [254]. This procentriole will become a parent itself during the next step and both parentcentrioles (one being fully mature and one being immature) start generating each a new procentriole perpendicularly during G1/S phase transition [255]. The process of generating only one procentriole each, is controlled by Plk4. The protein is recruited to the PCM components CP152 and CEP192 at the proximal end of the parentcentriole [256,257]. Plk4 phosphorylates SCL-interrupting locus protein (STIL), which recruits spindle assembly abnormal protein 6 homolog (SAS6). SAS6 is the key component of the cartwheel and evokes its formation. In the final step of procentriole formation, MTs deposit around the cartwheel, further relaying on the additional centriolar proteins CEP135 and centrosomal P4.1-associated protein (CPAP) [236]. During G2 phase, the newly established procentrioles elongate further. At the end of G2 phase, centriole duplication is completed and two pairs of centrioles are ready to overtake their task during mitosis. At this stage, the newly established procentrioles cannot recruit PCM whereas the parents can [236]. Even though, the younger parentcentriole is not fully mature yet, still missing the appendages. The Plk1-dependent process of PCM expansion that occurs during G2/M phase transition is termed centrosome maturation [247]. During mitosis, the two centrosomes position at the opposite end of the cell. They form the spindle poles from which MTs nucleate and attach to the kinetochores of the chromosomes [211], leading to proper segregation of genetic material into the newly formed daughter cells. At the end of mitosis, each daughter cell contains one

centrosome consisting of one pair of centrioles. An important aspect of the centrosome duplication cycle is that this process only starts once the pair of centrioles is further separated from each other. Plk1 and the protease separase activate this distancing of the procentrioles during mitosis/early G1 phase. Both proteins are described in the context of pericentrin cleavage, which is needed for the disengagement [258–260].

Taken together the centrosome is a highly multidimensional protein complex overtaking many critical functions during various cellular processes. During these processes, MTOC behavior and MT nucleation need to be understood in more detail. As has been reported only recently, MTs are responsible for directional persistence in migrating DCs along gradients of chemotactic cues [155] and the reorientation of the MTOC is crucial for proper vesicle transport toward the IS [197,198].
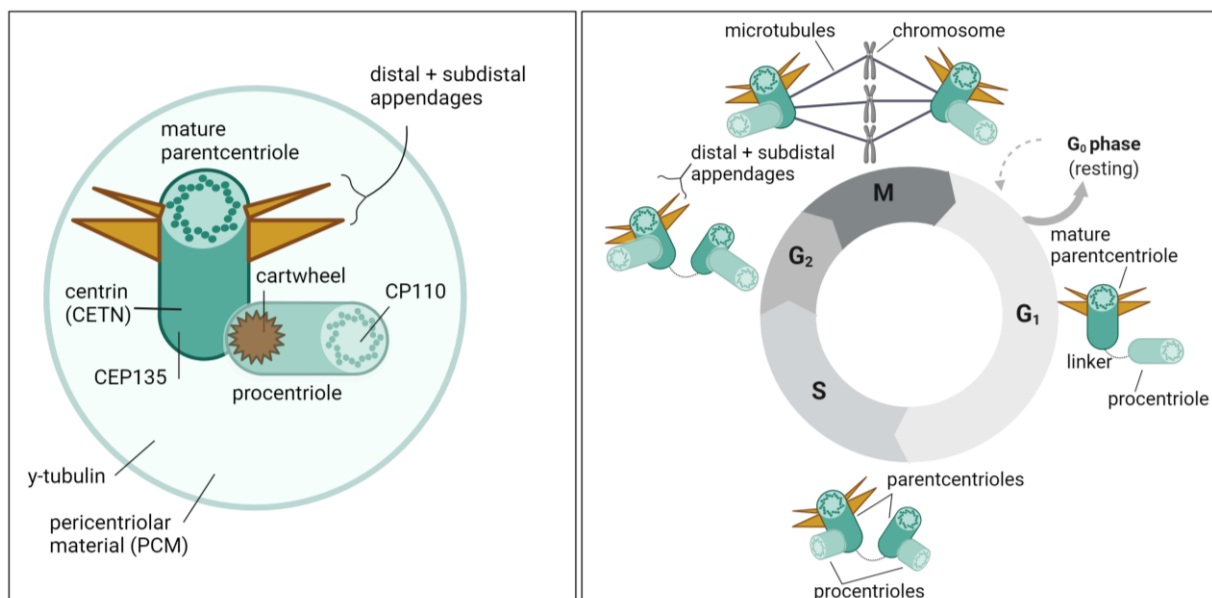


**Figure 1.6** Centrosome structure and duplication cycle.

(**a**) The Centrosome consists of two centrioles: a parentcentriole and a procentriole, both centrioles have a cylindrical structure formed of nine-triplets of microtubules (MTs), the mature parentcentriole additionally contains distal and subdistal appendages. Centrioles are surrounded by pericentriolar material (PCM). (**b**) Centrosomes duplicate once per cell cycle. In G1 one centriole pair is present, during G1/S phase transition the procentriole becomes a parentcentriole and two newly formed procentrioles are seeded from each parent. In G2 phase, procentrioles elongate, while during mitosis (M) both mature centriolar pairs separate from each other and function as spindle poles from which MTs nucleate that attach to the chromosomes and induce their proper segregation. Images adapted from Nigg and Holland, 2018.

## 1.5.     Aim of the present work

Fighting a disease is a daunting task for the human body. During such a process, the immune system overtakes important functions. It counteracts foreign pathogens such as bacteria and viruses as well as endogenous attacks from, for instance, cancerous cells. Our immune system consists of an ancient, innate and a highly specialized, adaptive framework. As both parts of the immune system overtake different aspects of the immune response this highlights the importance of their interaction and their need for close cooperation [261]. A critical linker between both parts of the immune system are DCs, which function as APCs thereby interacting with T lymphocytes. During this cell-cell interaction an IS is formed. The IS represents a highly specialized contact zone, which is dependent on dynamic cytoskeletal rearrangements and a complex signaling transduction network. As the DC side of the IS is insufficiently understood, the research aim of this study was to gain further knowledge on the molecular level, how the centrosome behaves and how it coordinates its function in nucleating MTs and as vesicle trafficking organizer.

# 2. Material and Methods

## 2.1. Material

### 2.1.1. Organisms

| Organism | Source |
|---|---|
| CCR4-KO mice (B6;129P-Ccr4$^{tm1Pwr}$/J) | Prof. Dr. Irmgard Förster, LIMES, Bonn University [262] |
| CETN2-GFP mice (CB6-Tg (CAG-EGFP/CETN2)3-4Jgg/J) | The Jackson Laboratory [263] |
| Flt3-Ligand producing hybridoma cells | Prof. Dr. Michael Sixt, IST Austria |
| GM-CSF producing hybridoma cells | Prof. Dr. Michael Sixt, IST Austria |
| HEK T293 (human embryonic kidney cells) | Sigma-Aldrich |
| Jurkat Clone E6-1 TIB-152 (human acute leukemia T cells) | Dr. Bettina Jux, Kolanus Lab, LIMES, Bonn University |
| One Shot Stbl3 Chemically Competent E. coli | Invitrogen |
| OT-II- mice (B6.Cg-Tg(TcraTcrb)425Cbn/J) | Prof. Dr. Sven Burgdorf, LIMES, Bonn University [264] |
| Subcloning Efficiency DH5α Competent Cells | Invitrogen |
| wildtype (WT) mice genetic background: C57BL/6JRcc | Dr. Joachim Degen, Genetic Resources Centre, LIMES, Bonn University |

### 2.1.2. Kits

| Kits | Company |
|---|---|
| BD Comp Beads anti-mouse compensation particles and negative control (FBS) particles set | BD Bioscience |

| Kits | Company |
|---|---|
| BD Comp Beads anti-rat/hamster compensation particles and negative control (FBS) particles set | BD Bioscience |
| BD Cytofix/Cytoperm Plus Fixation/Permeabilization kit | BD Bioscience |
| Cell Trace CFSE Cell Proliferation Kit | Molecular Probes |
| Click-iT Plus EdU Cell Proliferation Kit for Imaging, Alexa Fluor 555 dye | Thermo Fisher Scientific |
| EasySep Mouse Naïve CD4$^+$ T cell Isolation Kit | STEMCELL Technologies |
| EasySep Mouse Pan-DC enrichment kit | STEMCELL Technologies |
| eBioscience Foxp3/Transcription Factor Staining Buffer Set | Thermo Fisher Scientific |
| EndoFree Plasmid Maxi Kit | Qiagen |
| IL-6 Mouse ELISA Kit | Thermo Fisher Scientific |
| KC/CXCL1 Mouse ELISA Kit | Thermo Fisher Scientific |
| MDC (CCL22) Mouse ELISA Kit | Thermo Fisher Scientific |
| Monarch DNA Gel Extraction Kit | New England Biolabs |
| Monarch Plasmid Miniprep Kit | New England Biolabs |
| Mouse IL-2 Quantikine Elisa-Kit | R&D Systems |
| Pierce ECL Plus Western Blotting Substrate | Themo Fisher Scientific |
| Mouse Cytokine Antibody Array, Panel A | R&D Systems |
| RANTES (CCL5) Mouse Instant ELISA™ Kit | Thermo Fisher Scientific |
| Rneasy Mini Kit | Qiagen |
| TARC (CCL17) Mouse ELISA Kit | Thermo Fisher Scientific |
| TaqMan RNA-to-C$_T$ 1-Step Kit | Applied Biosystems |

### 2.1.3. Primer

Primer used for quantitative real-time polymerase chain reaction analysis

| Name | Company |
|------|---------|
| TaqMan Mm00446917_m1 PLK2 FAM | Thermo Fisher Scientific |
| TaqMan Mm01277042_m1 Tbp FAM | Thermo Fisher Scientific |
| TaqMan Mm00550358_m1 Plk4 FAM | Thermo Fisher Scientific |
| TaqMan Mm00516136_m1 CCL17 FAM | Thermo Fisher Scientific |
| TaqMan Mm00436439_m1 CCL22 FAM | Thermo Fisher Scientific |
| TaqMan Mm00446190_m1 IL-6 FAM | Thermo Fisher Scientific |
| TaqMan Mm01302427_m1 CCL5 FAM | Thermo Fisher Scientific |
| TaqMan Mm04207460_m1 CXCL1 FAM | Thermo Fisher Scientific |

Primer used for CRISPR/Cas9 based knock out generation

| Name | Sequence | Company |
|------|----------|---------|
| PLK2sg1a_fw | 5´CACCGGATTATAGTCGACCCCACGA3' | Eurofins |
| PLK2sg1b_rv | 5´AAACTCGTGGGGTCGACTATAATCC3' | Eurofins |
| PLK2sg2a_fw | 5´CACCGGCTGGTAGGTGATAGTCCGC3' | Eurofins |
| PLK2sg2b_rv | 5´AAACGCTGGTAGGTGATAGTCCGCC3' | Eurofins |
| scramble_fw | 5'CACCGGCCGTGGCGCATGGGTAGCA3' | Eurofins |
| scramble_rv | 5'AAACTGCTACCCATGCGCCACGGC3' | Eurofins |

### 2.1.4. Plasmid

| Plasmid | Resistance | Company |
|---------|-----------|---------|
| lentiCRISPRv2 | Ampicillin, puromycin | Addgene |
| pCMV-VSV-G | Ampicillin | Addgene |
| pdelta8.9 | Ampicillin | Addgene |

## 2.1.5. Reagents, media and enzymes

| Name | Company |
|---|---|
| 4–20% Mini-Protean TGX Gels | Bio-Rad Laboratories |
| ß-mercaptoethanol ( ß-ME) | Gibco |
| ß-mercaptoethanol ( ß-ME) | Bio-Rad Laboratories |
| acetic acid | Carl Roth |
| ACK Lysing Buffer | Life Technologies |
| agarose | VWR |
| ampicillin | Carl Roth |
| blotting-grade-blocker (milk powder) | Bio-Rad Laboratories |
| bovines serum albumin (BSA) | Sigma-Aldrich |
| BsmBI | New England Biolabs |
| Centrinone | Tocris |
| c0mplete protease inhibitor, EDTA-free | Roche |
| collagenase from clostridium hisolyticum | Sigma Aldrich |
| CountBright Absolute Counting Beads | Thermo Fisher Scientific |
| CutSmart 10 x Buffer | New England Biolabs |
| dimethylsulfoxid (DMSO) | Sigma |
| DMEM (Dulbecco's Modified Eagle Medium) Medium | Gibco |
| DNA loading dye 6x | Thermo Fisher Scientific |
| DNase I | Sigma |
| Dynabeads Mouse T-Activator CD3/CD28 | Gibco |
| EDTA ( Ethylenediaminetetraacetic acid ) (0.5 M), pH 8.0, RNase-free | Life Technologies |
| estradiol, | Sigma-Aldrich |
| ethanol (≥99.5%) | Carl Roth |

| Name | Company |
|---|---|
| FastAP thermosensitive alkaline phosphatase | Thermo Fisher Scientific |
| FastDigest Buffer 10x | Thermo Fisher Scientific |
| fetal bovine serum (FBS) | Gibco |
| Flt-3-ligand (supernatant from Flt-3-ligand-hybridoma cells) | produced by Stephanie Ebbinghaus, AG Kiermaier |
| Fluoromount-G Mounting Medium with DAPI | Thermo Fisher Scientific |
| formaldehyde 16%, methanol free | Thermo Fisher Scientific |
| GeneRuler 100 bp DNA Ladder | Thermo Fisher Scientific |
| GM-CSF (supernatant from GM-CSF-hybridoma cells), 150 ng/mL | produced by Stephanie Ebbinghaus, AG Kiermaier |
| glycine | Carl Roth |
| GolgiPlug (with Brefeldin A) | BD Biosciences |
| GolgiStop (with Monensin) | BD Biosciences |
| Hanks' Balanced salt solution (HBSS) | PAN-Biotech |
| HBSS 10x | Gibco |
| ICAM (CD54) recombinant protein | eBioscience |
| Laemmli Sample Buffer 4x | Bio-Rad Laboratories |
| LB (lysogeny broth) agar | Carl Roth |
| LB medium | Carl Roth |
| Lipofectamine 2000 Transfection Reagent | Invitrogen |
| lipopolysaccharide (LPS) | Sigma-Aldrich |
| MagicMarker XP Western Protein | Life Technologies |
| N-[Tris(hydroxymethyl)methyl]-2-aminoethanesulfonic acid (TES) | Sigma Aldrich |
| Opti-MEM, Reduced Serum Medium | Gibco |

| Name | Company |
|---|---|
| ovalbumin-peptide 323-339 (ova$_{323-339}$) | InvivoGen |
| ovalbumin | InvivoGen |
| paraffin wax | Sigma |
| PhosSTOP | Roche |
| phosphate buffered saline (PBS) (pH 7.4) | Gibco |
| penicillin/streptavidin | Gibco |
| Platinum Taq Green Hot Start DNA Polymerase | Invitrogen |
| Polybrene Infection/Transfection Reagent | Sigma-Aldrich |
| Ponceau S | Carl Roth GmbH & Co KG |
| Precision Plus Protein Standard | Thermo Fisher Scientific |
| PureLink RNase A (20 mg/mL) | Thermo Fischer Scientific |
| puromycin | Carl Roth |
| Quick-Load 1 kb DNA Ladder | New England Biolabs |
| recombinant Mouse CCL21/6Ckine Protein | R & D systems |
| recombinant Mouse CCL19/MIP-3 beta Protein | R & D systems |
| RIPA 10x | Cell Signaling Technology |
| RNAse inhibitor | Thermo Fisher Scientific |
| RPMI (Roswell Park Memorial Institute) 1640 Medium | Gibco |
| S.O.C. Medium | Thermo Fisher Scientific |
| sodium bicarbonate solution, 7.5% | Sigma |
| sodium chloride | Labochem International |
| SYBR Safe DNA Gel Stain | Thermo Fisher Scientific |
| T4 DNA Ligase Reaction Buffer 10x | New England Biolabs |
| T4 Ligase | New England Biolabs |

| Name | Company |
|------|---------|
| T4 Polynucleotide Kinase | New England Biolabs |
| TopVision Agarose | Thermo Fisher Scientific |
| Trans-Blot Turbo Transfer Pack | Bio-Rad Laboratories |
| tris-buffer-saline (TBS) 20x | Thermo Fisher Scientific |
| tris-glycine-SDS buffer (TGS) 10x | Bio-Rad Laboratories |
| Tris Pufferan | Carl Roth |
| Triton X-100 | Carl Roth |
| TRIzol Reagent | Thermo Fischer Scientific |
| trypsin-EDTA solution | Sigma-Aldrich |
| tween-20 | Sigma-Aldrich |
| UltraPure DNase/RNase-Free Distilled Water (=ddH2O) | Gibco |

## 2.1.6. Solutions

| Solution | Components |
|----------|-----------|
| 3% Formaldehyde | PBS<br>3% of 16% formaldehyde, methanol free |
| R10 medium | RPMI 1640 Medium<br>10% FBS,<br>2 mM L-Glutamine,<br>100 U/mL Penicillin,<br>100 $\mu$g/mL Streptomycin,<br>50 $\mu$M ß-ME |
| FACS Buffer | PBS<br>2 mM EDTA<br>2% FBS |

| Solution | Components |
|---|---|
| HEK T293 cell medium | DMEM Medium<br>10% FBS,<br>100 U/mL Penicillin,<br>100 μg/mL Streptomycin, |
| Hoxb8 medium | R10 medium<br>5% Flt-3 Ligand<br>1 μM estradiol |
| loading buffer | 4x Laemmli Sample Buffer<br>10% β-ME |
| PhosStop 10x | 1 tablet PhosStop<br>1 ml ddH2O |
| Proteinase-Inhibitor 25x | 1 tablet c0mplete protease inhibitor<br>2 mL ddH2O |
| Tris-Acetate-EDTA-Buffer (TAE) 50x | 40 mM Tris Pufferan<br>20 mM acetic acid<br>1mM EDTA<br>ddH2O |
| TBS-Tween (TBS-T) | 1x TBS<br>1% Tween-20 |
| TESCA Buffer | 50 mM TES<br>0.36 mM Calcium chloride, pH 7.4<br>ddH2O |
| Triton X-100 0.2% | 0.2% Triton X-100<br>PBS |

### 2.1.7. Antibodies

Antibodies for flow cytometry

| Target | Fluorochrome | Clone | Dilution | Company |
|---|---|---|---|---|
| CCL5 | PE | 2E9/CCL5 | 1:500 | Biolegend |
| CD103 | AlexaFluor488 | 2 E 7 | 1:500 | Biolegend |
| CD11b | PE | M1/70 | 1:500 | Biolegend |
| CD11b | APC | M1/70 | 1:500 | Biolegend |
| CD11c | APC | N418 | 1:500 | Invitrogen |
| CD11c | BV605 | N418 | 1:500 | Biolegend |
| CD11c | BV711 | N418 | 1:500 | Biolegend |
| CD115 | AlexaFluor488 | AFS98 | 1:500 | Invitrogen |
| CD135 (FLT3) | PE | A2F10 | 1:500 | Invitrogen |
| CD19 | APC-Cy7 | 6D5 | 1:500 | Biolegend |
| CD19 | Pacific Blue | 6D5 | 1:500 | Biolegend |
| CD197 (CCR7) | PE | 4B12 | 1:500 | Invitrogen |
| CD207 | APC | 4C7 | 1:500 | Biolegend |
| CD25 | PE | PC61 | 1:500 | Biolegend |
| CD3$\varepsilon$ | APC-Cy7 | 17 A2 | 1:500 | Biolegend |
| CD3$\varepsilon$ | PE-Cy7 | 17 A2 | 1:500 | Biolegend |
| CD4 | Pacific Blue | RM4-5 | 1:500 | Invitrogen |
| CD40 | PE/Dazzle 594 | 2 23 | 1:500 | Biolegend |
| CD44 | PE-Cy7 | IM7 | 1:500 | Biolegend |
| CD45 | BV421 | 30-F11 | 1:500 | Biolegend |
| CD45R7B220 | AlexaFluor700 | RA3-6B2 | 1:500 | Biolegend |
| CD49b | APC-Cy7 | DX5 | 1:500 | Biolegend |
| CD64 | PE-Cy7 | X54-5/7.1 | 1:500 | Biolegend |

| Target | Fluorochrome | Clone | Dilution | Company |
|---|---|---|---|---|
| CD69 | APC | H1.2F3 | 1:500 | Biolegend |
| CD70 | APC | FR70 | 1:500 | Biolegend |
| CD8α | PE | 53-6.7 | 1:500 | Biolegend |
| CD8α | FITC | 5H10-1 | 1:500 | Biolegend |
| CD80 | PE-Cy7 | 16-10A1 | 1:500 | Biolegend |
| CD86 | PE | GL1 | 1:500 | Invitrogen |
| F4/80 | BV605 | BM8 | 1:500 | Biolegend |
| F4/80 | APC-Cy7 | BM8 | 1:500 | Biolegend |
| Fc block cd16/cd32 | | | 5 mg/mL | eBioscience |
| phospho-histone H3 (pH3) | AlexaFluor647 | 11D8 | 1:500 | Biolegend |
| IL-6 | PE | MP5-20F3 | 1:500 | Biolegend |
| Ki67 | BV421 | 16A8 | 1:500 | Biolegend |
| Ly-6C | PE-Cy7 | HK1.4 | 1:500 | Biolegend |
| Ly-6G | APC-Cy7 | 1A8 | 1:500 | Biolegend |
| MHCII (I-A/I-E) | APC-Cy7 | M5/114.15.2 | 1:1000 | Biolegend |
| MHCII (I-A/I-E) | efluor 450 | M5/114.15.2 | 1:1000 | Invitrogen |
| MHCII (I-A/I-E) | PE/Dazzle 594 | M5/114.15.2 | 1:1000 | Biolegend |
| MHCII (I-A/I-E) | PerCp5.5 | M5/114.15.2 | 1:1000 | Biolegend |
| TER-119 | APC-Cy7 | TER-119 | 1:500 | Biolegend |

Antibodies for Immunoblotting

| Target | Species | Clone | Dilution | Company |
|--------|---------|-------|----------|---------|
| Plk2 | rabbit | polyclonal | 1:500 in 5% Milk, TBS-T | Abcam (ab71311) |

Antibodies for immunofluorescence staining

| Target | Species | Dilution | Company |
|--------|---------|----------|---------|
| α-tubulin | Rat | 1:600 | Invitrogen |
| y-tubulin | mouse | 1:600 | Sigma Aldrich |
| y-tubulin | rabbit | 1:600 | Abcam |
| acetylated (ac) tubulin | mouse | 1:600 | Sigma Aldrich |
| CEP110 | rabbit | 1:100 | Proteintech |
| CEP135 | rabbit | 1:300 | Abcam |
| CEP250 | rabbit | 1:300 | Proteintech |
| CEP97 | rabbit | 1:300 | Proteintech |
| CEP192 | rabbit | 1:300 | Proteintech |
| CETN1 | rabbit | 1:600 | Proteintech |
| pericentrin | rabbit | 1:600 | Abcam |
| phospho-histone H3 (Ser10) | rabbit | 1:600 | Cell Signaling |

Secondary Antibodies

| Target | Conjugate | Species | Dilution | Company |
|--------|-----------|---------|----------|---------|
| rabbit IgG | Horse-radish peroxidase (HRP) | goat | 1:10000 in 5% Milk, TBS-T | Bio-Rad Laboratories |
| rabbit IgG (H+L) | AlexaFluor488 | goat | 1:400 in 3% BSA, PBS | Jackson Immuno Research |
| rabbit IgG (H+L) | Cy3 | goat | 1:400 in 3% BSA, PBS | Jackson Immuno Research |
| rabbit IgG (H+L) | AlexaFluor647 | donkey | 1:400 in 3% BSA, PBS | Jackson Immuno Research |
| rat IgG (H+L) | AlexaFluor488 | donkey | 1:400 in 3% BSA, PBS | Jackson Immuno Research |
| rat IgG (H+L) | Cy3 | donkey | 1:400 in 3% BSA, PBS | Jackson Immuno Research |
| rat IgG (H+L) | AlexaFluor647 | donkey | 1:400 in 3% BSA, PBS | Jackson Immuno Research |
| mouse IgG (H+L) | AlexaFluor488 | donkey | 1:400 in 3% BSA, PBS | Jackson Immuno Research |
| mouse IgG (H+L) | Cy3 | donkey | 1:400 in 3% BSA, PBS | Jackson Immuno Research |
| mouse IgG (H+L) | AlexaFluor647 | donkey | 1:400 in 3% BSA, PBS | Jackson Immuno Research |

Additional dyes

| Target | Dilution | Company |
|--------|----------|---------|
| DRAQ7 DNA Dye | 1:1000 | Biolegend |
| Lysotracker Deep Red | 1:1000 | Molecular Probes |
| Propidium Iodide (PI) 1.0 mg/mL Solution in Water | 1:10 | Invitrogen |

| Target | Dilution | Company |
|---|---|---|
| Vybrant Dye Cycle Violet Stain | 1:100 | Invitrogen |

### 2.1.8. Plastic ware and consumables

| Item | Model | Company |
|---|---|---|
| Cell culture dishes | 6/24/48 well dishes | Greiner Bio-One International |
| cell strainer | EASYstrainer 70µm EASYstrainer 40 µm | Greiner Bio-One International Greiner Bio-One International |
| Costar transwell | 24 well plate, 3-µm pore size | fisher scientific |
| cover glasses | 10mm | VWR |
| filter tips | 10/200/1000 µL | Sarstedt |
| glass pasteur pipettes | | Brand |
| microscope slides | 76x26x1mm | Marienfeld |
| needles | Sterican | Braun Melsungen |
| PCR (polymerase chain reaction) tubes | 200 µL Thin Wall Tubes | Axygen |
| petri dishes | 10 cm (adhesive plastic) 10 cm (non-adhesive plastic) | Greiner Bio-One International Greiner Bio-One International |
| plastic tips | 10/200/1000 µL | Carl Roth |
| reaction tubes | 0.5/1/2 mL | Starlab |
| serological pipettes: | Cellstar: 5, 10, 25mL | Greiner Bio-One International |

| Item | Model | Company |
|---|---|---|
| syringes | Injekt 2/5/10 mL | Braun Melsungen |
| syringe filters | 0.45 µm | Carl Roth |
| tubes for flow cytometry | 5 mL | Sarstedt |
| tubes | 15/50 mL | Greiner Bio-One International |

## 2.1.9. Laboratory equipment

| Device | Model | Company |
|---|---|---|
| aspiration system | VHC$^{pro}$ | Vacuubrand |
| autoclave | DX-150 | Systec |
| blot transfer system | Trans-Blot Turbo Transfer System | Bio-Rad Laboratories |
| $CO_2$ incubator | Model C150 CB 210 E3 | Binder |
| centrifuges | 8510R 5415R 5424R | Eppendorf Eppendorf Eppendorf |
| counting chamber | Neubauer improved counting chamber | Marienfeld |
| electrophoresis chamber | Mini PROTEAN Tetra System | Bio-Rad Laboratories |
| electrophoresis chambers (SDS-PAGE) | Mini Trans-Blot Cell | Bio-Rad Laboratories |
| flow Cytometers | BD FACS Aria BD LSR II | BD Biosciences BD Biosciences |
| gel documentation device | ChemiDoc MP Imaging System | Bio-Rad Laboratories |
| heating block | ThermoMixer C | Eppendorf |

| Device | Model | Company |
|---|---|---|
| hotplate | HSC Ceramic Hotplate Stirrer | VELP Scientifica |
| incubator and shaker | Innova 44 | New Brunswick Scientific |
| laminar flow hood | HeraSafe KS | Thermo Scientific |
| microscope, laser scanning | LSM 880 | Carl Zeiss Microscopy |
| microscope, inverted light | Eclipse TS100-F | Nikon |
| pH meter | MP220 | Mettler Teledo |
| pipettes | Pipette boy accu-jet pro Research plus | Brand Eppendorf |
| plate reader | Infinite M200 | Tecan |
| rotator | Revolver Adjustable Lab Rotator | Labnet International |
| power supplies | PowerPac Basic Power Supply | Bio-Rad Laboratories |
| rocker | WS-10 | Edmund Bühler |
| scales | AG285(micro scale) JB2002-G | Mettler Toledo Mettler Toledo |
| shaker | WS-10 | Edmund Bühler |
| spectrophotometer | NanoDrop 2000 | Thermo Scientific |
| thermocyclers | C1000 Touch Thermal Cycler CFX96 Touch Real-Time PCR Detection System | Bio-Rad Laboratories Bio-Rad Laboratories |
| vacuum pump | AC02 | HLC BioTech |
| vortex mixer | UNIMAG ZX3 | VELP scientica |
| waterbath | | VWR |

### 2.1.10. Software

| Software | Company |
|---|---|
| ApE A plasmid Editor V3.0.5 | APE software GmbH |
| CFX Manager 3.1 | Bio-Rad Laboratories |
| FACS Diva Software | BD Bioscience |
| Fiji 1.53c | Schindelin, J. *et al.*[265] |
| FlowJo X 10.0.7r2 | BD Biosciences |
| GraphPad Prism Version 7.05 | GraphPad Software |
| ImageLab | Bio-Rad Laboratories |
| ND-1000 V3.5.2 | NanoDrop Technologies |
| ZEN 2.3 SPI | Carl Zeiss Microscopy |

## 2.2. Methods

### 2.2.1. Animal and cell based experimental techniques

#### 2.2.1.1. Mice

All mice used in this study were maintained at the institutional animal facility in accordance with the German law for animal experimentation. They were bred on a C57BL/6JRcc background. Centrin-2 (CETN2)-GFP (green fluorescent protein) mice were purchased from Jackson Laboratory [263]. OT-II mice, bearing an ovalbumin-peptide $_{(323-339)}$ specific TCR were a generous gift from Prof. Sven Burgdorf [264]. Mice lacking the *CCR4* gene (*CCR4$^{-/-}$*) were kindly provided by Prof. Irmgard Förster [262].

#### 2.2.1.2. Cell Isolation from primary organs

##### 2.2.1.2.1. Dermal DCs isolation from skin explants

For the isolation of dermal DCs, ears from 8-12 week-old wildtype (WT) or CETN2-GFP expressing mice were cut off and splitted with forceps into dorsal and ventral sheets. Ear sheets were transferred upside down into a 48-well plate containing 500 µL of full media (R10 medium) (RPMI 1640 Medium, 10% FBS, 2 mM L-Glutamine, 100 U/mL Penicillin, 100 µg/mL Streptomycin, 50 µM ß-mercaptoethanol (ß-ME)) supplemented with 25 µg/mL CCL19. Each day 500 µL of R10 medium was added until emigrated dermal DCs in suspension were harvested from the culture medium on day 3. Cells were further analyzed concerning their cell surface receptor expression as well as centrosome numbers and proliferation capacity.

##### 2.2.1.2.2. DC isolation from spleen and LNs

For the isolation of cDC1 and cDC2 DCs, spleen and mesenteric-, axillary-, brachial- and inguinal LNs of 8-12 week-old CETN2-GFP expressing mice were dissected and cut into small pieces. Cell pieces from spleen and LNs of one mice were transferred into a 12-well plate containing 2 mL of digestion buffer (Hanks' Balanced salt solution (HBSS) with Ca$^{2+}$, Mg$^+$; 0.1 mg/mL collagenase type IV and 50 µg/mL DNase I). Afterwards, the sell suspension was homogenized by forcing the tissue pieces through a 19 G needle and filtering through 70 µm strainer. Digestion was stopped by adding 15 mL of FACS buffer (phosphate buffered saline (PBS), 2% FBS, 2 mM EDTA). Erythrocyte lysis was performed using 1 mL ACK Lyse for 5 minutes, reaction was stopped with 15 mL FACS Buffer. Cell suspension was enriched for DCs by using EasySep Mouse Pan-DC enrichment kit according to the manufacturer's protocol. Afterwards, DCs subpopulations were separated using fluorescence-activated cell sorting (FACS) (cDC1: MHCII$^+$/CD11c$^+$/CD8$^+$ and cDC2: MHCII$^+$/CD11c$^+$/CD11b$^+$), were Ethynyl-2'-deoxyuridine (EdU) treated (see 2.2.1.4.2) and immobilized for microscopy to determine centrosome numbers and proliferation status.

### 2.2.1.2.3. Splenocyte and naïve CD 4⁺ T cell isolation

For the isolation of splenocytes and naïve CD4⁺ T cells, spleen and mesenteric-, axillary-, brachial- and inguinal LNs of 8-12 week-old OT-II or CCR4 $^{-/-}$ mice were dissected and filtered through 70 μm and 40 μm strainer. Erythrocyte lysis was performed using 1 mL ACK Lyse for 5 minutes. Reaction was stopped with 15 mL FACS Buffer. For naïve CD4⁺ T cell isolation EasySep Mouse Naïve CD4⁺ T cell Isolation Kit was used according to the manufacturer's protocol. Purity was assessed via FACS analysis and staining against CD3$\varepsilon$ and CD4. Splenocytes and naïve CD4⁺ T cells were used for further experiments.

### 2.2.1.3. Cell culture

### 2.2.1.3.1. Bone marrow-derived dendritic cell generation

Cultures were started from freshly isolated bone marrow of femurs and tibias from 8-12-week-old mice (WT, CETN2-GFP). Therefore, the bones were flushed with PBS and $2x10^6$ cells were seeded in 10 mL R10 medium containing 10% Granulocyte-Monocyte Colony Stimulating Factor (GM-CSF, supernatant from hybridoma culture). Cells were fed on day 3 and 6 with 10 mL R10 medium supplemented with 20% GM-CSF. Before adding the new medium on day 6, 10 mL from the cell culture were carefully removed and discarded. For maturation, cells were harvested and newly seeded in 20 mL R10 containing 20% GM-CSF and 200 ng/ml lipopolysaccharide (LPS) from *E. coli* 0127:B8 was added and stimulated overnight. Immature (im) cells were used on day 6 to 9 and mature (m) DCs (stimulated with LPS) on day 8 and 9.

### 2.2.1.3.2. Cell line maintenance

Jurkat E6.1 human acute leukemia T cells are suspension cells, which were cultured in R10 medium and split every 2 days.

HEK293 T cells were maintained in HEK T293 cell medium (Dulbecco's Modified Eagle Medium (DMEM) supplemented with 10% FCS, 100 U/mL Penicillin, 100 μg/mL Streptomycin). Cells were split every 2-3 days. Therefore, the adherent cells were washed with PBS once, detached from plates by adding 1 mL 1x trypsin-EDTA-solution for 5 minutes at 37°C, centrifuged at 300 rpm and seeded with new medium.

CETN2-GFP expressing Hoxb8 cells were maintained in Hoxb8 medium (R10 medium, 5% Flt-3 Ligand and 1 μM estradiol) and split every 2 days.

### 2.2.1.3.3. CRISPR/Cas9 based *Polo like kinase 2* knock-out generation

To generate *Plk2* knockout (KO) in DCs, a hematopoietic progenitor cell line expressing CETN2-GFP (CETN2-GFP expressing Hoxb8 cells) was used. Stephanie Ebbinghaus kindly provided this cell line. In brief, an estrogen-regulated form of *Hoxb8* is retroviral delivered into bone marrow of 8-12-week-old CETN2-GFP expressing mice [266]. Cells were cultured in Hoxb8 medium for 10 days and frozen in liquid nitrogen or differentiated into DCs (see 2.2.1.3.4.).

These cells were then used to generate *Plk2*^{-/-} via lentiviral transfection. For lentivirus production HEK T293 cells were used. Hence, $6\times10^6$ HEKT293 cells were plated in 100 mm petri dish, on the next day medium was replaced by 5 mL of Opti-MEM and transfection solution was prepared. Therefore, 5.4 $\mu$g of the cloned plasmid (see 2.2.2.1.), CRISPRv2 containing single guide RNA (sgRNA) for gene of interest, were co-transfected with 2.7 $\mu$g envelope plasmid pCMV-VSV-G and 4 $\mu$g packaging plasmid were added to 500 $\mu$L Opti-MEM. In a separate tube 500 $\mu$L Opti-MEM was supplemented with 30 $\mu$L Lipofectamine 2000 Transfection reagent. After 5 minutes of incubation, both solutions were combined and further incubated for 20 minutes. Thereafter, the transfection mixture was added dropwise to the cells in culture and incubated for 6 hours. Subsequently, medium was removed and replaced by 10 mL culture medium; this step was repeated the next morning. After 68 hours of transfection, the lentivirus-containing supernatant was harvested, centrifuged, filtered (0.45 $\mu$m syringe filter) and frozen in liquid nitrogen.

Next, lentivirus spin infection of CETN2-GFP expressing Hoxb8 cells was performed. Accordingly, $3\times10^5$ cells in 1 mL Hoxb8 medium were seeded into a 12-well plate and 500 $\mu$L of lentivirus dilution (1:1, 1:10 or 1:100) added together with 10 mg/mL polybrene beads. After 60 minutes centrifugation at 1500 g, 1.5 mL Hoxb8 medium was added. On the next day, 2 mL medium was carefully aspirated and replaced with 1 mL fresh medium. 72 hours post infection, medium was removed, cells were washed and 2mL new medium was added. Cells grew and were further expanded under the selection of 3 $\mu$g/mL puromycin. KO generation was confirmed using immunoblotting (see 2.2.3.3.) and precursor cells were differentiated into DCs (see 2.2.1.3.4.)

### 2.2.1.3.4. Hoxb8 derived dendritic cell generation

Hoxb8 derived DCs were generated with the same procedure as BMDCs but instead of $2\times10^6$ bone marrow cells per dish, $0.2\times10^6$ Hoxb8 progenitor cells were used, which were washed once with R10 medium to rinse out estradiol prior to cell seeding.

### 2.2.1.4.   Cell based assays

#### 2.2.1.4.1.   Centrinone treatment of BMDCs

BMDCs were treated with Centrinone during differing time points of differentiation. Therefore, cells were treated with dimethylsulfoxid (DMSO) (control) or Centrinone (250 or 500 nM). Either the medium was supplement with DMSO or Centrinone directly from day 0 on and then each time when the medium was added/replaced or only during maturation when LPS was given.

#### 2.2.1.4.2.   EdU incorporation assay

BMDCs, dermal DCs or sorted cDC1s/cDC2s were incubated in 10 $\mu$M EdU in R10 medium for 60 minutes. Cells were immobilized and EdU was detected using the Click-iT EdU Imaging Kit, according to the manufacturer's protocol. EdU positive cells were assessed by using laser scanning microscopy.

#### 2.2.1.4.3.   Flow cytometry

For cell surface staining of the cells, 1-2x10$^6$ cells were treated with 5 mg/mL anti-CD16/CD32 antibody (Fc block), stained with conjugated monoclonal antibodies diluted 1:500 (if not stated otherwise) and live/dead staining (DRQA7 1:1000) in 100 µL FACS buffer (1x PBS, 2% FBS, 2 mM EDTA). Samples were incubated for 30 minutes at 4 °C.

For intracellular cytokine staining, BD Cytofix/Cytoperm Plus Fixation/Permeabilization Kit was used. Therefore, 1x10$^5$ cells were permeabilized with 100 µL fixation/permeabilization solution for 30 minutes 4°C, washed and stained with conjugated monoclonal antibodies diluted 1:500 (if not stated otherwise) for 30 minutes at 4 °C in 100 µL washing buffer containing 5 mg/ml Fc block.

For intranuclear staining of phospho Histone H3 (pH3) and Ki67, eBioscience Foxp3/Transcription Factor Staining Buffer Set was used. For fixation/permeabilization 100 µL of Foxp3 fixation/permeabilization concentrate were mixed with 300 µL of Foxp3 fixation/permeabilization diluent. Cells were Incubated for 30 minutes at 4°C, washed with 1 mL of 1x permeabilization buffer and conjugated monoclonal antibodies diluted 1:500 (if not stated otherwise) for intracellular and cell surface staining were added in 100 µL 1x permeabilization buffer containing 5 mg/mL Fc block. Cells were incubated for 30 minutes at 4 °C.

For DNA content staining either PI or Vybrant Violet cell cycle dye was used. For the first one, cells were fixed for 30 minutes at 4 °C with 70% ethanol and washed with PBS. Thereafter, 190 µL H$_2$O containing 0,25 µL of 20mg/ml RNase and 10 µL of 1mg/mL PI and conjugated

monoclonal antibodies diluted 1:500 (if not stated otherwise) for cell surface staining were added to 1-2x10$^6$ cells. For the second DNA dye, live cells were used. Here a 1:100 dilution of Vybrant Violet cell cycle dye, conjugated monoclonal antibodies diluted 1:500 (if not stated otherwise) for cell surface staining and 5 mg/mL Fc block were used to stain 4x10$^6$ cells in 1 mL medium without phenolred (RPMI 1640 supplemented with 2% FBS) for 30 minutes at 37 °C.

Unstained samples, single-color stained samples, fluorescent minus one-control samples and BD Comp Beads were used for compensation set up, and samples were either analyzed using flow cytometry analyser LSRII or sorted with flow cytometry sorter ARIAIII. Data analysis was carried out using FlowJo X 10.0.7r2.

### 2.2.1.4.4. Sorting of DC subpopulations for DNA and centrosome content

Mature CETN2-GFP expressing BMDCs were harvested, counted and stained for live cells, DNA content and cell-surface markers as described above. Samples were sorted for mature BMDCs (MHCII$^+$/CD11c$^+$), diploid (2N) DNA content to get rid of tetraploid cells (4N) and their CETN2-GFP signal distribution. Diploid (2N) cells were gated into CETN2-GFP$^{low}$ (2N2C, diploid cells with 2 centrioles) and CETN2-GFP$^{high}$ (2NCA, diploid cells with centrosome amplification) expressing cells to separate them based on their centrosomal content. For determining the efficiency of separation, part of the sorted DC subpopulations were immobilized, fixed and centrosome numbers were assessed by confocal microscopy. The ratio of cells with centrosome amplification (CA) in 2NCA and 2N2C was determined to evaluate the efficiency of enrichment.

### 2.2.1.4.5. ImageStream assay

For ImageStream analysis, flow cytometry cell surface staining of emigrated dermal DCs was performed. Cells were adjusted to a concentration of 1x10$^6$ cells in 50 µL in PBS with 2% FBS in a 1.5 mL siliconized microcentrifuge tube. For compensation, single colour samples were included. The highest magnification of 60x was used to acquire images.

### 2.2.1.4.6. Immune synapse formation

To determine the MT nucleation capacity in BMDCs during IS formation, cells need to be very flat. To achieve this, special chambers were built containing a block of agarose. Hence, 0.2g ultra pure agarose was diluted in 5 mL nuclease-free and mixed with 5 mL R10 medium and 10 mL 2x HBSS and 0.4% sodium bicarbonate. 500 µL of agarose-mix was casted into custom-made 6 mm petri dish containing a 1 cm plastic ring glued with Paraffin wax into the middle of the dish. Within the ring, a small coverslip was placed. After polymerization, a 2 mm

hole was punched into the agarose pad and the outer part of the dish was filled with 5 mL ddH2O. After an incubation time of 45-60 minutes at 37 ˚C, 5% CO2 agarose was equilibrated. Then, 0.5 µL R10 containing $5\times10^4$ mature CETN2-GFP expressing BMDCs pretreated with 10 µg/mL ovalbumin for 2 hours were injected under the block of agarose, followed by 0.5 µL R10 containing $2.5\times10^5$ OT-II naïve $CD4^+$ T cells. The co-culture was incubated for 2 hours at 3 7˚C, 5% $CO_2$ to allow IS formation. Thereafter, cells were fixed with 4% para-formaldehyde (PFA) solution that was added on top of the agarose block and incubated overnight at 4˚C. Agarose was removed carefully using a forceps, coverslip with cells were washed three times with 1x PBS before immunostaining against α-tubulin was performed (see 2.2.3.1.).

To determine intercentrosomal distance and centrosomal location within BMDCs, $5\times10^4$ CETN2-GFP expressing BMDCS were seeded in 100 µL R10 medium into 96-well U-bottom plates and kept at 37 °C, 5% $CO_2$. 30 minutes post seeding, 10 µL/mL was added in 100 µL R10 medium and incubated for 2 hours at 37 °C, 5% $CO_2$. After antigen loading, supernatants were discarded and $2.5\times10^5$ OT-II naïve $CD4^+$ T cells were added. The co-culture was harvested after 10 minutes or 2 hours and immobilized on coverslips (see 2.2.3.1), which were further analyzed via confocal microscopy.

### 2.2.1.4.7.  Mixed lymphocyte reactions and IL-2 ELISA

$10^4$ cells from sorted DC subpopulations (2N2C, 2NCA) were seeded in 100 µL R10 medium into 96-well U-bottom plates and kept at 37 °C, 5% $CO_2$. 30 minutes post seeding, ovalbumin (1000 µg/mL; 500 µg/mL; 100 µg/mL and 10 µg/mL) or ovalbumin-peptide ($ova_{323-339}$ specific for $CD4^+$ T cell responses: 1 µg/mL; 0.1 µg/mL and 0.01 µg/mL) was added in 100 µL R10 medium and incubated for 2 hours at 37°C, 5% $CO_2$. For each condition, triplicates were prepared. After antigen loading, supernatants were discarded and $5\times10^4$ OT-II splenocytes were added in 200 µL R10 medium. 24 hours after co-culture, supernatants were harvested and IL-2 levels were determined using enzyme-linked immunosorbent assay (ELISA). Therefore, the Quantakine ELISA Kit was used according to the manufacturer's instructions. Colorimetric measurements were carried out on Infinite M200 spectrophotometer.

### 2.2.1.4.8.  T cell proliferation

$10^4$ cells from sorted DC subpopulations (2N2C, 2NCA) were seeded in 100 µL R10 medium into 96-well U-bottom plates and kept at 37 °C, 5% $CO_2$. 30 minutes post seeding, ovalbumin (1000 µg/mL 500 µg/mL; 100 µg/mL and 10 µg/mL) or ovalbumin-peptide ($ova_{323-339}$ specific for $CD4^+$ T cell responses: 1 µg/mL; 0.1 µg/mL and 0.01 µg/mL) was added in 100 µL R10 medium and incubated for 2 hours at 37 °C, 5% $CO_2$. For each condition, triplicates were prepared. After antigen loading, supernatants were discarded and $5\times10^4$ CFSE (fluorescent dye carboxyfluorescein succinimidyl ester) labelled OT-II splenocytes were added in 200 µL

full medium. CFSE labeling was performed using $2x10^6$ cells/mL with a concentration of 0.5 µM Celltrace CFSE in PBS for 7 minutes at 37 °C. 62 hours after co-culture, samples were stained (splenocytes from OT-II mice: CD11c$^-$, CD19$^-$, live cells, CD3$\varepsilon^+$, CD4$^+$) and flow cytometry analysis was performed on an LSRII flow cytometer. Data analysis was carried out using FlowJo X 10.0.7r2.

### 2.2.1.4.9.    Lysosomal content in sorted BMDCs

$5x10^4$ cells from sorted DC subpopulations (2N2C, 2NCA) were seeded in 100 µL R10 medium into 96-well U-bottom plates and kept at 37 °C, 5% $CO_2$ 30 minutes post seeding, 100 µL R10 medium containing 1:1000 of Lysotracker was added. For each condition, triplicates were prepared. After 2 hours of incubation at 37 °C, 5% $CO_2$ cells were analyzed via a flow cytometry approach using LSRII flow cytometer. Data analysis was carried out using FlowJo X 10.0.7r2.

### 2.2.1.4.10.    Inhibition of protein transport

Cells were sorted into 2N2C and 2NCA populations as described above. $4x10^5$ cells of each population were treated for 4 hours with 1:2000 dilution of Monensin (GolgiStop) and 1:2000 dilution of Brefeldin A (GolgiPlug) in 1.5 mL R10 medium at 37 °C, 5% $CO_2$. Afterwards, intracellular cytokine staining was carried out and cells were analyzed using LSRII flow cytometer. Data analysis was carried out using FlowJo X 10.0.7r2.

### 2.2.1.4.11.    Transmigration-assay of CD4$^+$ T cells

$1x10^6$ WT or CCR4 KO naïve CD4$^+$ T cells were seeded into a 24-well plate containing 2 mL R10 and 25 µL of Dynabeads Mouse T-Activator CD3/CD28. After 3 days of activation, T cell activation was assessed by flow cytometry and staining against CD3$\varepsilon$, CD4 CD8, CD25, CD69 and CD44. After cell activation, cells were used for transmigration assays. $2x10^5$ cells in 250 µL R10 medium were loaded to the upper chamber of a transwell apparatus (Costar, 24 well plate, 3-µm pore size). The lower chamber was loaded with either 600 µL R10 medium, R10 medium supplemented with 200 nM CCL19 or supernatant of sorted 2N2C and 2NCA DC subpopulations. Cells were harvested from the lower chamber after 2 h of transmigration at 37 °C, 5% $CO_2$; flow cytometry cell surface staining for CD4 was performed and analyzed by flow cytometry on a LSRII flow cytometer using 50 µL of absolute counting beads. Data analysis was carried out using FlowJo X 10.0.7r2.

2N2C and 2NCA supernatant was collected 16 hours post sort from $1x10^6$ sorted DC subpopulations, which were seeded into a 6-well plate containing 3 mL R10 medium.

### 2.2.2. Molecular biology assays

#### 2.2.2.1. Molecular cloning of single guide RNA into lentiviral vector

For the generation of *Plk2$^{-/-}$* CETN2-GFP expressing Hoxb8 cells were lentiviral transfected. For the lentivirus generation the packaging plasmid, the envelope plasmid and the lentiCRISPRv2 plasmid containing the sgRNA for the gene of interest is needed. To generate the latter one, the following procedure was performed:

First, the CRISPRv2 plasmid was digested, therefore an approach containing 50 µL of volume was used. The solution contained 5 µL of the restriction enzyme BsmBI, 5 µL CutSmart 10 x Buffer, 5 µg lentiCRISPRv2 and ddH$_2$O. Digestion was performed for 90 minutes at 55 °C, followed by inactivation for 20 minutes at 80 °C. Afterwards, 6x loading dye was added, incubated for 10 min at 65 °C, loaded on 1% agarose gel (1% agarose, 1x TEA buffer, 1:10000 SYBR Safe) and run at 80 V for 60 minutes. A separation into a 2 kilo baispairs (kb) DNA piece and 11 kb DNA piece happened. The larger one was cut and purified using Monarch DNA Gel Extraction Kit. DNA concentration was measured using a spectrophotometer. 100 ng of the plasmid was used for dephosphorylation by FastAP (alkaline phosphatase) for 30 minutes at 37 °C. Reaction was stopped by heat inactivation for 15 minutes at 65 °C. Phosphorylated and annealed pair of oligo's (Plk2 sg1, Plk2 sg2 and scramble) were prepared for ligation. Therefore, a reaction volume of 10 µL was used, containing 100 µM of each oligo, 1 µL 10x T4 ligation buffer (containing ATP), 0.5 µL T4 polynucleotide kinase and ddH2O. Reaction was performed under the following conditions: 30 minutes at 37 °C, 95 °C 5 minutes and then ramp down to 25 °C at 5 °C/minutes and subsequently diluted 1:200 in ddH$_2$O.

Afterwards, ligation of digested and dephosphorylated CRISPRV2 plasmid with phosphorylated and annealed pair of oligo's was performed. 20 µL of reaction volume was used, containing 100 ng digested plasmid, 1 µL diluted oligo-duplex, 2 µL 10x T4 ligation buffer, 1 µL T4 ligase and ddH20.The reaction was incubated over night at 16 °C.

Oligonucleotide-duplex

**PLK2 sg1**  5´CACCGGATTATAGTCGACCCCACGA3'
          5´AAACTCGTGGGGTCGACTATAATCC3'

**PLK2 sg2**  5´CACCGGCTGGTAGGTGATAGTCCGC3'
          5´AAACGCTGGTAGGTGATAGTCCGCC3'

**Scramble**  5'CACCGGCCGTGGCGCATGGGTAGCA3'
          5'AAACTGCTACCCATGCGCCACGGCC3'

### 2.2.2.2.   Transformation of bacteria

In the next step, 20 µL of ligated plasmid were transformed into One Shot Stbl3 Chemically Competent *E. coli* cells. Therefore, cells were thawed on ice and carefully mixed with DNA. Sample was incubated on ice for 30 minutes, then a heat shock of 45 sec at 42 °C was performed and sample placed back on ice for 2 minutes. 250 µL of pre-warmed S.O.C medium was added and the sample was incubated for 1 hour at 37 °C with shaking of 350 rpm. Afterwards, the sample was spread on a pre-warmed selective agar plate (100 µg/mL ampicillin) After incubation at 37 °C overnight, single colonies were picked and incubated in 3 mL LB medium containing 100 µg/mL ampicillin and incubated at 37 °C over night. Plasmid purification was performed using Monarch Plasmid Miniprep Kit according to the manufacturer's protocol and samples were sequenced by Eurofins Genomics. After the results were verified by sequencing (successful cloning of sgRNA into lentiCRISPRv2 plasmid), the construct was used for lentiviral production in HEK T293 cells.

### 2.2.2.3.   Messenger RNA expression levels

For RNA quantification, $1 \times 10^6$ cells were harvested into 350 µL lysis buffer (RNeasy Lysis Buffer containing 1% ß-ME), RNA isolation was carried out using the RNeasy Mini Kit and RNA concentration was measured with a spectrophotometer. Gene expression was assed using the TaqMan RNA-to-CT 1-Step Kit with a reaction volume of 20 µL containing 250 ng RNA template and 1 µL of Taq Man Gene Expression Assay. Triplicates were performed. Samples were run on a CFX96 Real-Time System with the conditions listed below. Analysis of relative gene expression was carried out using the CFX Manager Software Version 3.1, which depicted the threshold cycle value (Ct) of the amplified sample. Data were normalized according to the expression of a housekeeping gene in DCs (TATA-binding protein (TBP)). Therefore, the ΔΔCt method was applied. Results were depicted as fold change, calculated as follows:

ΔCT= Ct target gene – Ct housekeeping gene
ΔΔCt = ΔCt condition – ΔCt control
fold change expression = $2^{-\Delta\Delta Ct}$

Thermal cycling conditions

| Stage | Temperature (°C) | Time (minutes) |
|---|---|---|
| **Holding** | 48 | 15 |
| **Holding** | 95 | 10 |
| **Cycling** | 95 | 0.2 |
|  | 60 | 1 |

### 2.2.3. Biochemical assays

#### 2.2.3.1. Immunofluorescence staining and confocal microscopy

Small volume (1-3 μL) of cells was transferred on coated (2 μL of 1:1 (v:v) mixed 100 μg/mL ICAM-1 and 25 μg/mL CCL21 for 10 minutes at room temperature) coverslips which were placed into 24-well plates. Coverslips were incubated for 5 minutes at 37°C and subsequently fixed with 3% PFA diluted in 1x PBS and incubated for 15 minutes at 4 °C. Thereafter, samples were washed 3x10 minutes with 1x PBS.

For immunofluorescence staining, cells were permeabilized with 250 μL 0.2% Triton X-100 in 1x PBS for 20 minutes and washed 3x 10 minutes with 1x PBS. Afterwards samples were blocked to prevent unspecific antibody binding by blocking with 250 μL of 1% BSA in PBS blocking solution for 60 minutes. When EdU incorporation was performed, EdU staining was carried out according to manufacturer's protocol and after washing for 3x 10minutes with 1x PBS, staining with primary antibodies followed. When EdU was not present, primary antibodies were directly added after blocking. Primary antibodies (see 2.1.8 for dilution) were diluted in blocking solution and incubated over night at 4°C. Then, the samples were washed 3x 10 minutes with 1x PBS and incubated with the secondary antibody, which was diluted 1:400 in blocking buffer. After 60 minutes of incubation, samples were washed 3x 10 minutes with 1x PBS. Samples were conserved upside down on microscopy slide containing one drop of Fluoromount-G Mounting Medium with DAPI and sealed with nail polish. Samples were either directly imaged on LSM 880 or stored at 4 °C.

Confocal microscopy was applied for quantification of centrosome numbers in T cells and DCs as well as MT number determination and MTOC behavior studies. Therefore, cells were immobilised as described above and in section 2.2.1.4.6. Thereafter, samples were recorded using the inverted confocal microscope LSM 800, equipped with an Airyscan module, a Plan-Apochromat 63×/1.4 oil DIC objective, 488, 561 and 633 laser lines and a photomultiplier tube. For all experiments, imaging software ZEN Black 2.3 SP1 was used, Z-stacks with 200 nm sections were acquired, and maximal projected. When analyzing MT filament numbers, airy mode was applied and deconvolution performed after samples were acquired. MT filaments and centrosome numbers were validated manually using α-tubulin or ac-tubulin/CENT2-GFP/CEP135 signals respectively. For the processing steps and image analysis Fiji 1.53c was used. For measuring intercentrosomal distances and MTOC position during IS formation, Fiji multi-point tool was used to determine the X and Y position of single centrioles in 2D maximal projections. Hereafter the distinct coordinates were used to calculate the intercentrosomal

distance (d) between the center of one centriole pair to the center of the most distant centriole pair, by applying the following formula: $d = \sqrt{\left(\frac{x_1+x_2}{2} - \frac{x_3+x_4}{2}\right)^2 + \left(\frac{y_1+y_2}{2} - \frac{y_3+y_4}{2}\right)^2}$. To determine the MTOC position within the DC, first the center of mass was appointed by applying the Fiji freehand selection tool, thereby generating X/Y coordinates of the center from the selection. Thereafter, the distance from the centrosome center (CC) to the center of mass was analyzed using the following formulas CC $= \left(\frac{x_1+x_2+\cdots+x_n}{n} \Big| \frac{y_1+y_2+\cdots+y_n}{n}\right)$; n=number of centrioles and $d =$ $\sqrt{\left(\frac{x_1+x_2}{2} - \frac{x_3+x_4}{2}\right)^2 + \left(\frac{y_1+y_2}{2} - \frac{y_3+y_4}{2}\right)^2}$. When analyzing intercentrosomal distances and MTOC position, associated T cell numbers were taken in to account. Samples were distinguished for interacting with one T cell or more than one T cell.

### 2.2.3.2. Cytokine array and ELISA

2N2C and 2NCA supernatant was collected 16 hours post sort from 1x10$^6$ sorted DC subpopulations, which were seeded into a 6-well plate containing 3 mL full medium. The supernatant was used to determine cytokine concentrations via ELISA (CCL17, CCL22, CCL5, IL-6, CXCL1) according to the manufacturer's protocol or 500 µL supernatant were used for secretome analysis with the mouse cytokine antibody array panel A according to the manufacturer's instructions. For ELISA read out colorimetric analysis by Infinite M200 was performed and for secretome analysis chemiluminescence was acquired using a ChemiDoc Imaging System. Data analysis was carried out with Image Lab 6.1 Software.

### 2.2.3.3. Protein extraction and immunoblotting

For the analysis of *Plk2* KO generation in CETN2-GFP expressing Hoxb8 cells, 0.3x10$^6$ Hoxb8 derived DCs (scramble, Plk2 sg1 or Plk2 sg2) were lysed in 20 µL RIPA buffer (30 µL 10x RIPA, 0.8 µL 25x proteinase-inhibitor, 2 µL PhosStop and 15.2 µL PBS). Cells were lysed on ice for 30 minutes, being vortexed every 10 minutes in-between. Lysates were centrifuged at 15000 rpm for 10 minutes at 4 °C, supernatant collected and stored at -20 °C for further usage.

Before samples were applied for protein separation by Sodium Dodecyl Sulfate PolyAcrylamide Gel Electrophoresis (SDS-PAGE), 4 µL of 4x Laemmli sample buffer containing 10% β-ME was added to 12 µL lysate and boiled for 5 minutes at 95 °C. Thereafter, samples were loaded on precast gradient gel (4-20% Mini-PROTEAN TGX Stain-Free Protein Gel) together with 2 µL MagicMarker XP Western Protein. Proteins were separated using tris-glycine-SDS buffer (TGS) as running buffer and a voltage of 80 V for the first 15 minutes and thereafter voltage of 100 V. Proteins were transferred via Trans-Blot Turbo™ Transfer System with 1.3 A and 25 V for 7 minutes to a 0.2 µm nitrocellulose membrane in a semi-dry manner.

Following, staining for 5 minutes with Ponceau S solution (0.2% (v/w) Ponceau S, 5% acetic acid and ddH2O) was performed to confirm blotting efficiency. Then, the membrane was de-stained by washing with tris-buffer-saline-Tween (TBS-T). Membrane was blocked by applying 5% milk powder in TBS-T (blocking buffer) for 60 minutes. Primary rabbit polyclonal antibody against Plk2 was diluted 1:500 in blocking buffer and added to the membrane. The membrane was incubated overnight. Followed by 3x 10 minutes washing with TBS-T, anti-rabbit IgG secondary antibody conjugated to HRP was added for 60 minutes with the dilution of 1:10000 in blocking buffer. After the final washing steps (3x 10 minutes with TBS-T), 300 µL detection solution were applied (Pierce ECL Plus Western Blotting Substrate). Chemiluminescence signals were detected using the ChemiDoc MP Imaging System.

### 2.2.4. Schematic illustration
Schematic illustration were created with BioRender.com.

### 2.2.5. Statistical analysis
For Statistical analysis, the Software GraphPad Prism Version 7.05 was used. First, samples were tested via D'Agostino-Pearson omnibus normality test to identify for Gaussian distribution. If Gaussian distribution was given two tailed, paired (for sorted DC populations 2N2C and 2NCA) or unpaired, Student's *t*-test was applied. When unequal variances were present in paired samples, Wilcoxon test was performed. If Gaussian distribution was not given, Mann-Whitney test was carried out. Gaussian distribution was assumed for small datasets (n < 8) without being tested. Graphs display mean values $\pm$ standard deviation (s.d.) (95% Confidence Interval) or in Box-Whiskers blots the maximum and minimum value, median and the interquartile range. Significance levels were divided into the following values: *, $P < 0.05$; **, $P < 0.01$; ***, $P < 0.001$ and ****, $P < 0.0001$. The statistic test, which was applied and P value that was determined for each experiment, is indicated in the figure legend.

# 3. Results

## 3.1. Dendritic cells contain extra centrosomes

### 3.1.1. Extra centrosomes in bone marrow-derived dendritic cells

Centrosome behaviour is well studied in T cells during IS formation. How the centrosome operates on the DC side is less understood [163]. To visualize the centrosome in DCs, WT and CETN2-GFP expressing BMDCs were generated, stimulated with (mature) or without (immature) the TLR4 agonist LPS [267] and immobilized for immunofluorescence staining. First, we stained for the main PCM component γ-tubulin, which is located in close proximity to the nucleus (Figure 3.1 a,b). In addition, we stained for various centriolar and PCM proteins like CEP250, CP110, CEP97, CEP192, CETN1 and pericentrin. Yet, none of them led to a clear signal in BMDCs (data not shown). To verify that our staining protocol is working well, we tested these antibodies on T cells and received good signal-to-noise results (Figure 3.2 a). As it was previously reported that centriolar MTs get acetylated [268,269] we co-stained T cells with an anti-acetylated tubulin (ac-tubulin) antibody. We obtained clear colocalization with other centriolar and PCM markers and were able to visualize individual centrioles (Figure 3.2 a). From here on, we used ac-tubulin as marker for centrioles also in BMDCs and received excellent outcomes (Figure 3.1 a,b). Furthermore, we started another attempt by modifying the staining protocol and as a consequence were able to obtain good quality images of the centriolar protein CEP135 (Figure 3.1 b). In addition, we used BMDCs, which were generated from CETN2-GFP expressing reporter mice. CETN2-GFP colocalized nicely with the other centrosomal proteins (Figure 3.1 b).

When analyzing centrosomal markers, we noticed that in some BMDCs surprisingly more than two centrioles (one centrosome) and sometimes even more than four centrioles (two centrosomes or more) were present. We quantified ac-tubulin/CETN2/CEP135-positive foci and observed similar centrosome numbers for all stainings applied (Figure 3.1 c-e). In 20-25% of mature cells, two centrosomes are present and a smaller fraction of 5-10% carry more than two centrosomes. In contrast, immature cells only showed a small fraction of around 5% with two or more centrosomes (Figure 3.1 c).
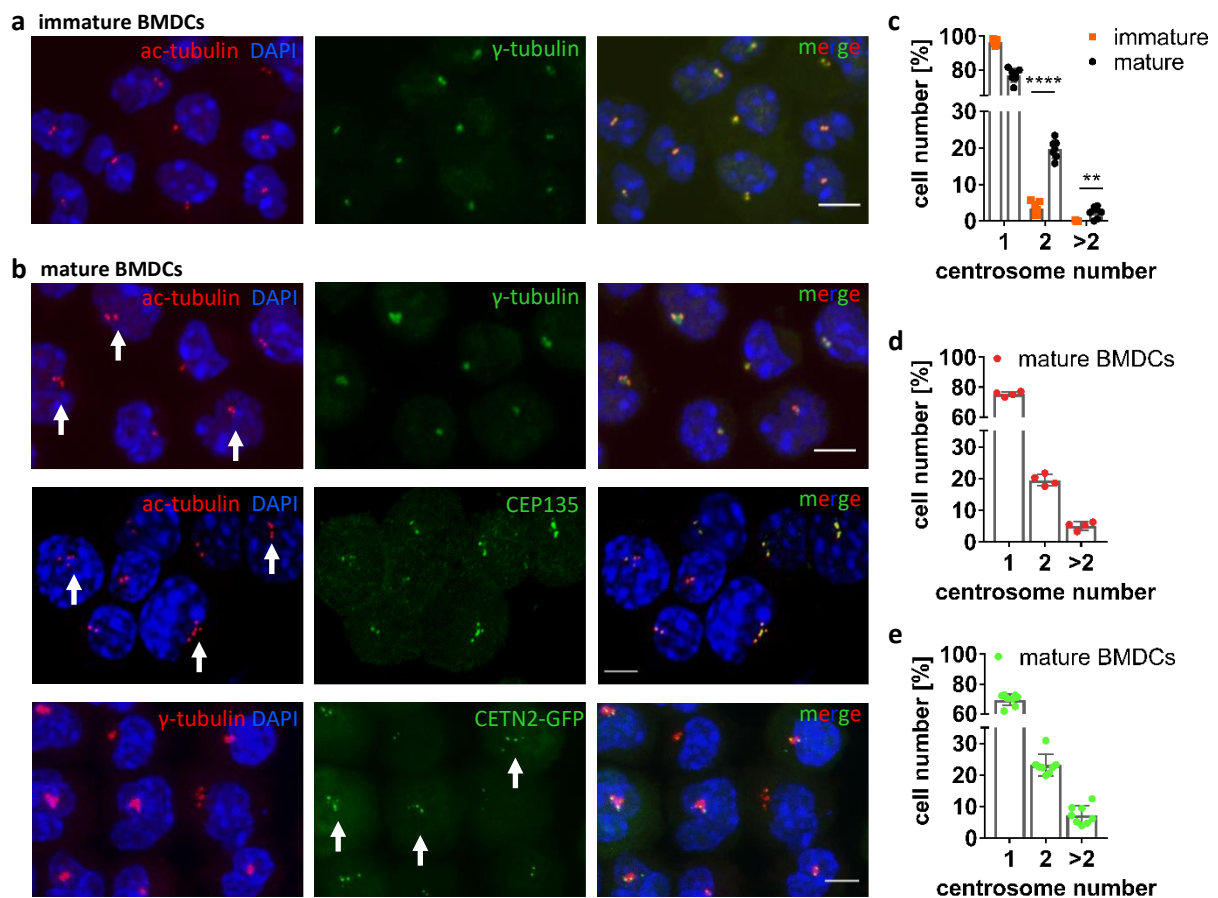
**Figure 3.1** Illustration and quantification of centrosomes in bone marrow-derived dendritic cells (BMDCs).

(**a**) Immunostaining of wildtype and CETN2-GFP immature and mature (**b**) BMDCs. Individual and merged channels of ac-tubulin (red), γ-tubulin (green, red), CEP135 (green) and CETN2-GFP (green). Nuclei were counterstained with DAPI (blue). ≥ 4 ac-tubulin/CETN2-GFP foci are highlighted by white arrows. Scale bar, 5 µm. (**c**) Quantification of centrosome numbers in immature and mature BMDCs according to ac-tubulin/γ-tubulin-positive foci. ****, $P < 0.0001$, **, $P = 0.002$ (two-tailed, unpaired Student's $t$-test). Graph displays mean values ± s.d. of 7 independent experiments. $N$ = 134/98/158/93/124/344/274 cells (immature) and $N$ = 141/203/158/127/128/200/175 cells (mature). (**d**) Enumeration of centrosome numbers in mature BMDCs corresponding to CEP135-positive foci. Graph shows mean values ± s.d. of 4 independent experiments with $N$ = 335/366/222/184 cells analyzed per experiment. (**e**) Quantification of centrosome numbers by CETN2-GFP/γ-tubulin-positive foci in mature CETN2-GFP expressing BMDCs. Graph shows mean values ± s.d. of 8 independent experiments with $N$ = 261/248/305/298/180/150/258/152 cells analyzed per experiment.
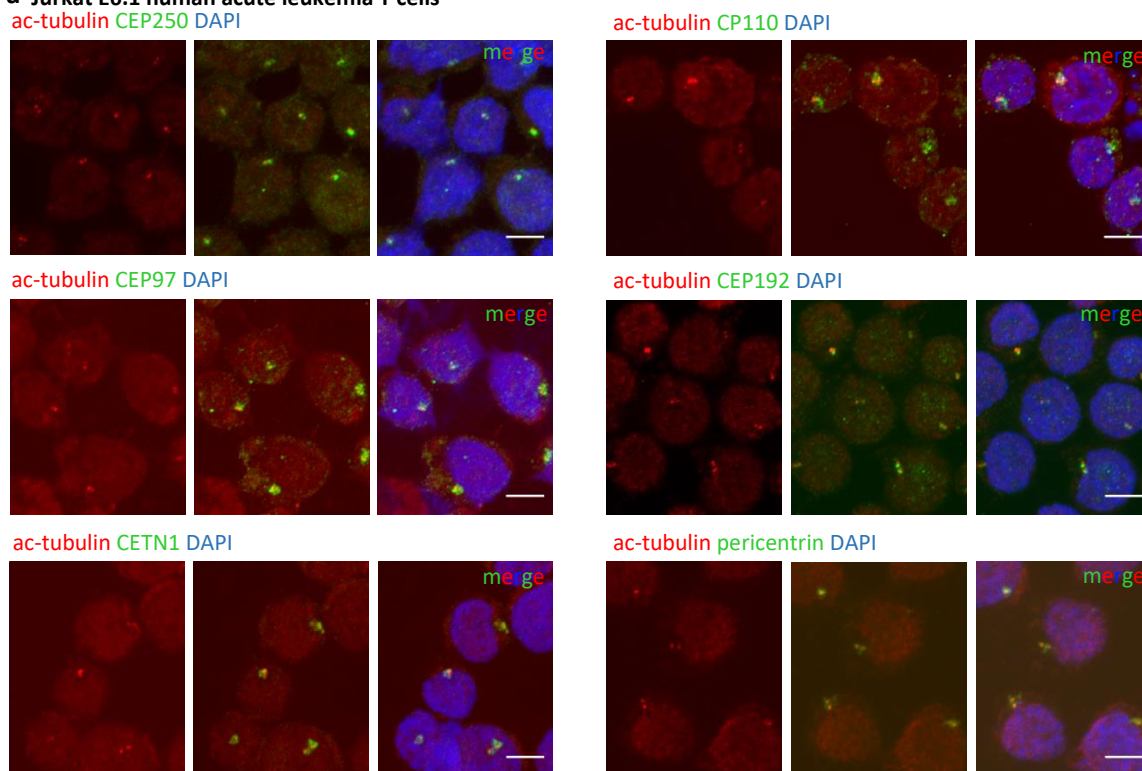
**Figure 3.2** Visualisation of centrosomes in T cells.

(**a**) Immunostaining of Jurkat E6.1 human acute leukemia T cells. Individual and merged channels of ac-tubulin (red), CEP250/CP110/CEP97/CEP192/CETN1/pericentrin (green). Nuclei were counterstained with DAPI (blue). Scale bar, 5 μm.

As the centrosome is duplicated in parallel to DNA in proliferating cells, we wondered whether cells that displayed increased centriole numbers are cycling cells. Therefore, EdU incorporation and pH3 as markers for S-phase and G2-M transition, respectively, were analyzed in immature and mature BMDCs (Figure 3.3 a,b). We observed that immature cells are cycling, as ~ 20% of the cells were EdU positive and ~ 15% pH3 positive, whereas mature cells did not proliferate, as only ~ 1% of the cells were EdU or pH3 positive. Therefore, we conclude that the cells with two or more centrosomes in immature cells represent proliferating cells while mature cells do not. As mature cells are not cycling, the phenomenon of elevated centrosome numbers cannot be explained.

We next sought to understand whether mature cells have exited the cell cycle. Therefore, we analyzed levels of Ki67 in BMDCs (Fig. 3.3 c). Nearly all cells were Ki67-positive, highlighting that the cells did not enter G0. As the cells are not in G0, we wondered if the profile of the DNA content could reveal additional information on the origin of extra centrosomes. Therefore, we visualised the DNA content (Figure 3.3 d) by flow cytometry. The profiles of mature BMDCs reveals two separated peaks: a major peak around 50 K, representing diploid cells (2N) and

a smaller fraction with twice the size at 100 K, representing cells with a tetraploid DNA content (4N). The quantification of the second peak is displayed in Figure 3.3 d and revealed that ~ 17% of cells are tetraploid. This cell subset together with the one displaying amplified centrosomes is of highest interest, as both together suggest alterations during proliferation. We conclude that *in vitro* cultured mature BMDCs show amplified centrosomes in ~ 30% of the cells and wonder if this phenomenon can also be observed in *in vivo* cells.
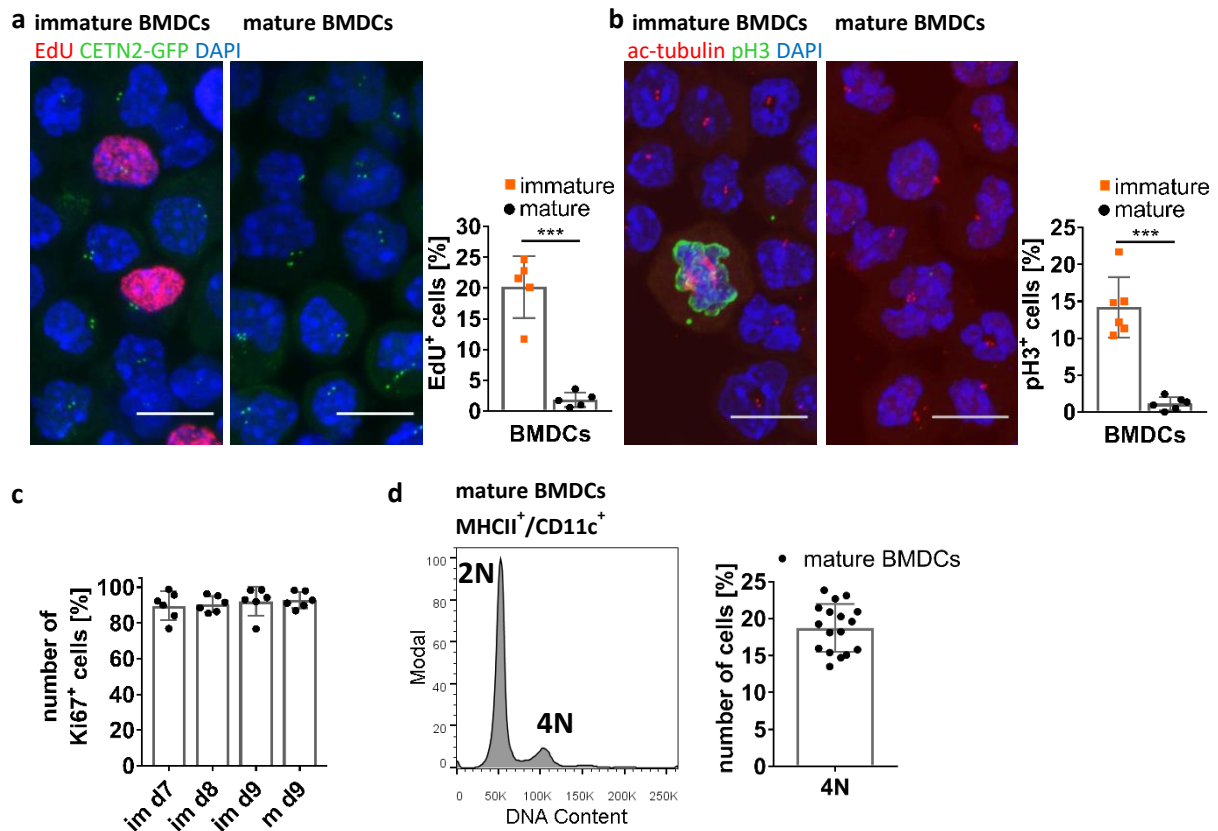


**Figure 3.3** Mature bone marrow-derived dendritic cells (BMDCs) do not transit through the cell cycle.
(**a**) Quantification of EdU-positive BMDCs. Left: EdU signal (red) and CETN2-GFP signal (green) in immature and mature BMDCs. Nuclei were counterstained with DAPI (blue). Scale bar, 10 µm. Right: Quantification of EdU-positive immature and mature BMDCs. ***, $P = 0.0009$ (two-tailed, unpaired student's *t*-test with Welch's correction). Graph shows mean values ± s.d. of 5 independent experiments. $N = 272/205/509/356/423$ cells (immature) and $171/192/286/286/217$ cells (mature). (**b**) Quantification of pH3-positive BMDCs. Left: Immunostaining of ac-tubulin (red) and pH3 (green) in immature and mature BMDCs. Nuclei were counterstained with DAPI (blue). Scale bar, 10 µm. Right: Quantification of pH3-positive immature and mature BMDCs. ***, $P = 0.0004$ (two-tailed, unpaired Student's *t*-test with Welch's correction). Graph shows mean values ± s.d. of 6 independent experiments. $N = 134/98/158/125/93/124$ cells (immature) and $141/203/158/204/127/128$ cells (mature). (**c**) Intracellular staining of Ki67 in immature (im) and mature (m) BMDCs at day (d7-9) of differentiation. Graph displays mean values ± s.d. of 6 independent experiments. $N = 10.000$ cells per experiment. (**d**) DNA content of mature BMDCs. Left: representative histogram of DNA content in MHCII+/CD11+ mature BMDCs. 2N (diploid), 4N (tetraploid). Right: Quantification of tetraploid cells. Graphs display mean values ± s.d. of 18 independent experiments. $N = 10.000$ cells per experiment.

### 3.1.2. Extra centrosomes within the dendritic cell compartment

To further validate the phenomenon of extra centrosomes, we studied *ex vivo* DCs isolated from WT mice (Figure 3.4 a-c). In dermal, splenic and LN DCs, extra centrosomes were observed. For studying dermal DCs, ear sheets were split and cells were harvested three days after emigration. These cells displayed typical DC cell surface markers during FACS analysis. Cells were analyzed for lineage (CD19, CD3$\varepsilon$, CD56, TER-119), CD45, MHCII, CD11c, CD103, CD207 and CD11b. As CD11b is a marker for cDC2s, most of the analyzed dermal DCs represent cDC2 (Figure 3.4 a). Immunostaining against centrosomal proteins (Figure 3.4 b) revealed amplified centrosomes. Around 20% of cells had two centrosomes and around 7% more than two (Figure 3.4 c). Similar to mature BMDCs, dermal DCs were not proliferating as the cells were EdU and pH3 negative (Figure 3.4 d,e) and did not enter G0 as the cells were Ki67-positive (Figure 3.4 f). Additionally, dermal DCs showed an increased DNA content, as depicted in Figure 3.4 g with around 7% of the cells being tetraploid.

As *in vivo* DC numbers are small, we tried to analyze further organs by using the ImageStream Amnis. This technique allows the user to combine flow cytometric aspects with imaging processes. Therefore, less cells are needed in comparison to the classical FACS combined with fluorescent imaging approaches. Unfortunately, the camera resolution was not high enough to quantify individual centriole numbers (Figure 3.5 a). Therefore, we isolated splenic and LN DCs by FACS and separated DCs into two subsets based on their cell surface marker expression: cDC1 (Lineage$^-$, CD45$^+$, F4/80$^-$, CD64$^-$, B220$^-$, MHCII$^+$, CD11c$^+$, CD8$\alpha^+$) and cDC2 (Lineage$^-$, CD45$^+$, F4/80$^-$, CD64$^-$, B220$^-$, MHCII$^+$, CD11c$^+$, CD11b$^+$) (Figure 3.5 b). Afterwards, immunofluorescence microscopy revealed the highest percentage of extra centrosomes in EdU negative CD8$\alpha^+$ cDC1s and to a lesser extend in EdU negative CD11b$^+$ cDC2s (Figure 3.5 c,d).

Therefore, we draw the conclusion, that DCs within different organs and distinct subsets display extra centrosomes, indicating that these variations could possibly be depended on the environment and the function of DCs. To better understand how extra centrosomes arise, the underlying mechanism(s) will be addressed in the next part. As DC subsets are a rare population of cells *in vivo*, we carried out all further experiments with BMDCs, which can be generated easily in large amounts *in vitro*.
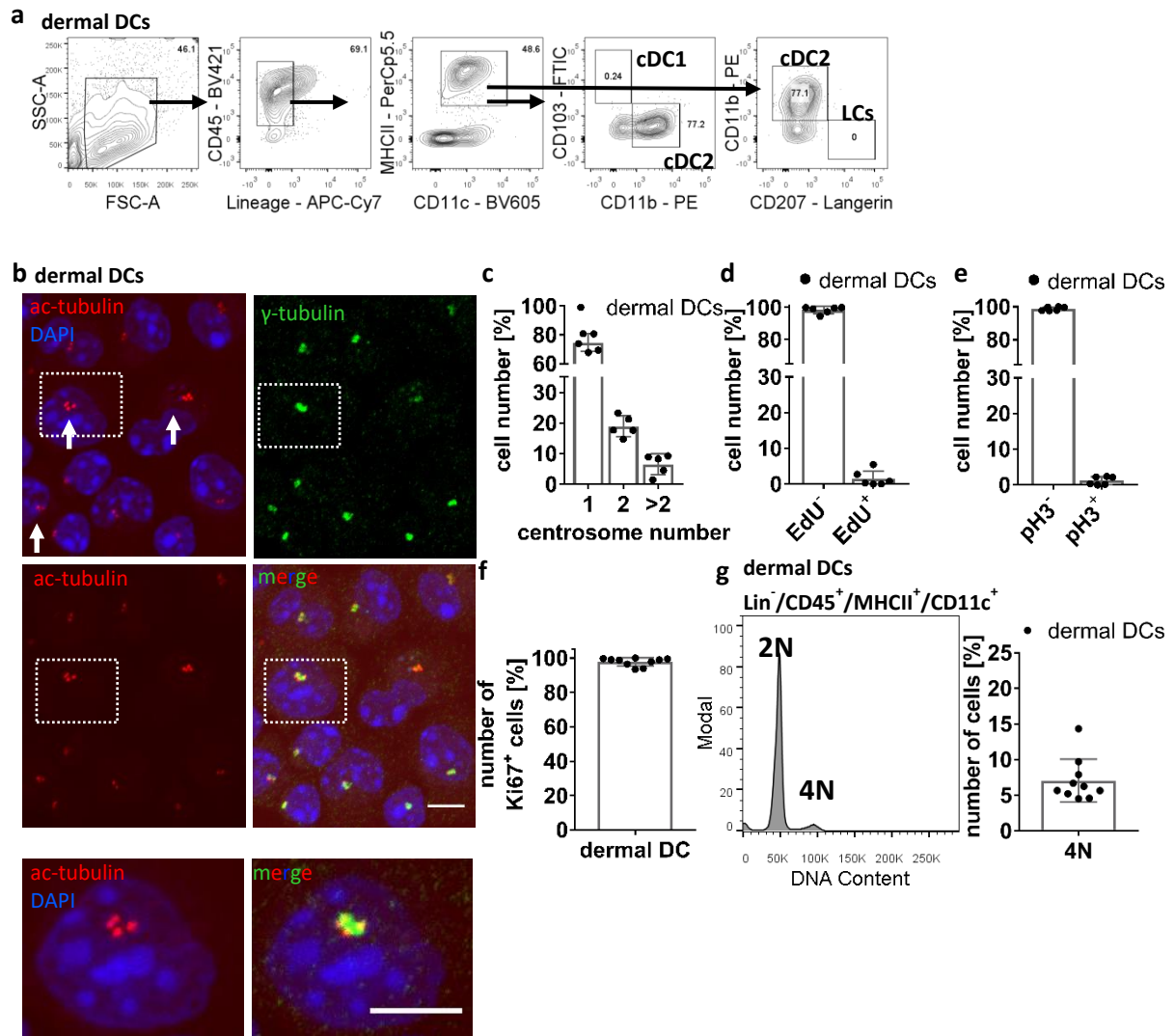
**Figure 3.4** Visualisation and analysis of centrosome numbers and cell cycle status in dermal dendritic cells (DCs).

(**a**) Cell surface analysis of skin emigrated dermal DCs into medium supplemented with CCL19. Dermal DCs were identified as cDC1, cDC2, and Langerhans cells (LCs) based on the following cell surface markers: Lineage (CD3$\varepsilon$, CD19, CD56, and TER-119), CD45, MHCII, CD11c, CD103, CD11b, and CD207. Black arrows indicate gating strategy. (**b**) Immunostaining of ac-tubulin (red) and γ-tubulin (green). Nuclei were counterstained with DAPI (blue). White arrows point to $\geq 4$ ac-tubulin. Scale bar, 5 µm. Lower panel: Magnification of boxed region. Scale bar, 5 µm. (**c**) Quantification of centrosomal numbers in dermal DCs according to ac-tubulin/γ-tubulin-positive foci. Graph displays mean values ± s.d. of 5 independent experiments. $N$ = 96/90/109/131/108 cells, pooled from three different mice for each experiment. (**d,e,f**) Quantification of EdU incorporation, pH3 staining and Ki67$^+$ dermal DCs. Graphs display mean values ± s.d. of 6 (EdU and pH3) and 11 (Ki67) independent experiments. $N$ = 84/119/316/181/191/183 cells, pooled from three different mice for each experiment (EdU, pH3). $N$ = at least 2100 dermal DCs analyzed per Ki67 experiment. (**g**) Dermal DCs contain tetraploid DNA. Left: Representative histogram of DNA content in MHCII$^+$/CD11$^+$ dermal DCs. 2N (diploid), 4N (tetraploid). Right: Quantification of tetraploid cells. Graphs display mean values ± s.d. of 11 independent experiments. $N$ = at least 2.100 cells per experiment.
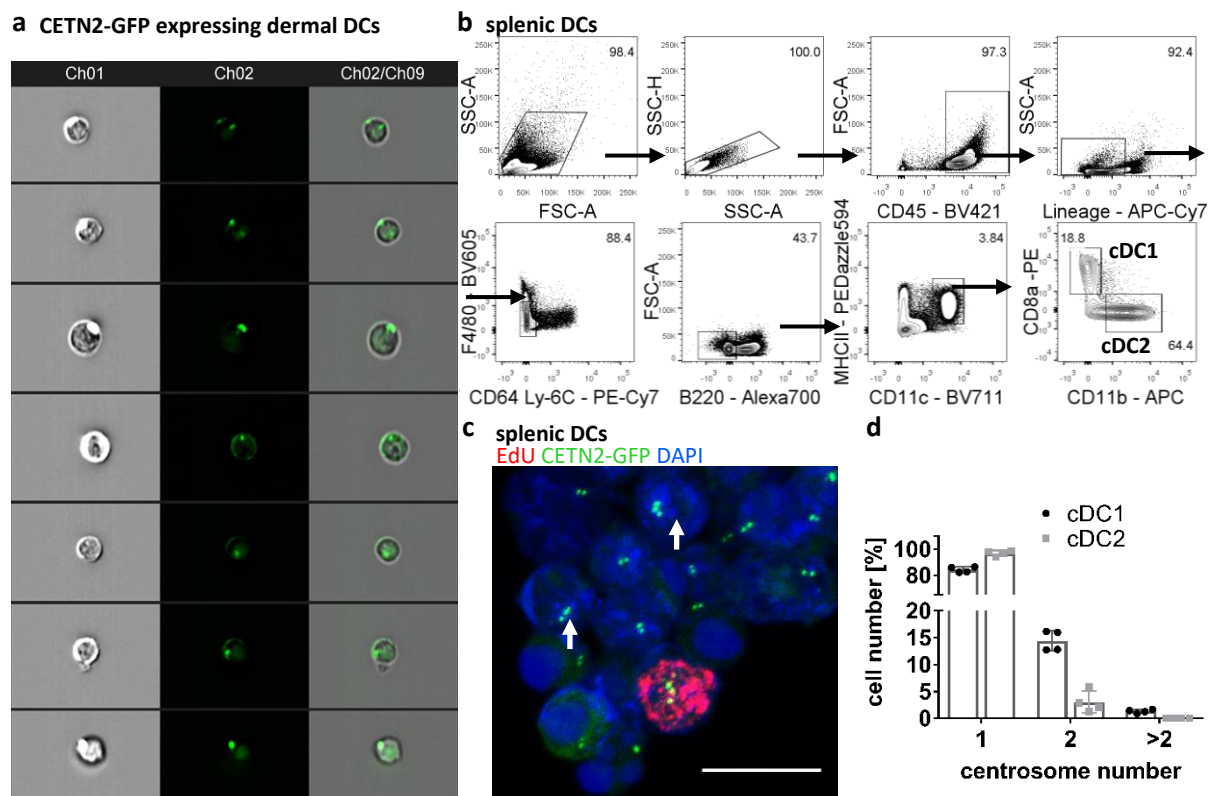
**Figure 3.5** Centrosome numbers in dendritic cell (DC) subpopulations.

(**a**) ImageStream analysis of CETN2-GFP expressing dermal DCs. Left panel: bright field, middle panel: CETN2-GFP, right panel: merge. (**b**) Fluorescent activated cell sorting on splenic DCs separated into cDC1 and cDC2 based on the following cell surface markers: CD45, Lineage (CD3$\varepsilon$, CD19, CD56, TER-119, Ly-6G), F4/80, CD64, Ly-6C, B220, MHCII, CD11c, CD8α, CD11b. Black arrows indicate gating strategy. (**c**) Visualisation of EdU incorporation (red) in CETN2-GFP (green) splenic DCs. Nuclei were counterstained with DAPI (blue). (**d**) Quantification of centrosome numbers in cDC1 and cDC2 according to CETN2-GFP-positive foci. Graph displays mean values ± s.d. of 4 independent experiments. N = 242/359/337/161 cells (cDC1) and 152/209/439/153 cells (cDC2).

## 3.2.　Centrosome duplication in dendritic cells

### 3.2.1. Alterations in cell division and polo like kinase 2 expression determine extra centrosome development

To date, two major mechanisms of how numerical centrosome abnormalities can arise are described: One is termed `overduplication´ and the other `centriole accumulation´ [270]. The first one relies on an unknown mechanism that evokes excess seeding of newly formed procentrioles leading to one parentcentriole with many procentrioles instead of only one new procentriole. For this to happen, deregulation of the centrosome duplication pathway needs to occur.

By contrast, the second pathway is not caused by deregulation of the centrosome duplication machinery but is rather associated with alterations in cell division, such as cytokinesis failure or mitotic slippage. As these cells do not divide properly into two daughter cells, the duplicated chromosomes as well as the amplified centrosomes stay within one cell. During the initiation of proliferation, the two centrioles of the initial centrosome both become parentcentrioles. Each of the two parentcentrioles then seed a new procentriole creating two complete centrosomes, each owning one parentcentriole and one procentriole. As the last steps of the cell cycle are not executed properly, both pairs of centrioles together with the duplicated chromosomes stay within the same cell. This polyploid cell habors a normal parent/procentriole ratio, as both of the two centrosomes contain one parent- and one procentriole (Figure 3.6 b).

As described, BMDCs exhibit ~ 17% of tetraploid cells (Figure 3.1), suggesting that this subset represents the `centriole accumulation´ pathway caused by an incomplete mitosis. This points out, that 54% of CA arise due to cell division alterations (17% of tetraploid cells from 30% that contain CA), leaving 46% of CA cells with diploid DNA content that arise due to the `overduplication´ pathway (Figure 3.6 a).
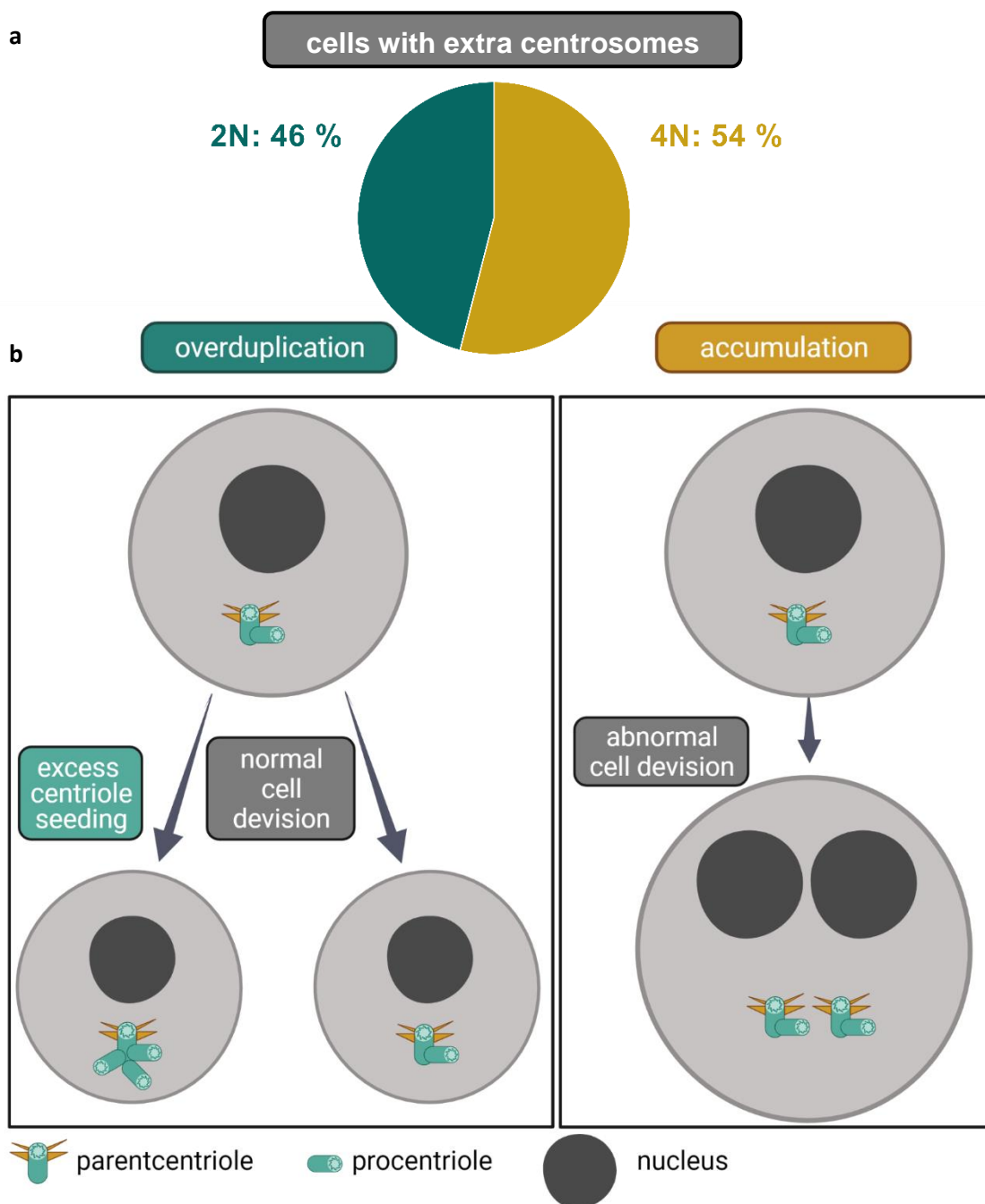
**Figure 3.6** Centrosome amplification pathways.

(**a**) Pie chart displays percentage of extra centrosomes in BMDCs belonging either to 'overduplication' (46%; diploid (2N) DNA content; green) or 'accumulation' pathway (54%; tetraploid (4N) DNA content; yellow). (**b**) Schematic representation displays normal (left) and abnormal cell division (right) and how this affects parent and procentriole numbers. In the 'overduplication' pathway (left), excess centriole seeding causes more than one procentriole. In the 'accumulation' pathway (right), abnormal cell division leads to twice the amount of DNA (here presented by two nuclei) and to too many centrosomes, each having one parentcentriole and one procentriole (normal parent/procentriole ratio of 1:1). (b) Image adapted from Cosenza and Krämer, 2016.

As demonstrated in Figure 3.1, elevated centrosome numbers are present in mature cells compared to immature cells, indicating that the mechanism of generating extra centrosomes is induced during the maturation process of centrosomes. Consequently, we wondered whether specific proteins that are known to overtake an important task during centriole duplication are altered during the process of maturation. We first focused on Plk4 and Plk2 messenger RNA (mRNA) expression during multiple time points after LPS induced stimulation. Plk2, as well as its family member Plk4, is an important protein during centriole duplication. Centrosome duplication is initiated in late G1 and early S phase. Here, one parent centriole serves as template for the production of one new procentriole. Thereby, acetylated Plk2 accumulates and phosphorylates several centrosomal associated proteins [271]. One of these proteins is the F-box protein F-box/WD repeat-containing protein 7 (Fbxw7), a subunit of the SKP1-CUL1-F-box protein complex (SCF) ubiquitin ligase [272]. When this protein is abrogated, SAS-6 is stabilized and increasingly recruited to the parent centriole, which cause multi-numerous centrioles [273]. Additionally, the destabilization of Fbxw7 via Plk2 mediated phosphorylation, also promotes increased cyclin E levels thereby coordinating cell cycle progression and centriole duplication [272].

We observed a 2-fold increase in the relative expression of *Plk4* shortly after LPS treatment and a more drastic increase of 12-fold for *Plk2*, reaching the highest expression 2 hours after stimulation (Figure 3.7 a,b).
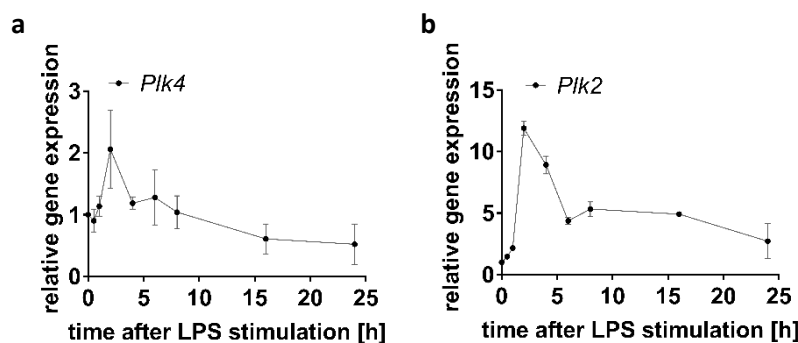


**Figure 3.7** Increased expression of genes involved in regular centriolar duplication.
(**a,b**) mRNA expression levels of *Plk4* and *Plk2* after lipopolysaccharide (LPS) stimulation of immature WT BMDCs (h, hours). For normalization, *TATA-box binding protein* was used. Graph displays mean values ± s.d. of three independent experiments.

To link the expression increase of both molecules to altered centrosome numbers, we first tested the Plk4 specific inhibitor Centrinone. This inhibitor functions in inhibiting Plk4 on a protein level. Therefore no new procentrioles can be formed during cell cycle progression, first leading to a loss of one centriole in the next daughter cell and eventually generating cells that do no longer contain any centrioles [274].

We tested several conditions, altering the concentration and time points of Centrinone admission. We observed that BMDCs treated with 250 nM or 500 nM Centrinone from day zero onwards differentiated and matured similar to the DMSO controls (Figure 3.8 a,b,c), showing high MHCII, CD11c and CD135 levels. Further, these cells expressed high levels of the co-stimulatory molecule CD86 and CCR7, both proteins that are upregulated during maturation. In addition, the percentage of polyploid cells did not alter between control and treated cells. These results confirm that PLK4 inhibition does not alter DC differentiation and maturation. Next, we quantified centrosome numbers in mature BMDCs treated with Centrinone or DMSO. As displayed in Figure 3.8. d, BMDCs treated with 250 nM Plk4 inhibitor from day zero onwards, exhibited around 30% of cells with no centrioles, around 20% with one centriole, a majority of cells with two centrioles and about 20% of the cells showed amplified centrosomes. These were separated in cells with three to four centrioles and more than four centrioles. In the control samples on the other hand a similar result for amplified centrosomes were detected and the majority of cells harbored two centrioles. The results obtained from cells that were treated during maturation, revealed similar percentage of amplified centrosomes in control and inhibited samples (Figure 3.8 e), but did not contain cells with no centriole and only very little with one centriole, indicating that the mechanism of action from Centrinone could no longer be effective, as cells stop proliferating during maturation. Comparing the different conditions, it was obvious that the percentage of cells owning amplified centrosomes is not altered significantly with or without Plk4 inhibition. From these results, we conclude that Plk4 does not seem to be directly involved in the amplification of centrosomes after LPS stimulation in DCs.
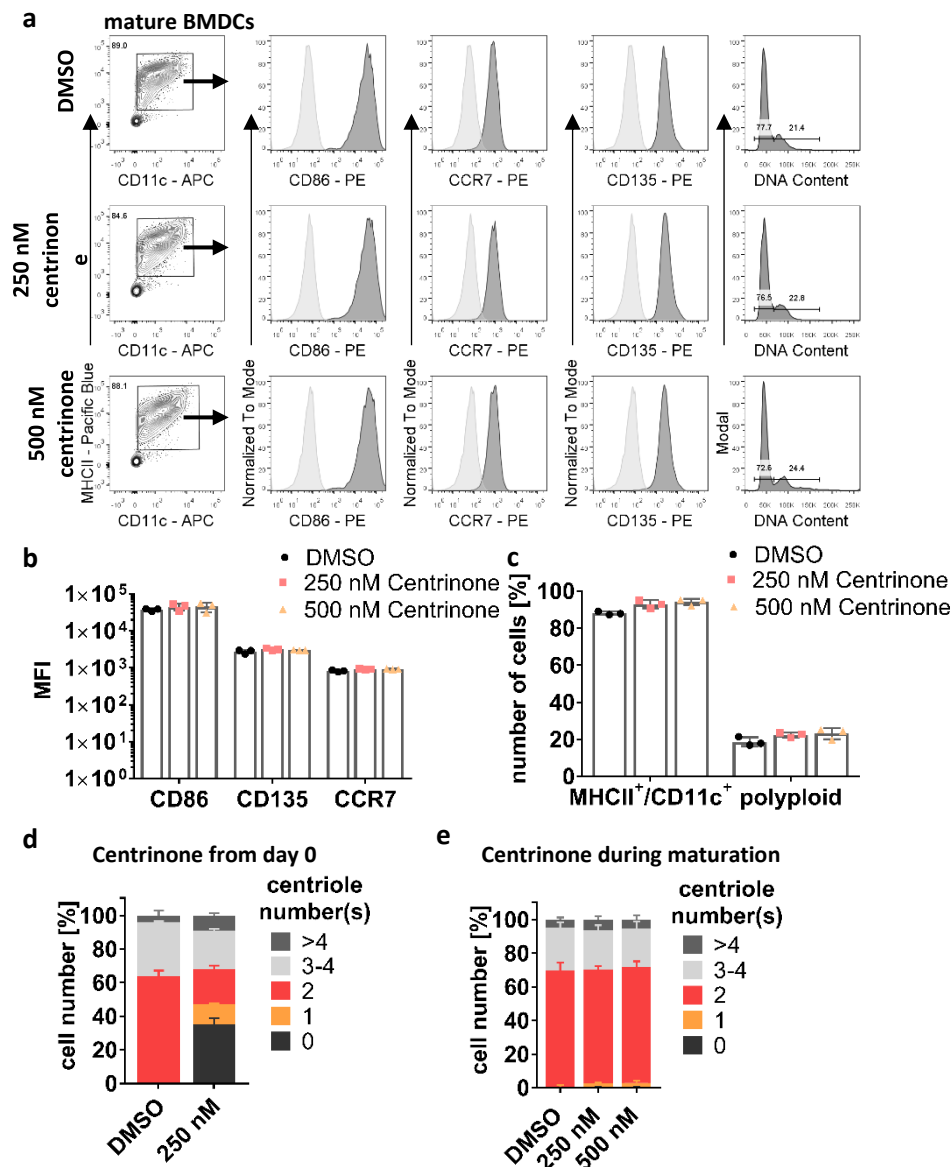
**Figure 3.8** Pharmacological depletion of centrioles using Centrinone.

(**a-c**) Analysis of CETN2-GFP expressing BMDCs differentiation and maturation during Plk4 inhibition by Centrinone. (**a**) Flow cytometry analysis of MHCII, CD11c, CD86, CCR7, CD135 and DNA content in mature BMDCs treated with DMSO (control), 250 nM or 500 nM Centrinone. Unstained samples served as control and were included as light grey filled line. Staining for DC marker has been conducted in parallel with PE-conjugated antibodies. Representative histograms of one out of three independent experiments are shown. $N$ = 10.000 cells per experiment.(**b**) Quantification of CD86, CD135 and CCR7 in CETN2-GFP expressing BMDCs treated with or without (DMSO) Centrinone. Graph displays mean values of mean fluorescence intensities (MFI) ± s.d. Each data point represents one independent experiment. (**c**) Quantification of MHCII/CD11c-positive and polyploid CETN2-GFP expressing BMDCs treated with or without (DMSO) Centrinone. Graph displays mean values ± s.d. of three independent experiments. $N$ = 10.000 cells per experiment. (**d**) Quantification of centriole numbers in CETN2-GFP expressing BMDCs by CETN2-GFP-positive foci treated with 250 nM Centrinone or DMSO from day 0 onwards. Graph displays mean values ± s.d. of three independent experiments. $N$ = at least 156 cells analyzed per experiment. (**e**) Quantification of centriole numbers in CETN2-GFP expressing BMDCs by CETN2-GFP-positive

foci treated with 250 nM or 500 nM Centrinone or DMSO during maturation. Graph displays mean values ± s.d. of three independent experiments. *N* = at least 146 cells analyzed per experiment.

After that, we sought to identify the impact of Plk2 on the generation of extra centrosomes. To this aim, we generated CRISPR/Cas9 knockouts on the 78 kDa protein in CENT2-GFP expressing precursor cell line Hoxb8 [275]. *Plk2-deficiency* was confirmed using immunoblotting against Plk2 in control (scramble) and KO cells. In the lysate of KO cells, the band at the size of 78 kDa was missing (Figure 3.9 a). We next differentiated the precursors into DCs and analyzed their differentiation and maturation profile. Similar to BMDCs that were treated with Centrinone, Hoxb8-derived DCs showed high levels of MHCII, CD11c, CD135 as well as the maturation markers CD86 and CCR7 (Figure 3.9 b). No alterations could be detected in the percentage of polyploid cells comparing controls and KOs (Figure 3.9 c). In addition, proliferation (pH3) and cell cycle arrest (Ki67) were checked over the time course of differentiation and maturation from day 6 to day 9 (Figure 3.9 d,e). No alteration between control and KO was observed. As the cells developed normally, we analyzed centrosome numbers by quantifying CENT2-GFP-positive foci in mature DCs. Comparing scramble and *Plk2*$^{-/-}$, a significant reduction of cells having two or more centrosomes was demonstrated within the KO sample (Figure 3.9 f). In particular, cells containing more than two centrosomes were essentially absent after plk2 depletion. These results point to a `rescue´ effect of extra centrosomes in mature DCs and highlight that Plk2 is involved in extra centrosome generation in DCs.
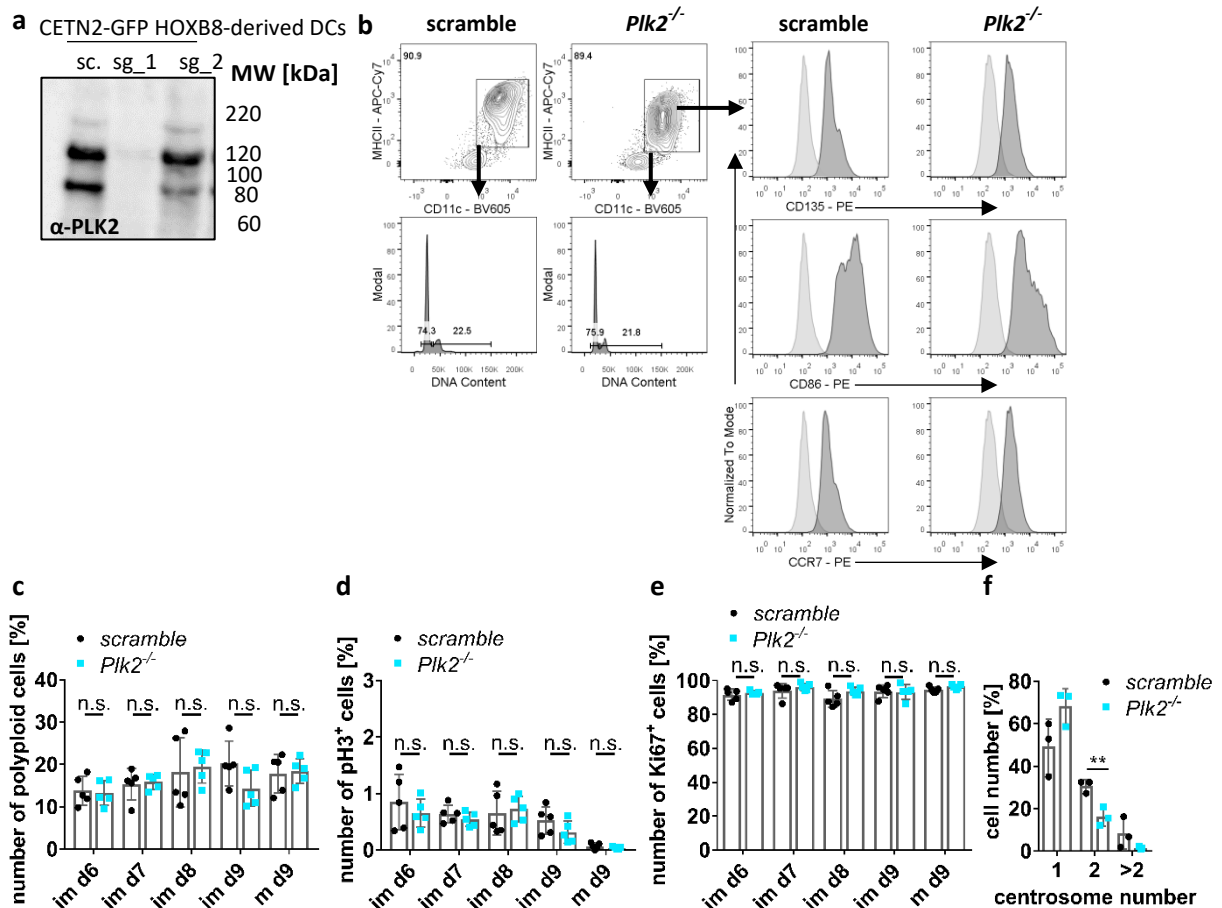
**Figure 3.9** Centriole amplification depends on polo like kinase 2 (Plk2).

(**a**) Immunoblotting against Plk2 of lysates from mature control (scramble (sc)) and $Plk2^{-/-}$ (sg_1 and sg_2 (single guide)) CETN2-GFP expressing Hoxb8-derived DCs. Only sg_1 lead to a KO generation. (**b**) Flow cytometry analysis of MHCII, CD11c, DNA Content, CD135, CD86 and CCR7 in control (scramble) and $Plk2^{-/-}$ mature CETN2-GFP expressing Hoxb8-derived DCs. Unstained samples served as control and were included as light grey filled line. Black arrows indicate gating strategy. Staining for DC marker has been conducted in parallel with PE-conjugated antibodies. Representative histograms of one out of 4 independent experiments are shown. $N = 10.000$ cells per experiment. (**c-e**) Quantification of polyploid cells, pH3 positive and Ki67 positive cells of control (scramble) and $Plk2^{-/-}$ mature CETN2-GFP expressing Hoxb8-derived DCs. Graph displays mean values ± s.d. of 4 independent experiments. $N = 10.000$ cells analyzed per experiment. n.s., non-significant (Multiple, two tailed, unpaired $t$-tests). (**f**) Quantification of centrosome numbers by CETN2-GFP-positive foci in control (scramble) and $Plk2^{-/-}$ mature CETN2-GFP expressing HOXb8-derived DCs. ***, $P = 0.0095$ (two-tailed, unpaired Student's $t$-test). Graph displays mean values ± s.d. of three independent experiments. $N = 315/263/155$ cells (*scramble*) and 295/268/130 cells ($Plk2^{-/-}$).

Taken together, we conclude that both pathways, the `centriole accumulation´ and the `overduplication´ pathway, take place in DCs promoting the generation of extra centrosomes. 54% arise due to cell division alterations and 46% of CA due to overduplication of procentrioles. In the latter one, Plk2 as a centrosome duplication protein, seems to be involved. To further analyze the role of Plk2 and its interaction partners, additional studies will

be necessary. Besides that, extra studies are needed to understand the physiological role and functional consequences of these extra centrosomes in immune cells.

## 3.3.     Physiological function of extra centrosomes

### 3.3.1. Microtubule nucleation capacity is increased when having amplified centrosomes

So far, extra centrosomes have been associated to malignancy and are a well-described phenomenon in cancer cells [236,276]. Their physiological role within DCs needs to be enlightened. The centrosome functions as MTOC, thereby forming and organizing MTs. As MTs overtake important functions during antigen uptake and processing, migration and IS formation, we hypothesized that it would be beneficial for these processes to have additional centrosomes.

The first question raised was whether extra centrosomes evoke a higher MT nucleation capacity. We visualised individual MT filaments in DCs by staining against α-tubulin during IS formation. Therefore, mature CETN2-GFP BMDCs were fed with the model antigen ovalbumin and injected under a blog of agarose to mimic confined environments. Then, freshly isolated naïve CD4$^+$ T cells from OT-II transgenic mice were injected. Their T cells carry a transgenic TCR that pairs with the CD4 co-receptor and is specific for ovalbumin-derived peptide$_{323-339}$ (ova$_{323-339}$) in the context of MHCII I-A$^b$ [264]. By analyzing MT numbers in DCs, which are interacting with T cells, we could identify that extra centrosomes indeed nucleate more MTs (Figure 3.10). One centrosome nucleates 35 MT filaments, whereas amplified centrosomes produce 42 MT filaments, a significant increase of 20%. From here on, we focused on the DCs' capacity to activate T cells, as this is the final read out for a successful signal transduction.

**a** co-culture of antigen loaded mature CETN2-GFP expressing BMDCs with OT-II naïve CD4+ T cells
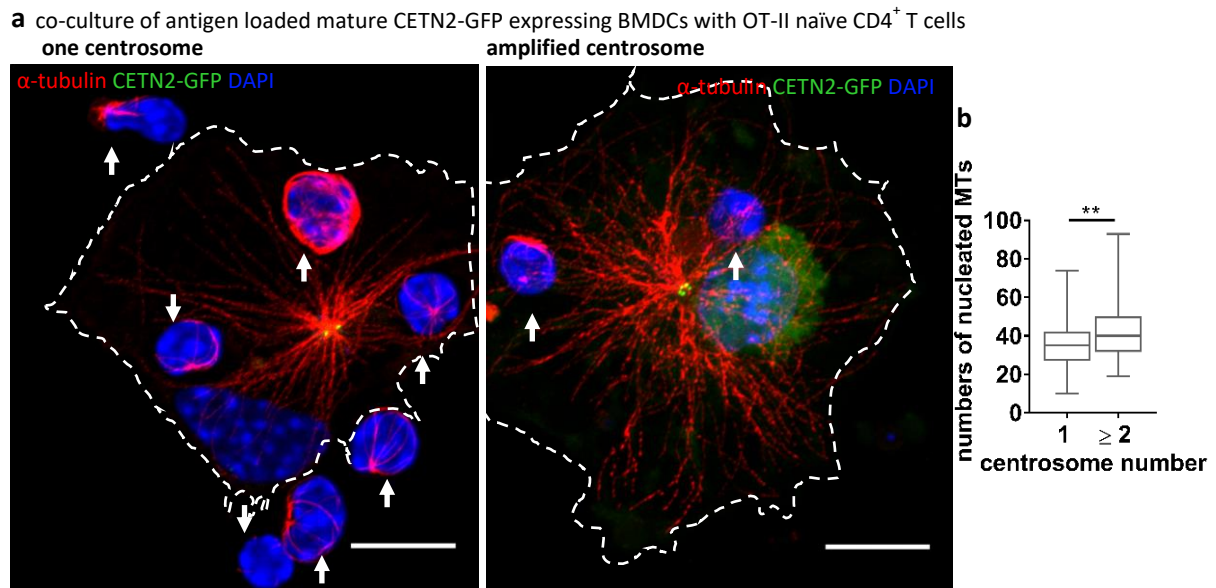
**Figure 3.10** Amplified centrosomes promotes microtubule (MT) nucleation capacity during immune synapse formation.

(**a**) Immunostaining of ovalbumin loaded mature CETN2-GFP expressing BMDCs with OT-II naïve CD4+ T cells. MTs are labelled in red (α-tubulin), centrioles are visualised by CETN2-GFP (green). Nuclei were counterstained with DAPI (blue). White arrows indicate T cells. Left: DC with 2 centrioles (1 centrosome). Right: DC with 5 centrioles (amplified centrosome). Scale bar, 10 μm. (**b**) Quantification of nucleated MTs from 1 centrosome and ≥ 2 centrosomes. **\*\***, *P = 0.0014* (Mann-Whitney test). Graph displays shape of distribution, central value and variability of data analyzed of 4 independent experiments. *N* = 93 (1 centrosome) and 85 (≥ 2 centrosomes) cells analyzed.

## 3.3.2. BMDC separation based on centrosomal content

To analyze T cell activation, we looked into the proliferation profiles of T cells as well as their capacity to release IL-2 after co-culture with antigen-loaded DCs. For this experimental set up, we first needed to separate the heterogeneous BMDC population into DCs with normal centrosome numbers and those having CA. To achieve this aim, we sorted cells based on the fluorescent reporter signal of CETN2-GFP (Figure 3.11 a). First, tetraploid cells were excluded from the analysis, as these cells contain a surplus of DNA and show variations in protein expression depending on altered gene-dosage [277]. In the next step, diploid cells were sorted based on a low or high signal intensity of CETN2-GFP. This separation led to a CETN2-GFPlow population that from here on is termed 2N2C (diploid cells with two centrioles) and a CETN2-GFPhigh population which will be referred to as 2NCA (diploid cells with centrosome amplification) (Figure 3.11 b). After sorting, a small fraction of cells was analyzed by confocal microscopy to identify centrosome numbers and consequently the efficiency of enrichment. This separation strategy led to an enrichment of centrosome numbers by the factor of at least 1.5 (Figure 3.11 c), ranging from 8-42% of amplified centrosomes within the 2N2C population and 21-70% for the 2NCA population.
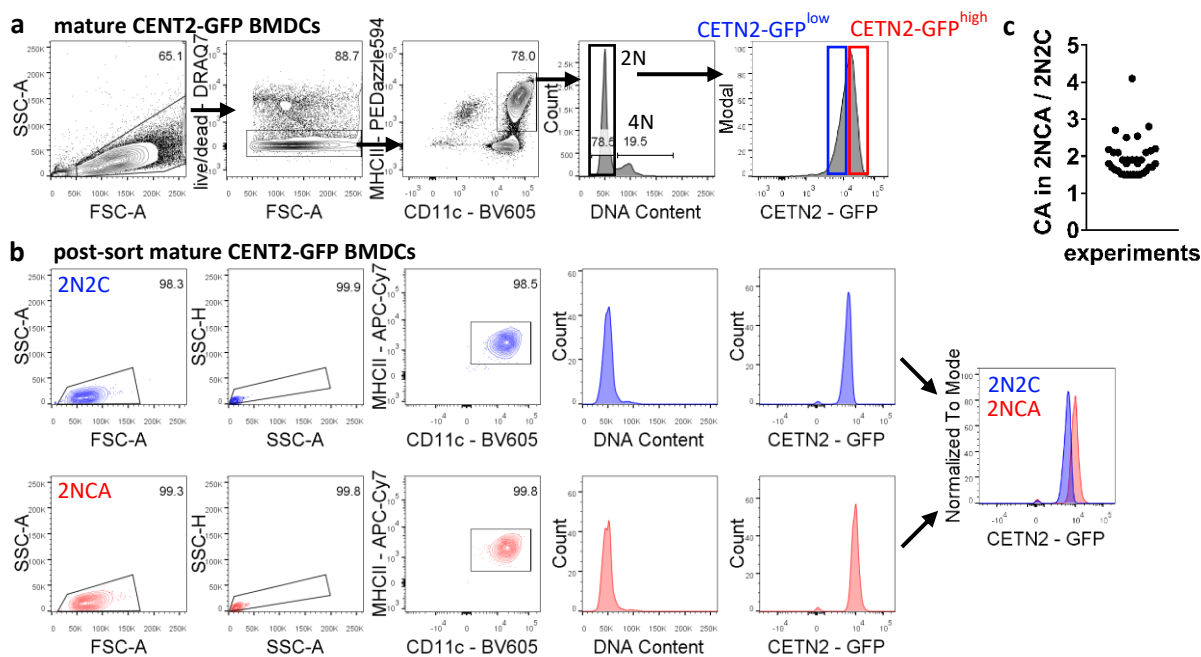
**Figure 3.11** Centrosome separation in CENT2-GFP expressing bone marrow-derived dendritic cells (BMDCs). (**a**) Sorting strategy of mature CETN2-GFP expressing BMDCs for live, MHCII, CD11c, diploid DNA content (black box) and CETN-2GFP$^{low}$ (blue box) or CETN-2GFP$^{high}$ (red box). (**b**) Post-sort analysis of CETN2-GFP$^{low}$ (2N2C) and CETN2-GFP$^{high}$ (2NCA) for diploid DNA content and CETN2-GFP. (**c**) Graph displays ratio of amplified centrosome numbers analyzed in 2N2C and 2NCA populations for each experiment performed. Centrosome numbers were determined in sorted DC populations by confocal microscopy based on CETN-2GFP-positive foci.

Both populations were further characterized on DC, monocyte, macrophage and granulocyte markers to ensure that the separation does not cause distinct cell populations (Figure 3.12 a). We also sorted the diploid cells based on size, and quantified centrosome numbers in smaller and larger cells, to exclude the possibility that DC enrichment was efficient due to differences in cytosolic GFP signal or cell size. Amplified centrosome numbers in small and large cells were essentially the same excluding the possibility that size effects account for any observed effect (Figure 3.12 b).
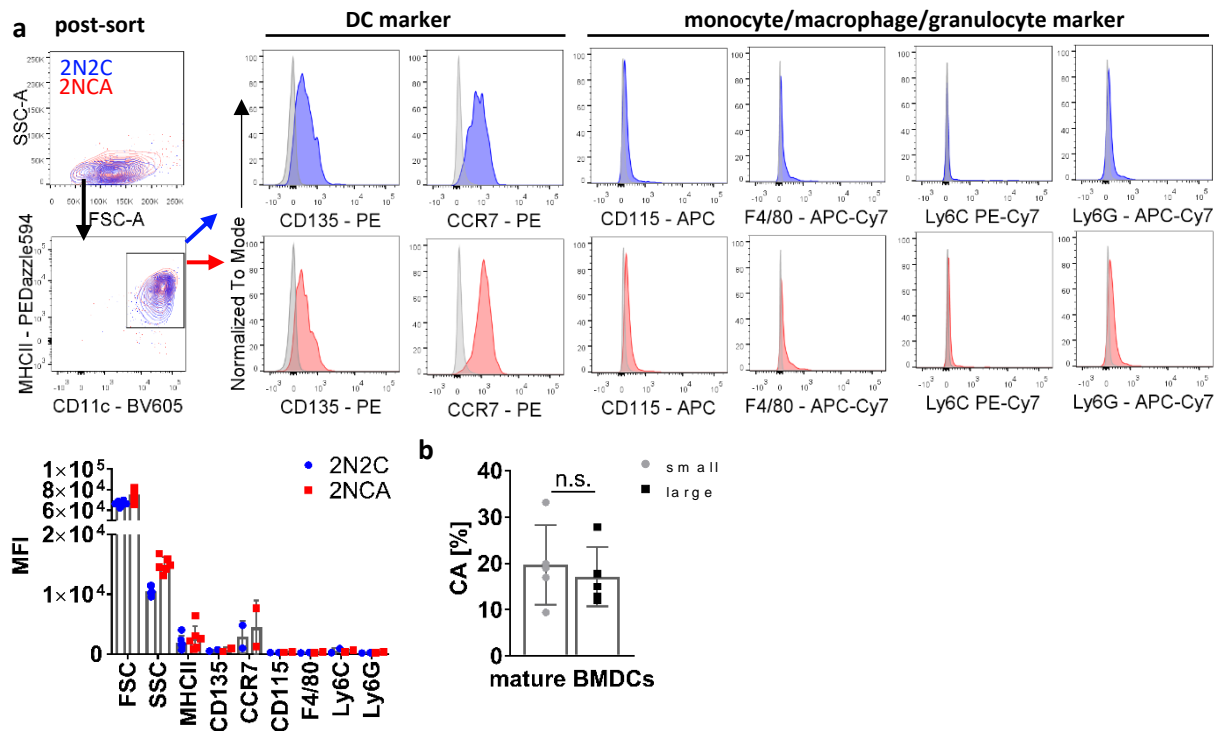
**Figure 3.12** Phenotype analysis of 2N2C and 2NCA bone marrow-derived dendritic cells (BMDCs) population. (**a**) Cell-surface expression of DC, monocyte, macrophage and granulocyte markers on enriched MHCII^{+}/CD11c^{+} 2N2C and 2NCA CETN2-GFP expressing BMDCs subpopulations. Histograms include unstained controls in light grey. Representative histograms of one out of at least two independent experiments are shown. Graph below shows quantification of cell-surface markers indicated as mean fluorescence intensity (MFI). Mean values ± s.d. are depicted. (**b**) Quantification of centrosome amplification (CA) in diploid mature MHCII^{+}/CD11c^{+} CETN2-GFP expressing BMDCs sorted based on their size (FSC-A, small and large). n.s., not significant (two tailed, paired Student`s t-test). Graph displays mean values ± s.d. of 5 independent experiments. $N$ = at least 139 individual cells analyzed per experiment.

### 3.3.3. Dendritic cells with extra centrosomes lead to optimized T cell activation

After centrosome separation into 2N2C and 2NCA populations, we performed mixed lymphocyte reactions. Here, sorted DCs were loaded with the model antigen ovalbumin and cultured with freshly isolated splenocytes from OT-II transgenic mice. After 24 hours, supernatants were collected and IL-2 concentrations determined. The release of IL-2 was induced after successful signal transduction from the DCs to the T cell. At all ovalbumin concentration tested, higher amounts of IL-2 were measured when the co-culture was performed with DCs that contained higher levels of CA (Figure 3.13 b).

In the next step, we measured T cell expansion to directly address T cell activation. For this assay, we labeled the cells with CFSE [278] and followed their proliferation cycle by analyzing the dilution of the fluorescent dye after 62 hours in CD4^{+} T cells (Figure 3.13 a). Here, we observed similar results as for the IL-2 secretion. If the co-culture was carried out with DCs

harboring amplified centrosomes, T cells were more proliferative than when DCs with lower centrosome numbers were used. This holds true for all ovalbumin concentrations tested (Figure 3.13 c).
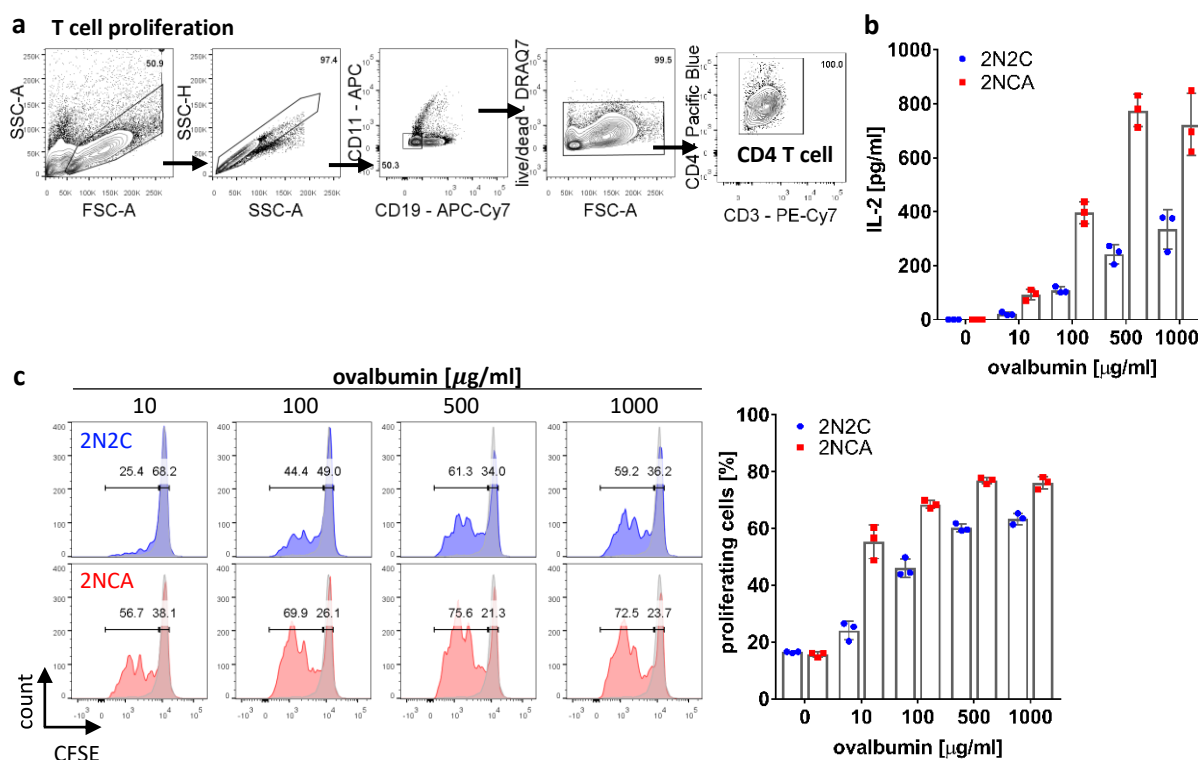


**Figure 3.13** Bone marrow-derived dendritic cells (BMDCs) enriched in multiple centrosomes lead to optimized T cell activation.

(**a**) Gating strategy for CD4$^+$ T cells. (**b**) Graph displays quantification of IL-2 levels after co-culture of ova-treated 2N2C (blue, cells enriched for one centrosome) or 2NCA (red, cells enriched for multiple centrosomes) DC populations with OT-II CD4$^+$ T cells. Graph displays mean values ± s.d. of one representative out of four experiments. Data points represent technical replicates. (**c**) Left panel: representative histogram of T cell proliferation of co-cultured OT-II CD4$^+$ T cells with enriched BMDC subpopulations (2N2C (blue) and 2NCA (red)) treated with different ovalbumin-concentrations. Unprimed T cells (-ovalbumin) served as negative control and are displayed as grey filled line. Right: graph shows quantification of OT-II CD4$^+$ T cells that divided after co-culture with ova-pulsed enriched DC subpopulations and displays mean values ± s.d. of one representative out of four experiments. Data points represent technical replicates.

Overall, we conclude that DCs with amplified centrosomes are more potent in activating T cells. Whether this is due to enhanced intracellular antigen processing, altered vesicle trafficking or improved cytokine secretion needs to be discovered. To face these questions, we performed T cell activation assays with ovalbumin-peptide $_{323-339}$ (ova$_{323-339}$). The peptide does not need to be internalized and therefore bypasses the intracellular antigen processing. We received similar results for IL-2 secretion and CFSE T cell proliferation when cells were treated with peptide instead of the whole antigen. In both cases, T cell responses were

increased when T cells were treated with BMDCs enriched in amplified centrosomes (Figure 3.14 a,b). Therefore, we excluded improved antigen processing as major reason for the optimized T cell activation capacity of DCs carrying amplified centrosomes.
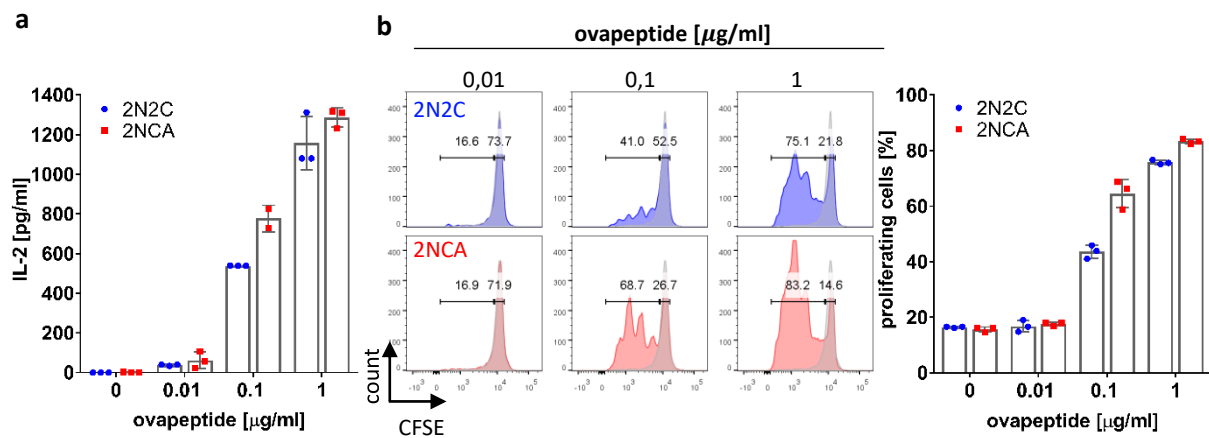


**Figure 3.14** Antigen processing is not involved in optimized T cell activation.

(**a**) Graph displays quantification of IL-2 levels after co-culture of ova$_{323-339}$-treated 2N2C (blue, cells enriched for one centrosome) or 2NCA (red, cells enriched for multiple centrosomes) DC populations with OT-II CD4^{+} T cells. Graph displays mean values ± s.d. of one representative out of four experiments. Data points represent technical replicates. (**b**) Left panel: representative histogram of T cell proliferation of co-cultured OT-II CD4^{+} T cells with enriched BMDC subpopulations (2N2C (blue) and 2NCA (red)) treated with differing ova$_{323-339}$-concentrations. Unprimed T cells (-ova$_{323-339}$) served as negative control and are displayed as grey filled line. Right: graph shows quantification of OT-II CD4^{+} T cells that divided after co-culture with ova$_{323-339}$-pulsed enriched DC subpopulations and displays mean values ± s.d. of one representative out of four experiments. Data points represent technical replicates.

In the following, we analyzed the expression of co-stimulatory molecules, as for some of them the intracellular trafficking has been reported to rely on MTs [231]. For CD40, CD70, CD86 no significant difference was observed when analyzing cell surface expression in 2N2C and 2NCA populations, whereas CD80 seems to be slightly increased on cells with amplified centrosomes (Figure 3.15 a). From these results, we reasoned that the expression of co-stimulatory molecules does not account for optimized T cell activation in response to DCs with extra centrosomes.
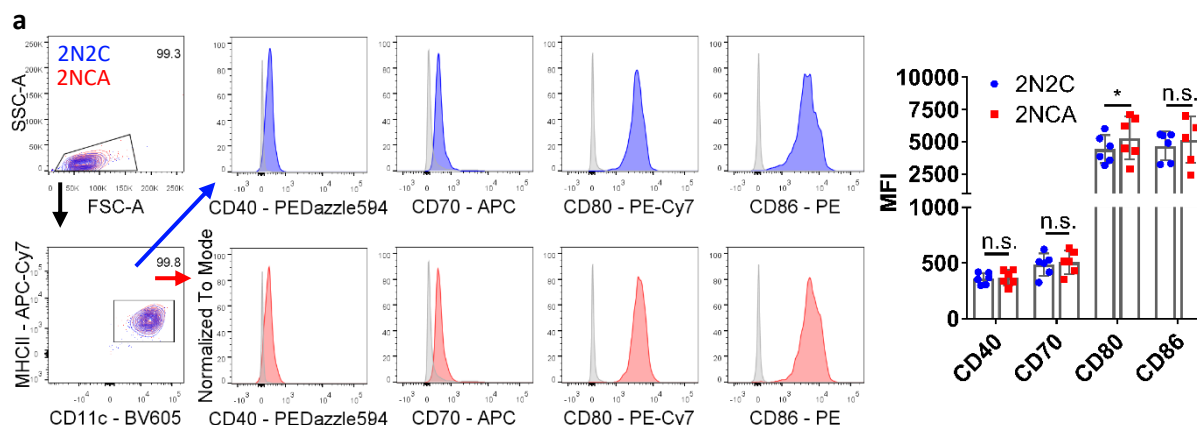
**Figure 3.15** Co-stimulatory molecules in bone marrow-derived dendritic cells (BMDCs) separated on centrosome content.

(**a**) Left panel: Representative histogram of co-stimulatory molecules on 2N2C (blue, cells enriched for one centrosome) and 2NCA (red, cells enriched for multiple centrosomes) BMDCs. Unstained control served as negative control and are displayed as grey filled line. Right: Graph displays mean values of mean fluorescence intensities (MFI) ± s.d. of co-stimulatory molecules in enriched DC subpopulations of six individual experiments. *, $P = 0.027$ n.s., non-significant (all, two-tailed, paired Student's *t*-test).

### 3.3.4. Dendritic cells with extra centrosomes exhibit increased cytokine secretion

Not only co-stimulatory molecules rely on MTs, but also compartments involved in endocytosis such as the endo- and lysosomes [107,279]. Lysosomal staining using the Lysotracker Deep Red, indicated that the 2NCA has markedly higher numbers of lysosomes compared to 2N2C (Figure 3.16 a). Lysotracker probes are fluorescent acidotropic probes that function in staining acidic compartments. The fluorophore is linked to a weak base. At neutral pH, only partial protonation can happen [280]. Based on the larger number of lysosomes present in cells with amplified centrosomes, we wondered whether this has an impact on cytokine secretion as cytokines can be released by secretory lysosomes [281–283]. In addition, data on inflammatory stimulated macrophages highlighted the role of centrosomes for cytokine production [284] and a pathway termed the extra centrosome-associated secretory pathway (ECASP) has been introduced [285], thereby highlighting centrosome function during secretion. When testing cytokine release in cells with different centrosome numbers, we used a cytokine array, which gave us a broad overview of the secretome of mature BMDCs (Figure 3.16 b). Besides other cytokines, we identified IL-6, CCL5, CXCL1, CCL17 and CCL22 to be released at higher levels by DCs that were enriched in extra centrosomes. Those data were confirmed by performing single ELISAs with the supernatant of 2N2C and 2NCA DCs (Figure 3.16 c). These cytokines are well described for their function in attracting and activating T cells as well as neutrophils [63,286–289].
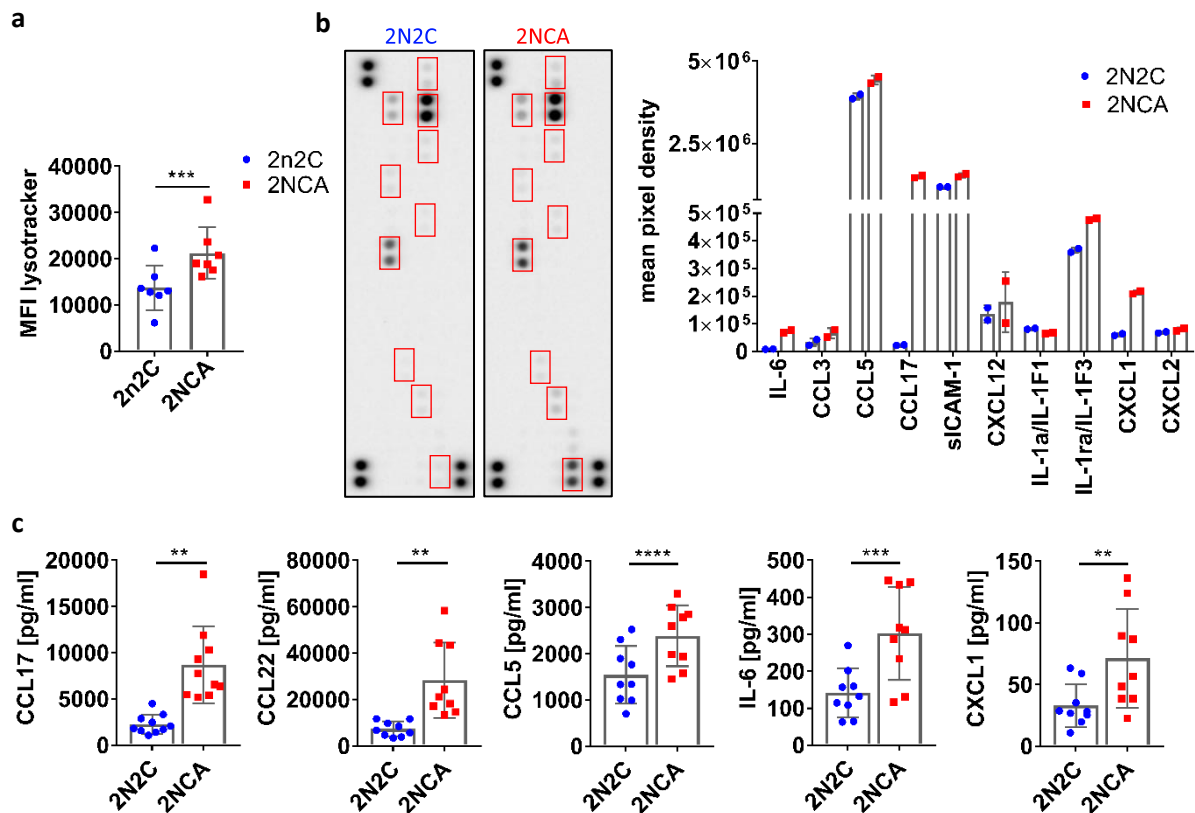
**Figure 3.16** Cells with multi-numerous centrosomes exhibit enhanced lysosome numbers and cytokine secretion. (**a**) Quantification of lysotracker intensity in enriched DC subpopulations (2N2C (blue) and 2NCA (red)). Graph displays mean values of mean fluorescence intensities (MFI) ± s.d. of seven individual experiments. ***, P = 0.0001 (all two-tailed, paired Student's *t*-test). (**b**) Cytokine array analysis of conditioned medium harvested from sorted 2N2C and 2NCA DC subpopulations. Sorted 2N2C and 2NCA cells were cultured and supernatants harvested after 16 hours. Left panel: Cytokine array of supernatants harvested from enriched DC populations. Quantified cytokine signals are highlighted with red boxes. Right panel: quantification of cytokine signal intensities. Graph shows mean pixel intensities ± s.d. of one out of two independent experiments. Data points represent technical replicates. (**c**) Sorted 2N2C and 2NCA cells were cultured and supernatants harvested after 16 hours. Cytokine levels were quantified by ELISAs. Graph shows mean values ± s.d. of at least 9 independent experiments. **, *P* = 0.0020 (CCL17); **, *P* = 0.0039 (CCL22) (CCL17 and CCL22 Wilcoxon test), ****, *P* < 0.0001 (CCL5); ***, *P* = 0.0005 (IL-6) and **, *P* = 0.0057 (CXCL1) (CCL5, IL-4 and CXCL1, two-tailed, paired Student's *t*-test).

To test whether only the transportation or secretion is altered or if these changes are due to altered gene expression, we carried out mRNA analysis (Figure 3.17 a). For IL-6, CCL5 and CXCL1 we could not detected significant differences in relative gene expression, however for CCL17 and CCL22 expression levels were altered in cells with elevated centrosome numbers. The relative gene expression of CCL17 and CCL22 is 1.5-2.5 fold increased in DCs with amplified centrosomes. These results point out that the production of certain cytokines was not influenced by extra centrosomes while others might be.

From here on, we focused on two aspects. First, we focused on the trafficking and secretion of cytokines that are not altered in production. We inhibited the intracellular protein transport with Monensin and Brefeldin A and observed for the T cell stimulating cytokines IL-6 and CCL5 increased intracellular levels in cells having amplified centrosome numbers (Figure 3.17 b), promoting the concept, that optimized T cell activation is at least partly due to enhanced cytokine trafficking.

The other aspect we focused on was T cell attraction due to increased cytokine release. In particular, CCL17 and CCL22 have been reported to be responsible for CCR4 dependent T cell attraction. CCR4 is the receptor of both cytokines and holds different binding regions for its ligands [290]. We performed transmigration assays with WT or CCR4 KO CD3/CD28 activated CD4$^+$ T cells in the upper chamber of the transwell device and distinct fluids in the lower chamber. After two hours, cells that transmigrated to the lower chamber were quantified (Figure 3.17 c). The fluids consisted of supernatant from sorted diploid cell populations (2N2C and 2NCA) or media supplemented with or without CCL19. CCL19 served as positive control, as this chemokine is known for attracting T cells [291]. Indeed, WT T cells migrated best towards CCL19-containing media and only poorly towards media controls (Figure 3.17 c). The same was observed for CCR4 KO T cells, which migrated only poorly on simple media (Figure 3.17 c). When comparing the transmigration towards the supernatants of 2N2C or 2NCA, WT T cells were translocated more efficiently into the 2NCA supernatant containing chamber. This effect though did not exist for CCR4 KO T cells (Figure 3.17 c), indicating that elevated release of chemoattractant cytokines, in particular CCL17 and/or CCL22 by DCs owning amplified centrosome numbers, lead to more potent T cell attraction.

Overall, these data demonstrate the importance of amplified centrosomes in increased secretion of immune stimulatory cytokines and the subsequent effect on optimized T cell activation.
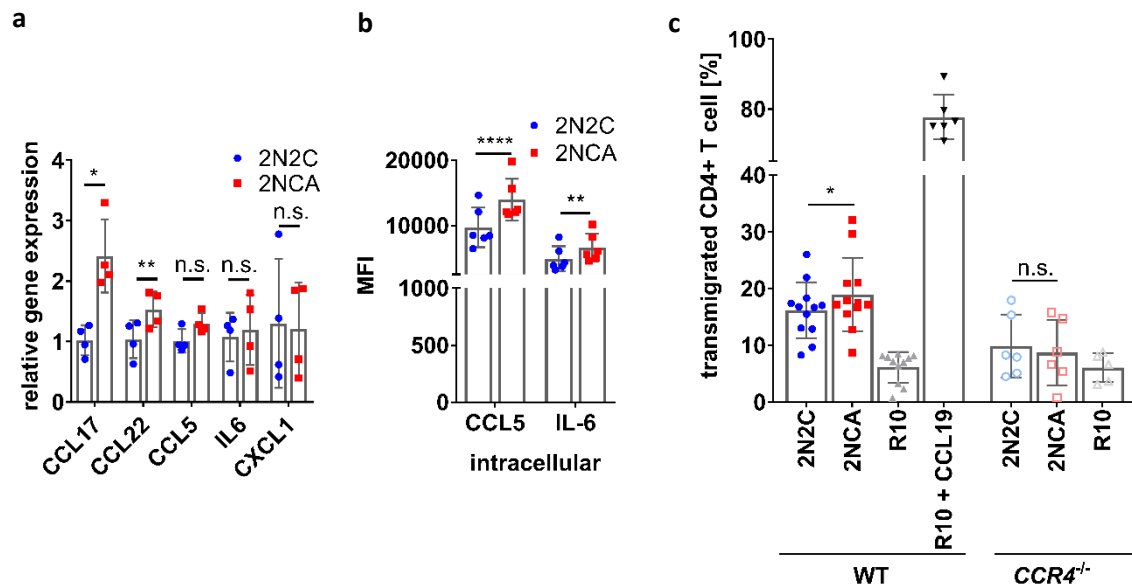
**Figure 3.17** Amplified centrosomes correlate with increased cytokine secretion and T cell activation.
(**a**) Relative gene expression levels of indicated cytokines in sorted 2N2C and 2NCA DC subpopulations. For normalization, *TATA-box binding protein* was used. Graph displays mean values ± s.d. of at least three independent experiments. *, $P$ = 0.012 (CCL17), **, $P$ = 0.0019 (CCL22) n.s., non-significant (all, two-tailed, paired Student's *t*-test). (**b**) Intracellular staining of cytokines upon blocking protein transport along MT filaments. Sorted 2N2C and 2NCA DC subpopulations were treated with Monensin and Brefeldin A and intracellular levels of CCL5 and IL-6 were determined by flow cytometry. Graph displays mean values of mean fluorescence intensities (MFI) ± s.d. of 6 independent experiment. ****, $P$ < 0.0001 (CCL5), **, $P$ = 0.002 (IL-6) (both two-tailed, paired Student's *t*-test). (**c**) Transmigration of WT and *CCR4*$^{-/-}$ naïve CD4$^+$ T cells toward supernatant harvested from 2N2C and 2NCA cells and toward control media. Graph displays mean values ± s.d. from at least 6 independent experiments. *, $P$ = 0.033 (WT naïve CD4$^+$ T cells on 2N2C vs. 2NCA supernatant), n.s. not significant (*CCR4*$^{-/-}$ naïve CD4$^+$ T cells on 2N2C vs. 2NCA supernatant), (two-tailed, paired Student's *t*-test).

## 3.3.5. MTOC localization in cell-cell conjugates

Our data demonstrate that amplified centrosomes correlate with a higher capacity of DCs to elicit T cell responses. We next sought to understand these data in more detail on a single cell level. Therefore, we were interested in MTOC behavior, in particular when DCs interact with several T cells simultaneously. The characteristic of forming an IS with several cells simultaneously, is termed multi-conjugated IS. This feature together with a multicentric structure are special attributes of ISs between DCs and T cells [178–180].

It is well established that dynamic MT filaments in T cells play a crucial role during IS formation allowing to exchange signals that are required for T cell activation [208,216,221]. Yet, there is limited knowledge on how antigen-presenting cells organize MT growths and dynamics and how centrosomes behave during these processes. For several cell types, a reorientation of the centrosome has been linked to successful signal transduction during IS formation. However, in DCs this process has not been studied satisfyingly, therefore we addressed the question, if

the centrosome relocalizes towards the IS and how this influences the activation of effector cells in a multi-conjugated ISs.
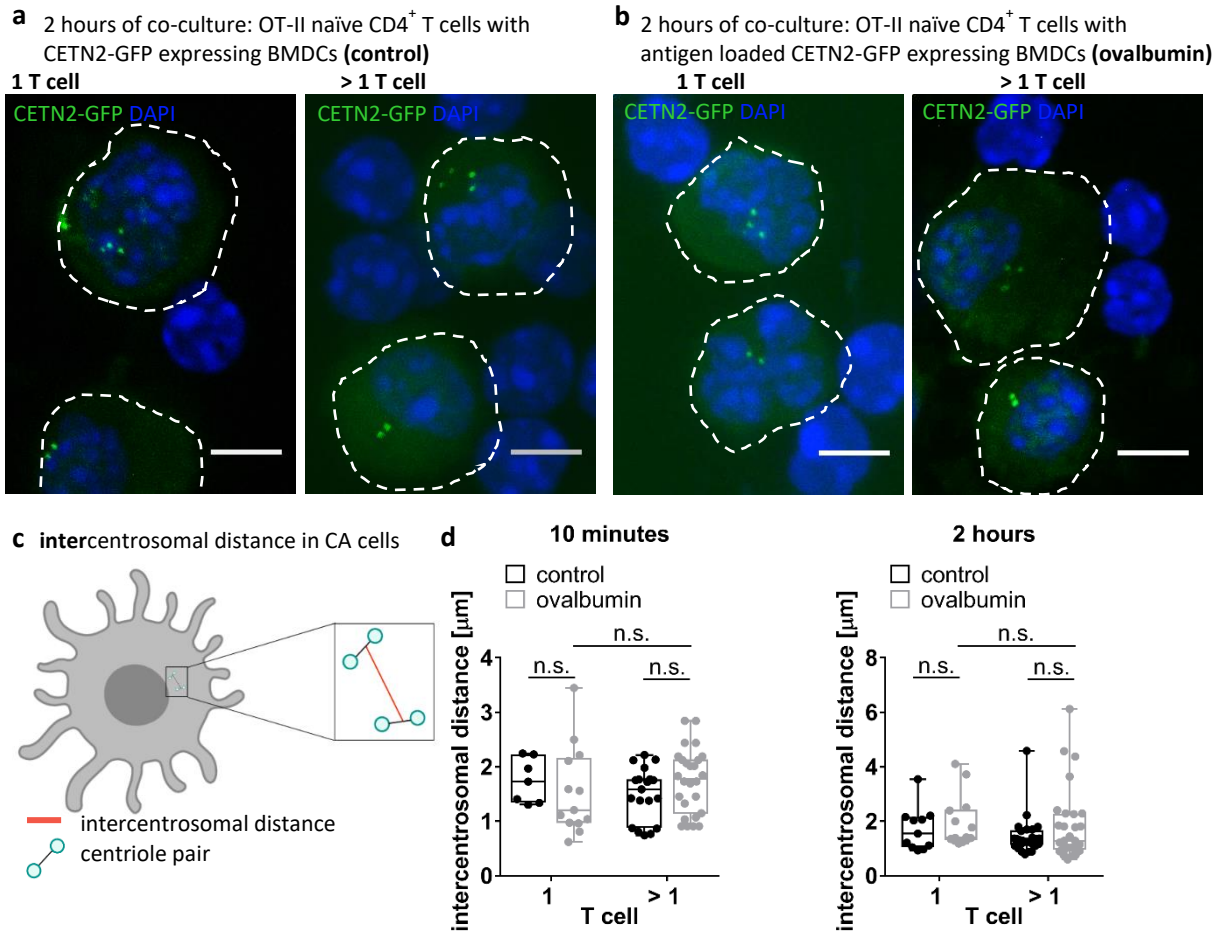
Additionally, we were interested in the conformation of multi-numerous centrosomes, as we observed extra centrosomes in DCs. Therefore, we wondered, if individual centrosomes display a dynamic behaviour or if the extra centrosomes form a cluster during IS signaling. The latter one is a phenomenon that has been described previously for mitotic cancer cells. Here, amplified centrosomes cluster to avoid a multipolar spindle formation as a multipolar spindle promotes nuclear fragmentation and subsequent cell death [292].

When addressing these open questions, we aligned our experiments based on existing studies [213,215] and focused on two time points after IS formation.

MTOC polarization towards the IS has been described in multiple settings for different cell types. The study carried out by Pulecio and colleagues reports that after 7 minutes MTOC relocalization happens in a fraction of BMDCs [213]. Another study by Ueda and colleagues characterizes the different stages of IS formation between BMDCs and CD4+ T cells. Thereby, they term stage 3 "centriole proximity". This stage happens after 2 hours of co-culture and a centriole reorientation towards the IS is reported for T cells, but not for the engaged BMDCs [215]. Therefore, we analyzed an early time point of around 10 minutes and a later time point of 2 hours of DC-T cell engagement. We first sorted CETN2-GFP BMDCs on diploid DNA content and treated them with or without ovalbumin for two hours. Following, we added naïve OT-II CD4+ T cells and immobilized the cells after the indicated time points (Figure 3.18 a,b).

When measuring the intercentrosomal distances between pairs of centrioles to determine whether extra centrosomes cluster during IS formation (Figure 3.18 c), preliminary results did not show significant changes for all conditions tested (Figure 3.18 d). The intercentrosomal distance in diploid BMDCs was around 2 μm, independent of T cell number encountered or antigen treated. All centrosomes stayed in close proximity to each other during early time points (10 minutes) of IS formation as well as in mature ISs (2 hours) [293,294]. Consequently, we conclude that extra centrosomes in BMDCs cluster during antigen presentation and T cell activation under the tested conditions.

**a** 2 hours of co-culture: OT-II naïve CD4⁺ T cells with CETN2-GFP expressing BMDCs **(control)**

**b** 2 hours of co-culture: OT-II naïve CD4⁺ T cells with antigen loaded CETN2-GFP expressing BMDCs **(ovalbumin)**

**c** **inter**centrosomal distance in CA cells

**d**

**Figure 3.18** Centrosome clustering during immune synapse (IS) formation.

(**a,b**) Immunostaining of OTII naïve CD4⁺T cells co-cultured for 2 hours with either control (a) or ovalbumin loaded (b) CETN2-GFP expressing mature diploid BMDCs. Left panels (a,b) show BMDCs with amplified centrosomes interacting with 1 T cell. Right panels (a,b) show BMDCs with amplified centrosomes interacting with more than 1 T cell. Centrioles are visualised by CETN2-GFP (green). Nuclei were counterstained with DAPI (blue). White lines depict BMDC cell outlines, whereas T cell outlines are not surrounded. Scale bar, 5 µm. (**c**) schematic representation of intercentrosomal distance (red) between two centriole pairs in DCs. (**d**) Quantification of intercentrosomal distance of amplified centrosomes in control and ovalbumin-pulsed diploid DCs co-cultured for 10 minutes (left) or 2 hours (right). Analysis was separated based on the conjugate number that was formed between DC and OT-II naïve CD4⁺ T cells (1 or more than 1 T cell). Graph displays shape of distribution, central value and variability of data analyzed. Each data point represents an individual cell. Data collected from three independent experiments performed by Peter Konopka. n.s. not significant (two-tailed, unpaired Student's *t*-test (10 minutes), Mann-Whitney test (2 hours)).

Throughout the next analysis, we focused on MTOC localization in BMDCs. We could readily observe that the T cell MTOC is relocalized during IS formation (Figure 3.19 a), but on the DCs side the result was not that clear (Figure 3.19 a-c). For the analysis, we determined the center of mass (CoM) and measured the distance to MTOC position (Figure 3.19 d). Thereby we distinguished between the following parameters: 1. Whether the DC forms a conjugate with one T cell or with multiple T cells, as this might influence the force that is generated by MTs

anchoring to the cell surface at the side of IS formation. 2. We separated the analysis based on centrosome numbers, whether one or more centrosomes are present as this influences MT nucleation capacity (Figure 3.10). 3. DCs treated with or without antigen (Figure 3.19 e), as an active IS requires p-MHC recognition by a cognate T cell via its TCR.

The data unveiled no major distance alterations between the centrosome and the CoM in all tested conditions (Figure 3.19 e). Hence, we infer that the MTOC in BMDCs is not relocated toward the IS as previously suggested for T helper synapses [213].
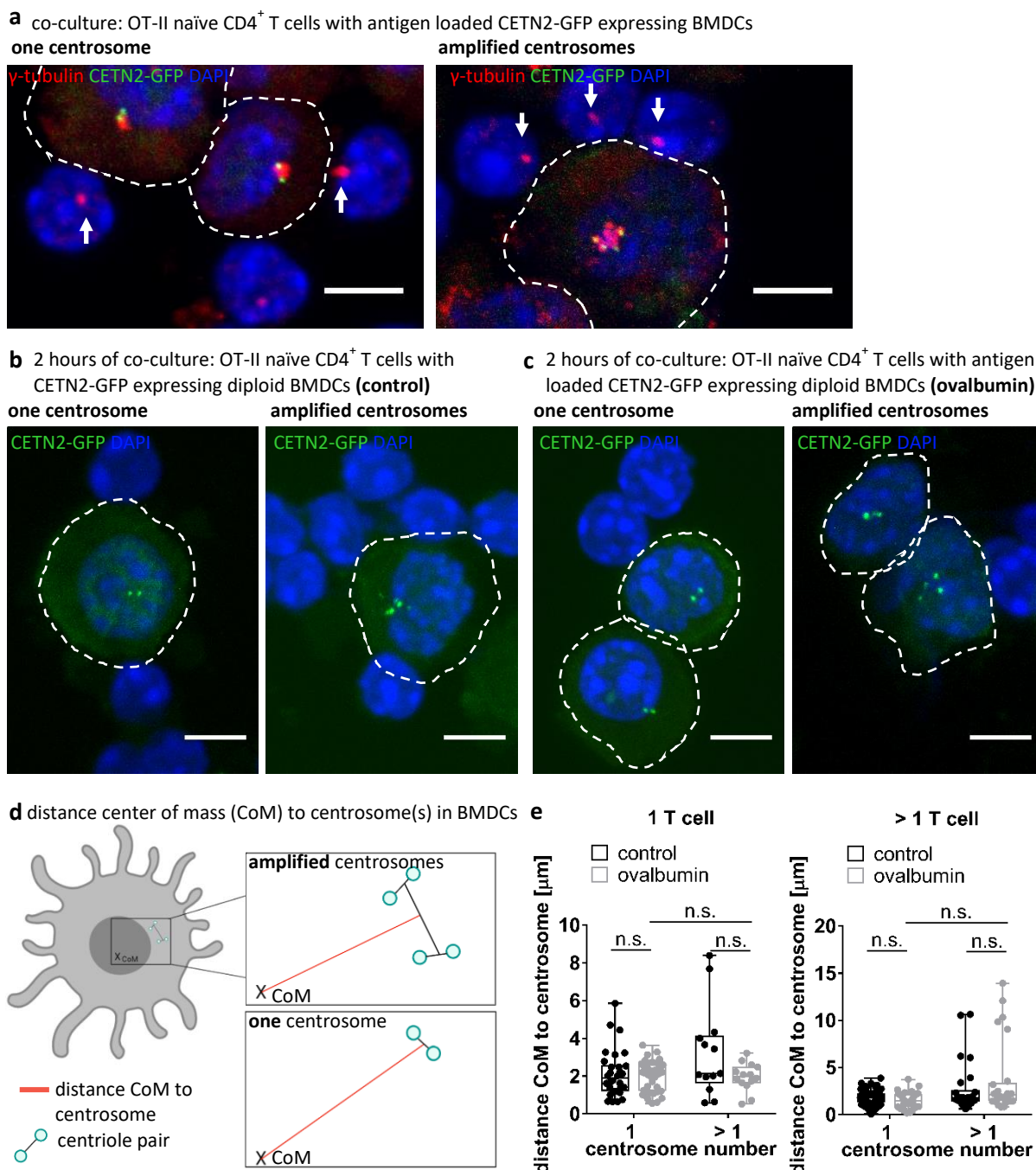


**Figure 3.19** Centrally localized centrosome in DCs during immune synapse (IS) formation.

(**a,b,c**) Immunostaining of OTII naïve CD4$^+$T cells co-cultured either control (b) or antigen loaded (a,c) CETN2-GFP expressing mature diploid BMDCs. Left panels (a,b,c) show BMDCs with one centrosome interacting with T cells. Right panels (a,b,c) show BMDCs with amplified centrosomes interacting with T cells. Centrioles are visualised by CETN2-GFP (green) and γ-tubulin (red, only in a). Nuclei were counterstained with DAPI (blue). White lines depict BMDC cell outlines, whereas T cell outlines are not surrounded. (a) White arrows indicate centrosome relocalization in T cells. Scale bar, 5 μm. (**d**) schematic representation of distance between the center of mass (CoM) and the centrosome(s) in DCs. (**e**) Quantification of distance between the center of mass (CoM) to centrosome in control and ovalbumin-pulsed diploid DCs when forming conjugates with 1 OT-II naïve CD4$^+$ T (left) or more than 1 OT-II naïve CD4$^+$ T (right) after 2 hours of co-culture. Graph displays shape of distribution, central value and variability of data analyzed. Each data point represents an individual cell. Data collected from three independent experiments performed by Peter Konopka. n.s. not significant (all, Mann-Whitney test).

Altogether, our results elicit a phenomenon of amplified centrosomes within various DC subsets. During IS formation extra centrosomes cluster and are centrally localized. Additionally, we could demonstrate that DCs with amplified centrosomes nucleate more MTs, which are linked to increased inflammatory cytokine secretion. As a consequence of this and probably further yet unknown mechanisms, T cells are activated more efficiently when primed by amplified centrosomes.

# 4. Discussion

## 4.1. Extra centrosomes in dendritic cells

This study aimed to gain a better understanding of the DC side of the IS, as many important aspects are insufficiently studied. On the T cell side as well as in B cells and NK cells, a reorientation of the centrosome takes place, which induces efficient signal transduction and activation response [197–199,295,296].

While establishing immunofluorescence stainings against centrosomal markers, we identified that 20-25% of mature BMDCs carry 2 centrosomes and 5% even higher centrosomal numbers, a phenomenon referred to as centrosome amplification. Thereby, we could confirm that ac-tubulin is an excellent marker for quantifying centriole numbers in non-adherent immune cells. Ac-tubulin nicely colocalized with other centriole and PCM components (for example CEP135, CETN2, y-tubulin) in BMDCs and T cells (Figure 3.1 a,b and Figure 3.2 a) confirming that extra centrosomes indeed represent bona fide centrioles.

Cells owning 2 centrosomes is a neglectable phenomenon in cycling cells. During proliferation, centrosome duplication occurs concomitantly to DNA duplication, leading to the presence of 2 pairs of centrioles in G2/M phase [236]. Certainly, after analysing cell cycle progression of these cells, thereby identifying that BMDCs are arrested during the cell cycle (Figure 3.3 a,b), we could no longer neglect the observation of 2 or more centrosomes. We analyzed further subsets of DCs and could identify that dermal DCs as well as splenic and LN DCs show increased centrosome numbers emphasizing that this phenomenon must have a physiological relevance *in vivo*. This led to the expansion of our initial goal and we formulated additional questions addressing different aspects of centrosome amplification in DCs: First, we wanted to understand the underlying mechanism(s) of CA and second, we wondered whether increased centrosome numbers are beneficial for a proper immune response or present a disadvantage. Thereby, we focused on the impact of extra centrosomes during T cell activation.

To address the first question, we sought to understand the underlying mechanisms of CA. Therefore, we analyzed immature BMDCs, in which the phenomenon of higher centrosome numbers was significantly decreased (Figure 3.1 c), indicating that BMDCs maturation, which was caused via TLR4 stimulation, has an influence on centrosome numbers. TLR signaling is a complex pathway, which can be separated into three major branches of activation: mitogen-activated protein kinase (MAPK), nuclear factor-κB (NF-κB) and IRFs (Figure 4.1). Depending on the nature of stimuli, differing TLRs are induced, which lead to distinct signal transduction through the TIR-domain signaling adapter molecules: MYD88, TRIF, TRAM and TIRAP/MAL, eventually activating MAPK, NF-κB and/or IRFs. Those promote the induction of pro-

inflammatory cytokines and type I INFs, among other factors. As TLR4 represents a special receptor, which can interact with various TIR-domain signaling adapter molecules [80], a wide field of possible molecules arise that could influence centrosome numbers. Therefore, it could well be conceivable that the stimulation of other TLRs or other PRR also lead to increased centrosome numbers. By analyzing different TLR agonists and their downstream targets, this could narrow down molecules, which might be involved in the pathway of generating extra centrosomes. To go one-step further, the generation of extra centrosomes could also be a more general response from DCs to stress. So far, we cannot rule out the possibility that stress induces CA and vice versa that CA favours a stress response as reported in the studies by Arnandis and colleagues, in which amplified centrosomes evoke oxidative stress and non-cell-autonomous invasion [285].

Thereby, it might be of relevance that the stimulus does not reach higher than a certain threshold, as otherwise cell-death pathways are induced rather than a protective cellular response [297].

As dermal DCs have been isolated from split ear sheets, which were separated by mechanical force and subsequently floated 3 days in media containing a chemoattractant, these cells represent a stimulated stage, whereas DCs taken from spleen and LNs of healthy mice are taken under steady state conditions, potentially clarifying why centrosome numbers overall are a bit lower in this fraction (Figure 3.4 b,c and Figure 3.5 c,d). It would be of interest to study mice under inflammatory conditions to determine the influence on centrosome numbers. Thereby, differing stimuli as well as various concentrations should be tested.
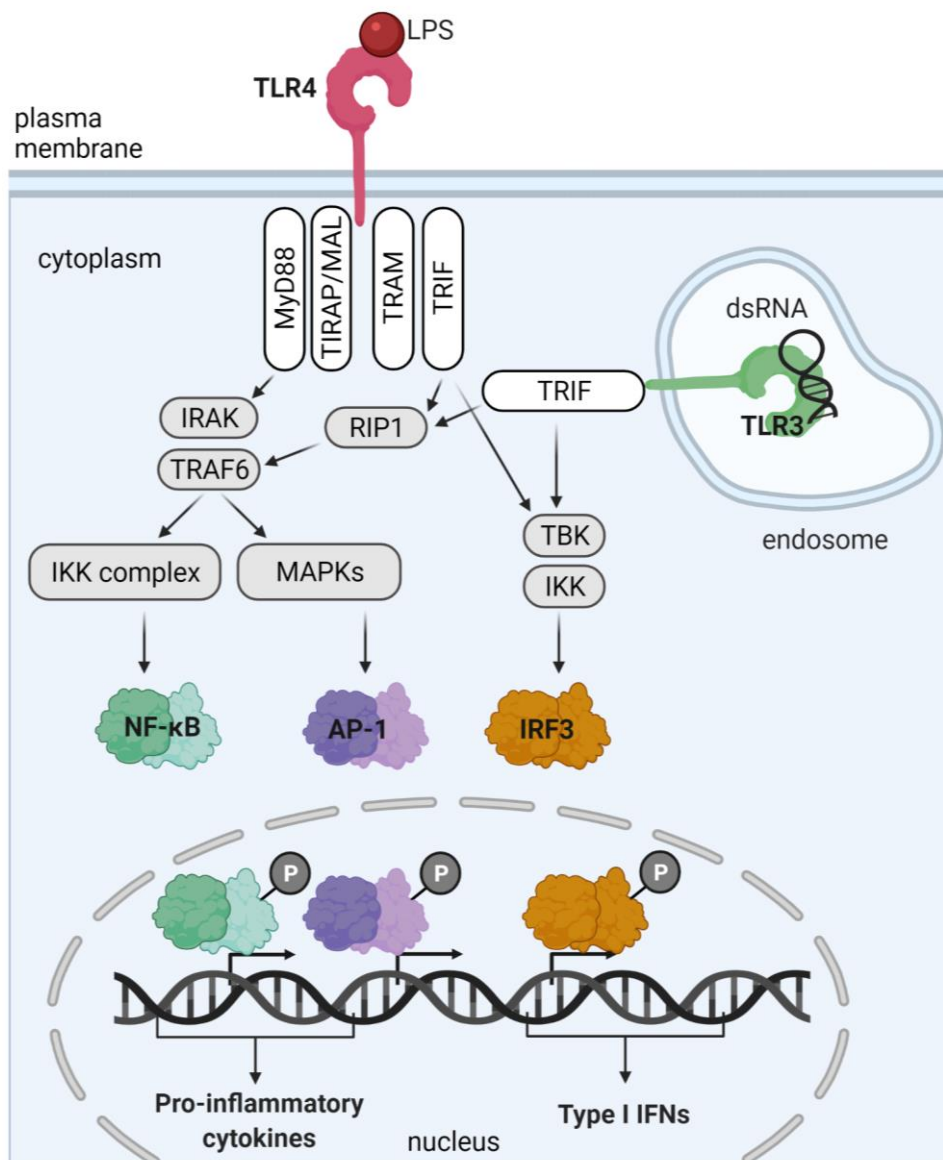
**Figure 4.1** Toll-like receptor (TLR) signaling pathways.

After antigen recognition by a specific TLR, adaptor molecules (MyD88, TIRAP/MAL, TRAM or TRIF) are recruited which initiate intracellular signaling cascades. MyD88 recruits IRAK4 and TRAF6 upon ligand stimulation, leading to further downstream activation of the IKK complex and MAPKs signaling. Activation of these proteins cause phosphorylation (P) of transcription factors NF-κB and AP-1, respectively. The adaptor molecules TRAM and TRIF recruit TBK. TBK together with IKK phosphorylate (P) the transcription factor IRF3. Phosphorylated transcription factors translocate into the nucleus and bind to DNA, thereby initiating the transcription of pro-inflammatory cytokines and type I IFNs. Image adapted from Takeuchi and Akira, 2010.

The alterations in the overall number of amplified centrosomes as well as the differences in specific DC subsets (Figure 3.4 b,c and Figure 3.5 c,d) can possibly be explained by their specific tissue environment and the specialized functions, which influence the DC status [298]. Dermal DCs for instance are constantly exposed to foreign substances due to their location in peripheral barrier tissues. Hence, DCs from distinct tissues should be analyzed separately, as this might give additional details on the pathway how extra centrosomes arise and their physical function. We used an ImageStream analyzer, which is able to work with small cell populations, to identify single centrioles which have a size of 450-500 nm in length and 200-250 nm in diameter, but the resolution was not high enough (Figure 3.5 a). This led to additional steps when investigating on centrosome numbers, as we first had to apply FACS followed by high-resolution imaging. As both aspects are combined in the ImageStream analyzer, less starting material is needed as fewer intermediate steps take place where cells can be lost.

When analyzing single tissues, one could expect that DCs from barrier organs such as lung, intestine nasal- or oral mucosa own higher centrosome numbers as these cells are constantly exposed to local microbiota, food particles, inhaled particles such as pollutants as well as mechanical processes that occur in certain tissue, e.g. peristalsis in the intestine or breathing in the lung.

Another aspect, which might be of interest is the analysis of pDCs, which has not been conducted so far. pDCs leave the bone marrow fully differentiated whereas cDCs derive from pre-committed precursor cells that leave the bone marrow [5,24,32]. This could lead to further insights whether the differentiation process has an influence on extra centrosome generation. At the same time, it is also of highest interest to clarify if the phenomenon of extra centrosomes in DCs is also present in other cells of the immune compartment and whether human DCs contain extra centrosomes. The procurement of human samples is difficult, yet the use of foreskin could conceivably be used to answer this question. So far, we were able to gain preliminary data from peripheral blood mononuclear cells of fresh human blood and post-mortem tissue of spleen and LNs. MHCII+/CD11c+ cells isolated from fresh blood samples did not possess extra centrosomes, whereas MHCII+/CD11c+ cells isolated from post-mortem tissue showed about 10% of extra centrosomes (data not shown).

### 4.2. Mature dendritic cells arrest during cell cycle progression

Amplified centrosomes/centrioles are a well-appreciated hallmark of various types of cancer and can cause chromosomal instability, which can lead to aneuploidy and chromosome missegregation during proliferation [276]. They additionally correlate with advanced tumor progression and an overall poor clinical outcome. Besides tumor cells, it has only recently been reported that cycling progenitors of olfactory sensory neurons contain amplified centrioles. In these cells, amplified centrioles seem to be part of normal developmental programming [299].

Focusing on DCs, we noticed that cancers arising from this cell type are extremely rare. Cancer of DC origin belong to the group of neoplasms, which are divided into the one's that derive from precursor cells, to which the blastic plasmacytoid dendritic cell carcinoma (BPDCN) belongs and into a mature lymphoid neoplasm where the heterogeneous group of histiocytic/dendritic cell neoplasms is part of [300]. The incidence of BPDCN is 0.000045% [301] whereas the latter one makes up less than 1% of all neoplasms [302].

This made us wonder whether a possible explanation for such low case numbers is the proliferation capacity of DCs and whether the proliferation capacity influences the generation of extra centrosomes. In particular, as it is known, that malignant as well as normally developing cycling cells own amplified centrosomes, this seemed to be a fundamental concern that needed to be addressed.

Therefore, we analyzed cell cycle progression to identify if DCs are proliferating. The canonical cell cycle has four consecutive phases: G1, S, G2 and M, whereby the progression is regulated by cyclin-dependent kinases (Cdks) and their association with cell cycle specific cyclins [303]. We could detect that dermal DCs as well as mature BMDCs are not transiting through S-phase (EdU incorporation) and G2-M phase (staining against pH3) (Figure 3.3 a,b and Figure 3.4 d,e). Additionally, we analyzed Ki67, a protein that functions during interphase and mitosis [304] and drew the conclusion that cells do not arrest in G0, as the cells were Ki67 positive (Figure 3.3 c and Figure 3.4 f). At the same time, we also had a look at the DNA content by flow cytometry. Thereby, we observed that a smaller fraction of dermal as well as mature BMDCs showed twice the amount of DNA, indicating that these cells are either transitioning through S/G2/M phase during proliferation or, which seems to be more likely, that these cells arrested during cell cycle progression. Due to our EdU and pH3 analysis, we concluded that the latter case is more relevant in DCs.

There are three possibilities how the cells could have gained twice the amount of DNA. One could be explained by DCs arresting in G2 phase were the cells normally own duplicated DNA. The second possibility could be that cells successfully replicated their genome but did not perform cell division. This alternative cell cycle is termed endoreplication and two forms have

been described: Endocycling, where cells alternate between G and S-phase, or endomitosis, where cells slip through mitosis. A third explanation for an increased DNA content could be a failure during cytokinesis. Both, endoreplication as well as cytokinesis failure leads to cells, which are arrested in G1 phase, but contain twice the amount of DNA [303].

To address these aspects, further studies are needed, for example by analyzing cell cycle specific proteins such as cyclins, Cdks and Cdk inhibitors. This could clarify in which cell cycle stage the cells arrest. By evaluating the nucleus, one could address the second possibility in the absence of cell division. Cells that have performed endoreplication should be mononucleated (nuclear polyploidy: increase of the amount of DNA per nucleus) while cells that failed during cytokinesis should have two nuclei (cellular polyploidy: increase of nuclei number per cell) [303]. Another solution to this problem would be the use of fluorescent, ubiquitination-based cell cycle indicator (Fucci). This system allows to explore cell-cycle dynamics in a spatio-temporal pattern. Using targets (chromatin licensing and DNA replication factor 1 (Cdt1) and Geminin) of E3 ubiquitin ligases, SCF$^{Skp2}$ and APC/C$^{Cdh1}$ (anaphase-promoting complex/cyclosome). SCF$^{Skp2}$ targets Cdt1 during S/G2 for degradation, whereas APC$^{Cdh1}$ targets Geminin during M/G1 phase for degradation, leading to an accumulation of Cdt1 in G1 and Geminin in S/G2/M. Both ligases thereby function in a cell cycle dependent manner, as the SCF$^{skp2}$ is a direct target of the second ligase, hence generating a feedback loop. Sakaue-Sawone and his colleagues used this dependency to track the cell cycle stage; therefore, they fluorescently tagged Cdt1 with a red fluorescent protein and Geminin with a green fluorescent protein. This generates in the end red cells in G1, yellow cells during G1/S transition and green cells during S/G2/M phase [305].

Even though we can clearly identify that DCs demonstrate a heterogeneous cell cycle position, we claim that DCs are terminal differentiated, as they do not proceed through the cell cycle. As we observed that a certain percentage of cells are tetraploid, cells started proceeding through the cell cycle in which they did not only replicate their DNA but also duplicated the centrosome. The phenomenon of being polyploid during homeostasis has been described for approximately 30% of human hepatocytes before. Liver cells experience whole-genome duplications as well as supernumerary centrosomes [303]. As only 17% of mature BMDCs own higher DNA content, this explains only approximately half of the higher centrosome numbers (~ 30% of mature BMDCs) but not why some cells have more than 2 centrosomes. This prompted us to search for secondary pathways that could initiate centrosome amplification.

### 4.3. Polo like kinase 2 is a critical player during extra centrosome development in dendritic cells

Centriole biogenesis is a tightly controlled process, securing that the centrosome is duplicated only once per cell cycle. Yet, there are two mechanisms described in the literature how centrosomes can overamplify. One is termed 'overduplication', where excess seeding of new procentrioles happens, and the second one is termed 'centriole accumulation', where alterations in cell division induce higher centrosome numbers. Observing around 17% of polyploid BMDCs under the tested conditions (Figure 3.3 d), CA in this subset is probably caused by the centriole accumulation pathway whereas CA in diploid DCs is linked to overduplication of centrioles as described above (Figure 3.6).

The serine/threonine kinases Plk4 and Plk2 are two out of many proteins that are localized to the centrosome and are involved in its replication. We started analyzing these two proteins, because Plk4 is considered the master regulator of centriole duplication. In previous studies, it has been shown that no new procentrioles could be assembled when lacking *Plk4* and that excessive numbers of new centrioles were sprouting when *Plk4* was overexpressed. This led to CA and furthermore to spontaneous initiation of tumorigenesis [296,306,307]. Similar results for centriole numbers were obtained when *Plk2* was down- [308] or upregulated [272].

As we detected extra centrosomes in mature BMDCs, we analyzed mRNA levels from both kinases during the maturation process and noticed that the expression levels of both kinases are drastically increased shortly after LPS stimulation. Thereby, *Plk4* increased by 2-fold and *Plk2* by 12-fold (Figure 3.7 a,b). From here, we went on by manipulating expression levels of Plk4 and Plk2 to establish a causative link between elevated expression levels and centrosome numbers. For Plk4, we used the pharmacological inhibitor Centrinone, but did not receive drastic changes in the number of extra centrosomes (Figure 3.8 d,e). In contrast to these results, we observed a rescue effect of extra centrosome numbers in mature *Plk2*$^{-/-}$ Hoxb8 derived DCs, which exhibit a significant decrease of cells with 2 or more centrosomes (Figure 3.9 f). Thus, we concluded that the formation of extra centrosomes in DCs is linked to Plk2, yet it needs to be clarified if this is the only centriole-associated molecule that is involved as well as the underlying molecular mechanism(s). Interesting candidates are Fbxw7, nucleolar protein nucleophosmin 1 (NPM1), glycogen synthase kinase-3 (GSK3) and cyclin E/Cdk2 complex, as all of these proteins interact with one another [272,273,309–313].

Fbxw7 is part of the SCF ligase complex and gets phosphorylated by Plk2 conducting the degradation of Fbxw7 [272]. When Fbxw7 is abrogated, SAS-6 is stabilized and increasingly recruited to the parent centriole, which contribute to multi-numerous centrioles [273]. Furthermore, the destabilization of Fbxw7 also leads to increased cyclin E levels, thereby

controlling cell cycle progression and centriole duplication [272]. Tarapore and colleagues reported that when they ectopically expressed cyclin E, this caused a persistent activation of cyclin E/Cdk2, which in turn resulted in a miss-coordination of centrosome and DNA duplication cycle. More precisely, this process initiated centrosome duplication way earlier than DNA replication [309].

On the other hand, it has been reported that Fbxw7 is stabilized through the interaction of the subunit Fbwx7γ with NPM1 in the nucleus [312]. NPM1 itself is important for the induction of centriole duplication. Thereby, centrosome-bound NPM1 is removed from the centrosome via phosphorylation by Plk2 and/or cyclin E/Cdk2 complex [310,311,313].

Besides Fbxw7 and NPM1, GSK3 is also phosphorylated by Plk2 [314]. GSK3 inhibition has been described to induce cellular senescence in human amnion cells [315]. Additionally, GSK3 interacts with cyclin E/Cdk2 complex leading to its degradation [316]. Evidence pointing out how this complex system is involved in extra centrosome generation in DCs is currently missing, therefore, DC specific $Plk2^{-/-}$ mice would be extremely helpful.

Next to the function in centrosome biogenesis and the cell cycle, Plk2 has also been described in the context of mitochondrial dysfunction promoting oxidative stress, cellular response to DNA damage and in post-mitotic neurons during neurodegenerative disease development [314,317,318], indicating a complex role of Plk2 during various stress-dependent situations.

As Plk2 is activated during G1/S transition when procentriole formation is initiated, the question remains whether other centriole-associated proteins are involved in CA generation, as some of the cells might be arrested in G2 phase of the cell cycle. Therefore, Plk2 might rather be part of the 'centriole overduplication' process (excess seeding of procentrioles) than being involved in the 'centrosome accumulation' (alterations in cell division) pathway. An interesting candidate for the second pathway could be Plk1. Plk1 is another Plk family member, but is predominantly expressed during late S/G2 and M-phase and responsible for diverse mitotic and centrosomal events [319]. Of note, phosphorylation of Plk1 has been linked to Plk2 before [320].

Taken together, we conclude that Plk2 is an important driver of CA in DCs, however we do not yet fully understand the underlying mechanism, therefore further studies will be necessary. Besides that, additional studies are needed to understand the physiological role of extra centrosomes in DCs.

## 4.4. Dendritic cells with amplified centrosomes nucleate more microtubule filaments

It was reported that extra centrosomes fulfil their function by nucleating MTs and even being capable of generating higher MT numbers, which led to invasive cell behaviour [321]. Consequently, we wondered whether DCs with increased centrosome numbers nucleate more MTs or contain an altered cytoskeletal structure. We tested this under co-culture conditions, when ovalbumin loaded DCs were able to interact with OT-II naïve CD4+ T cells. We observed indeed that DCs with 1 centrosome nucleated on average 20% less MTs than cells owning 2 or more centrosomes (Figure 3.10, Figure 4.4).

As mentioned above, cells with elevated MT numbers showed altered invasive behaviour. This phenomenon was described in tumor cells giving them an advantageous feature that led to increased metastasis and tumor progression [321]. Having this in mind, it would be extremely interesting to investigate whether migratory DCs demonstrate an altered migration behaviour. Nevertheless, we postponed this aspect and instead concentrated on the initial goal to analyze DC behaviour during IS formation as MT are central players during this operation. Most of the MT-dependent tasks during IS formation have been described in T helper or cytotoxic T cells [198,208,216]. For example, the MT-dependent delivery of secretory vesicles to the plasma membrane and the transport of recycling endosomes containing TCRs and additional signaling transduction molecules [222–224]. On the DCs side of the IS, studies have highlighted the role of MT-dependent transport for multivesicular late endosomal-lysosomal antigen-processing compartments, also known as MIIC, which deliver p-MHCII to the IS via MT-dependent trafficking [102,103]. Still, the knowledge gained on how the centrosome acts as vesicle trafficking organizer and how MT-transport is regulated during IS formation on the DC side is less well understood.

Thus, we went on with a more general approach analyzing T cell activation by measuring their IL-2 release and proliferation capacity after performing a mixed lymphocyte reaction with 2 distinct DC subsets. One termed 2N2C and one termed 2NCA, both owning diploid DNA content but the latter one possessing higher extra centrosome numbers.

To achieve the separation based on centrosome numbers in DCs we used CETN2-GFP expressing mature BMDCs and enriched the diploid fraction on either low or high GFP expression (Figure 3.11 a,b). A small fraction of sorted cells was used for quantifying centrosome numbers. Samples showed at least a ratio of 1.5 of CA in 2NCA over CA in 2N2C (Figure 3.11 c). After ensuring that these populations carry the same lineage characteristics (Figure 3.12 a), we proceeded with T cell activation analysis. We determined that DCs with

extra centrosomes optimize CD4^{+} T cell activation (Figure 3.13 a-c, Figure 4.4), raising the question of how this is accomplished.

For B cells, it has been reported that when artificially inducing CA by *Plk4* overexpression, multiple MTOCs promote antigen presentation by improved antigen processing. We wondered whether this also holds true for DCs and analyzed T cell activation after loading DCs with ovalbumin-peptide. In this set up, the antigen bypasses the processing part and can directly be loaded on the cell surface expressed MCHII molecules. When performing this assay, we obtained similar results when DCs were treated with the whole protein (Figure 3.14 a,b), indicating that peptide processing might not the source of optimized T cell activation caused by extra centrosomes in DCs.

Next, we wanted to address whether peptide presentation by MCHII-complex could cause the optimization. p-MHCII move along MT to the cell surface [102,103]. Since more MT are present, it could be that more antigen is presented. So far, we were not able to address this question, since there is no specific antibody available against the MHCII-peptide. To circumvent this technical problem, we purified an antibody that is supposed to target MHCII- loaded with the model antigen hen egg lysozyme (HEL) (I-Ak:HEL46-62) from hybridoma cells AW 3.18.14 CRL-282 [322]. Unfortunately, we did not detect any specific binding, neither with an imaging approach nor with flow cytometry (data not shown). Consequently, we cannot draw any conclusions about the relationship of peptide presentation and extra centrosome numbers. For an alternative approach, the use of an auto-quenched version of ovalbumin could be used. The protein becomes fluorescent during proteolytic cleavage, allowing its visualization and tracking at the end of the processing step and during presentation [323].

We could already demonstrate an optimized T cell activation capacity for CD4^{+} T cells and wondered whether cross presentation of antigens from DCs to CD8^{+} T cells could also be improved under altered centrosome numbers. As this process involves a distinct antigen processing and presentation machinery [110] it may help to shed further light on the underlying molecular mechanisms, which are involved.

In the next section we addressed vesicle trafficking, as this process has been demonstrated to be MT-dependent [197,198]. Hence, we analyzed lysosome numbers in both DC subsets, and observed significantly higher lysosome numbers in 2NCA cells (Figure 3.16 a). From here on, we focused on cytokines as these belong to the molecules that are transported in MT-dependent vesicles and have been associated to centrosomes [198,221]. For example, it was recently reported that centrosomes in macrophages take over an important role in the production of cytokines to inflammatory stimuli [284]. Further data demonstrated that cells with extra centrosomes harbor a distinct secretory phenotype so called centrosome–associated

secretory pathway (ECASP) [285]. In agreement to these reports, we could present that DCs containing higher centrosome numbers secrete larger amounts of T cell and neutrophil attracting and activating cytokines (Figure 3.16 b,c, Figure 4.4) [286,288–290].

We further analyzed their relative gene expression and observed for 2 (CCL17 and CCL22) out of 5 an alteration between 2N2C and 2NCA, whereas the other 3 (CCL5, IL-6 and CXCL1) showed similar mRNA levels in the tested conditions (Figure 3.17 a). A possible explanation for this could be that expression of CCL17 and CCL22 is regulated by a feedback loop, which leads to higher expression after increased secretion of CCL5, Il-6 or CXCL1. For the micro RNA (miRNA) miR-9, it has been reported that CCL17 and Plk2 are both gene targets, which are downregulated after miR-9 overexpression, linking both molecules to the same partner [324]. Additionally, Plk2 was linked to IL-6 and CXCL1 regulation in diabetes. The depletion of Plk2 significantly suppressed the production of these inflammatory cytokines [325]. A possible link is presented by the transcription factor NF-κB, which targets all of these cytokines [326–330] and as has been linked to Plk2. In activated neurons, Plk2 regulates NF-κB thereby overtaking an important task during homeostatic synaptic plasticity [331]. In the future, it needs to be clarified, if these aspects are of relevance in DCs.

We further focused on the function of CCL22 and CCL17. Both cytokines are responsible for CCR4-mediated T cell attraction by binding to different binding sides at the receptor [290]. By performing transwell migration assays with WT or CCR4$^{-/-}$ T cells, we observed that for CCR4$^{-/-}$ T cells, the supernatant of 2N2C and 2NCA (having more CCL17 and CCL22) cells led to no significant change in transmigration, whereas we observed elevated transmigration in WT T cells (Figure 3.17 c). From this we conclude that the increased amount of both cytokines, as a response to extra centrosomes in DCs, overtake an important function in attracting T cells. To gain an even deeper knowledge, CCL17 neutralizing RNA aptamers could be added as an additional control in the transmigration assay [63]. Even so, we could demonstrate that T cells are more easily recruited to DCs with amplified centrosomes due to increased cytokine secretion; this aspect may not be of relevance for the mixed lymphocyte reaction that was performed in a small reaction tube and may rather play a more prominent role under *in vivo* conditions.

As CCR4 is expressed by Th2 and T regs cells [289], CCR5 a receptor of CCL5 on Th1 cells [332] and IL-6 and CXCL1 has been linked to induce Th17 T cell differentiation [287,333], it would be crucial to analyze in which T helper subset CD4$^+$ T cells differentiated and which memory cells are recruited to evaluate further immune responses.

Besides the function of CXCL1 in T cell differentiation, the cytokine also functions in recruiting and activating neutrophils to the site of action [288]. Therefore, analysis of neutrophil behaviour would be a nice aspect for future studies. Thereby, one could use a bigger approach studying

the *in vivo* situation, comparing DCs with normal centrosome numbers with DCs showing altered centrosome numbers and how those influence migration and immune cell responses. Considering that an inflammatory cytokine milieu is dependent on the microenvironment and needs to be precisely controlled as too much can promote autoimmune defects and other pathogenic conditions [287,289].

So far, we did not have a good model system in hands, which allows us to address these last points, but as Plk2 seems to be a promising tool to alter centrosome numbers, these studies could be performed in the near future. For now, it has to be kept in mind that DC separation based on centrosome numbers by FACS is not ideal, as it did not lead to a complete separation of cells. Nevertheless, studies in which CA was artificially induced only led to 10-20% of cells with CA, which was already enough to cause significant changes in cellular behaviour [296], similar to what we observed with FACS-based separation. Therefore, the effects have to be even more drastic on a single cell level in comparison to the previously described bulk analysis.

### 4.5. MTOC behavior during immune synapse formation

We were able to demonstrate that amplified centrosomes in DCs correlate with an optimized T cell response and increased secretion of immune cell activating and attracting cytokines. Additionally, we wondered how centrosomes behave during the process of forming multicentric ISs in particular when multiple T cells interact with one DC.

As centrosomes function in nucleating MTs, we addressed whether extra centrosomes have a higher capacity to nucleate MTs, which was indeed the case (Figure 3.10). This analysis was done comparing centrosome numbers independent of DNA content and independent of the number of interacting partners. Both aspects are important to gain a deeper understanding, as polyploid cells are generally larger, therefore providing more space for spatial expansion, which might lead to less steric hindrance during MT nucleation and elongation. Additionally, polyploid cells display a greater cell surface area, offering more space for conjugate formation. As the formation of multiple synapses could influence the generation of new MTs or alter MT stability, this might further affect MT numbers. That is why also the number of interacting T cells should be taken into account when analyzing MT numbers. To address both of these aspects, it would be helpful to sort for diploid BMDCs before performing further analysis. In the next step, a separation based on interacting T cell numbers could be performed.

In cancer cells, it has been described that amplified centrosomes form a cluster, in this way avoiding the formation of a multipolar spindle, which can cause cell death [292]. We wondered what the conformation of multi-numerous centrosomes is during IS formation and if a dynamic

behaviour of individual centrosomes can be observed. Preliminary data were generated during early and late IS formation between naïve T cells and diploid BMDCs treated with or without ovalbumin. Under all condition tested, no significant increase in the distance between pairs of centrioles (intercentrosomal distance) was observed. These results suggest that extra centrosomes cluster in DCs during IS formation (Figure 4.4). These preliminary data were generated under fixed conditions. To mimic a more physiologically approach *in vitro*, we could use microfabricated devices to reconstitute 3D cellular environments. These devices are commonly referred to as 'Lab-on-a-Chip' or 'Micro Total Analysis Systems' [334] and allow imaging of the immunological synapse as well as the underlying cytoskeletal dynamics with high spatio-temporal resolution as demonstrated before [196].

Additionally, we did not formally take into account whether an active IS is present. To address this aspect, one should include the activation status of the interacting partner (T cells). For instance, one could perform immunofluorescence stainings against activated signaling molecules such as phosphorylated VAV (pY174-VAV) or PKC-θ [214]. When performing life cell imaging, measurement of calcium flux could be included [190].

An experimental approach on how centrosome clustering influences T cell activation could be performed by using so called "declustering agents". These agents create a change in centrosome conformation, from clustered centrioles to separated centrioles. This makes them interesting candidates for cancer treatments, as the declustering of centrosomes leads to major mitotic errors in cycling cells and eventually ensures cell death [335]. Nevertheless, these drugs have also been reported to not only influence centrosome conformation but also MT formation [335], thereby altering cytoskeletal dynamics in an unspecific manner. To avoid these secondary aspects an alternative approach could be performed by using a modelling system, which combines mathematical calculations with the obtained experimental data.

Finally, we investigated MTOC positioning in BMDCs. For many other immune cells, it has been described that reorientation of the centrosome occurs during IS formation. This reorientation influences downstream signaling cascades and induces polarized delivery of cytokines [213]. In the conditions we tested, we could not observe such a reorientation, as the centrosome(s) showed similar distance to the center of mass in control and ovalbumin treated samples, no matter whether they interact with one or multiple target cells. We conclude that under our conditions the centrosome is centrally localized (Figure 4.4). It could well be that a reorientation of the centrosome in monofocal synapses is more beneficial but that in the formation of multiple synapses with a multicentric conformation, which happens to be the case for DCs, a centrally localized centrosome is the preferential option. To compare whether MTOC translocation is favourable or centrosome localization in the center is the preferred

configuration, a modelling approach could be useful to answer which centrosome configuration is best suited under which condition.

Sarkar and colleagues introduced such a modelling system, in which they studied MT capture time at the IS in T cells [212]. They conclude that the site of IS formation is an essential factor, which determines the underlying kinetics. When extending the initial model with our parameters such as centrosome polarization and alteration in MT numbers, we could gain information on how T cell activation in a multi-conjugated IS is influenced.
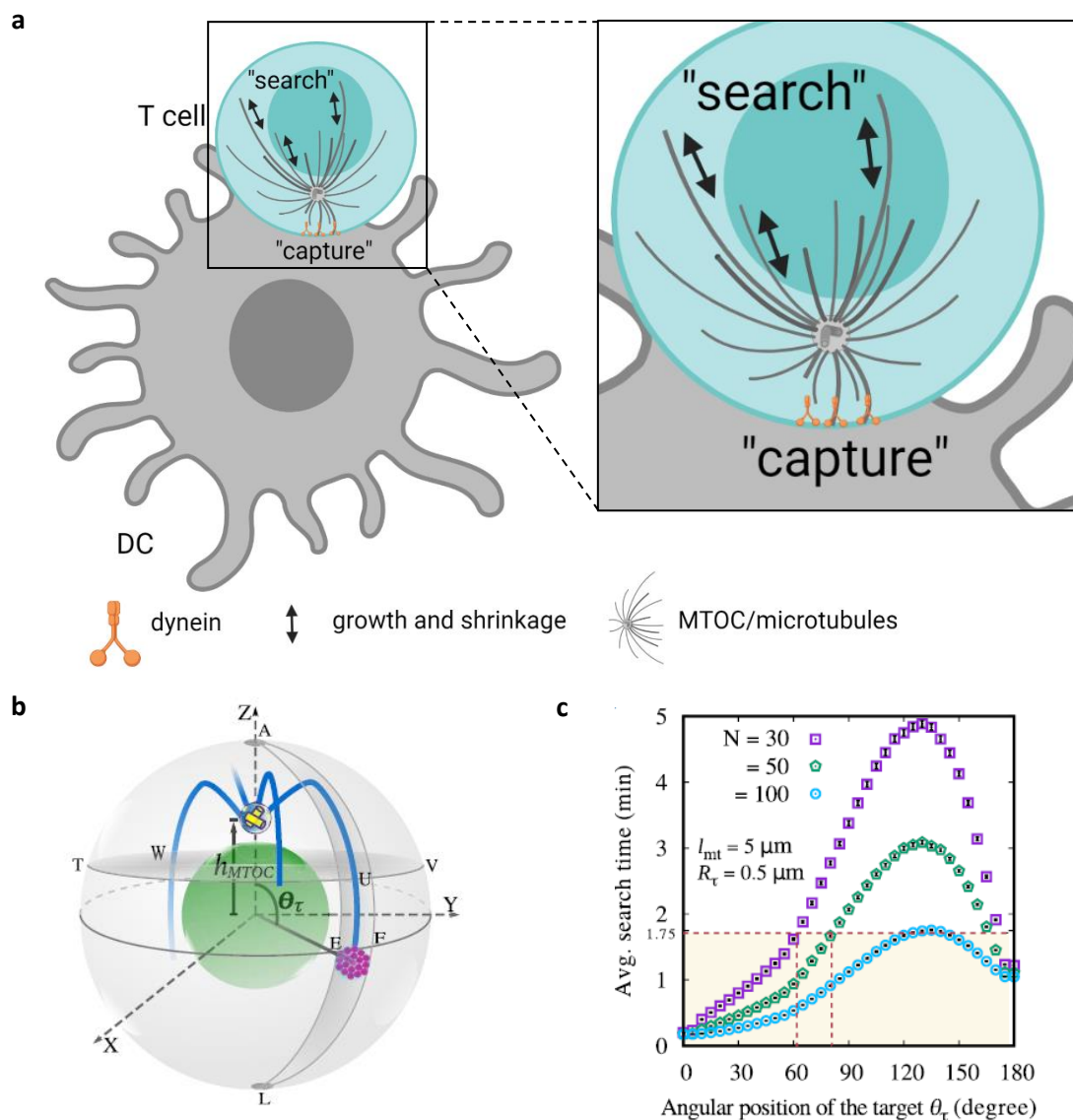


**Figure 4.2** Schematic representation of an immune synapse (IS) modelling system.
(**a**)The focus is on the search and capture efficiency of dynamic microtubules (MTs) from the microtubule organizing center (MTOC) in T cells. Thereby, "search" refers to MT growth and shrinkage into the periphery, whereas "capture" refers to MT anchoring to the cell cortex at the side of the IS via dynein. (**b**) Graphical sketch of the mathematical modelling system, indicating the parameters that are taken into account. (**c**) Graph displays average search time of MTs in dependency to the angular position in which MTs nucleate from the MTOC. (b, c) Graphics taken from Sarkar et al., 2019.

A missing key component in understanding MT behaviour during IS formation are the underlying mechanisms of how MTs attach to the cell cortex. When analyzing MT numbers in DCs, we observed that MTs mostly approach the T cell horizontally (Figure 3.10 a), indicating that the proposed model of "cortical sliding pathway" could apply in DCs. This model describes dynein in a fixed position at the cell cortex and a sliding of MTs along them [200]. As we observed the horizontal approach in 2D settings, there is still the possibility that MTs reach the target cell perpendicularly under physiological conditions. The perpendicular approach is represented by a second model, the "capture-shrinkage pathway" where dynein attaches (capture) to the MT plus ends which undergo dynamic instability (shrinkage) [201]. So far, we cannot draw any conclusion if one or both models apply in DCs, hence this should be included in the proposed experimental set up for analyzing MTOC behaviour with 'Micro Total Analysis Systems'.
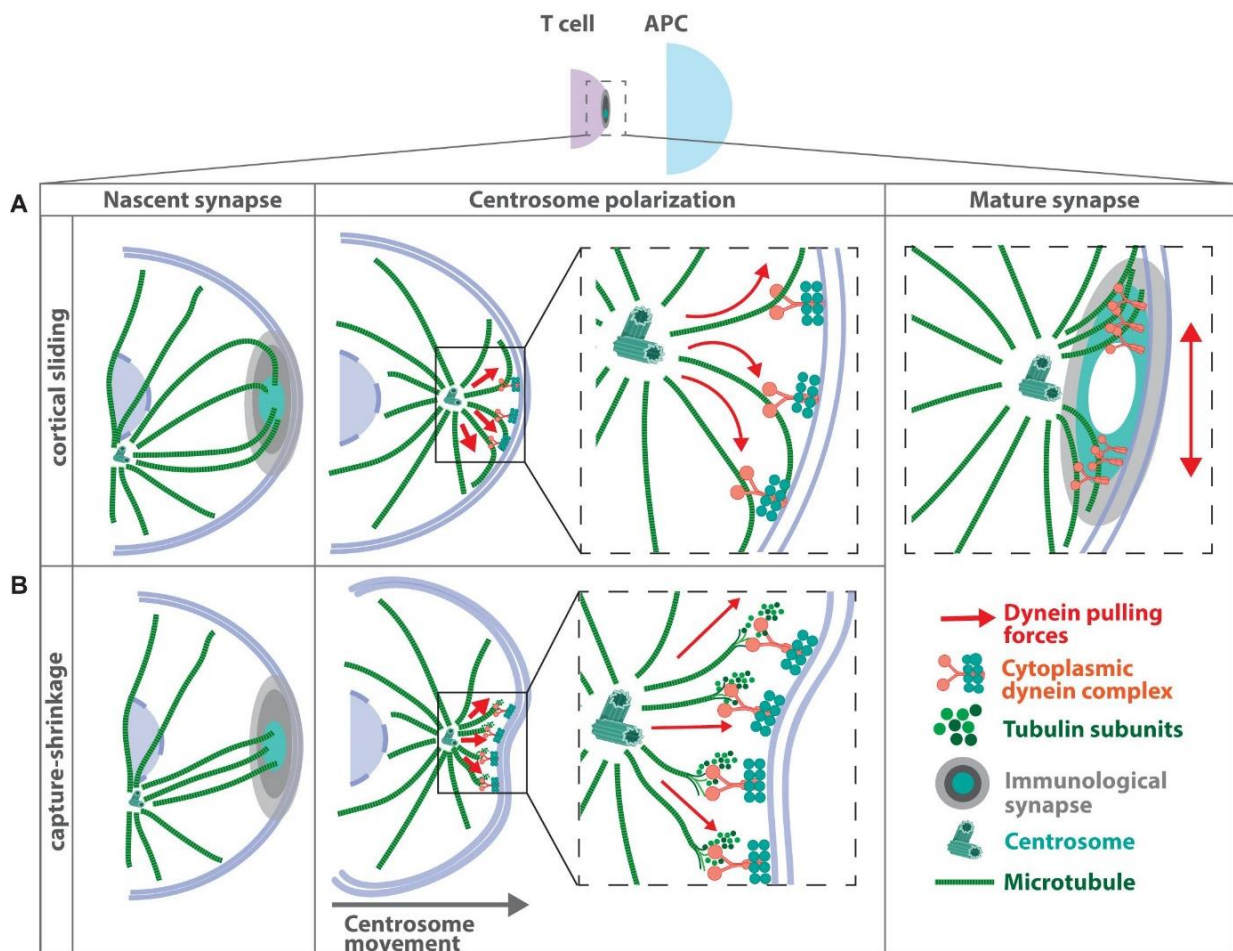


**Figure 4.3** Mechanisms of microtubule (MT) anchoring to the cell cortex.

In T cells, a reorientation of the centrosome takes place during the formation of an immune synapse. Two models have been introduced how MTs are anchored on the cell wall, thereby generating force on the centrosome leading to its reorientation. In A, the cortical sliding mechanisms is depicted and in B, the capture-shrinkage model. Picture taken from Kopf and Kiermaier, 2021.

These microfabricated devices are typically made of silicone rubber. In more detail, they consist of chambers that can be formed between glass and polydimethylsiloxane (PDMS). PDMS is a biocompatible and optically transparent elastomer, making it powerful tool for light microscopy. These chambers formed of PDMS can be produced in various shapes, thereby being able to mimic and manipulate 3D cellular environmental parameters such as pore sizes, micro-geometry and micro topology. To be able to build such chambers in various conformations, first wafers need to be fabricated that serve as templates. These wafers can be generated by photolithography, therefore photosensitive material is coated on a silicon ship and a photomask applied. The photomask is designed beforehand by computer assisted design software and bears microscale patterns. When exposing the silicon ship to high-intensity ultraviolet light, the photomask protects some regions of the photosensitive material whereas the exposed material dissolves. In this way, wafers containing specific microscale pattern are generated. Another approach to generate 'Micro Total Analysis Systems' without the need of first producing wafers is by using three-dimensional bio printing, here biocompatible ink is processed through a nozzle and printed directly in the desired shape [336].

Taken together, we observed that the centrosome is centrally located in DCs with extra centrosomes clustered during IS formation. Nevertheless, additional questions arise which need to be answered to gain a better picture of the underlying processes.

## 4.6. Conclusion and outlook

In summary, we aimed to increase the knowledge on DC behaviour during IS formation, as this process represents a complex network of signal transduction and overtakes indispensable functions during immune responses.

During this study, we observed that DCs obtain extra centrosomes upon immune activation and wondered whether this so far unidentified phenomenon is beneficial or disadvantageous for immune cell biology. Thereby, we could demonstrate that mature DCs are terminal differentiated cells that show a heterogeneity in their DNA content. Some cells were polyploid. What causes this polyploidy can only be speculated, but will be addressed in future experiments.

Additionally, we were able to link extra centrosomes to the expression of Plk2; this kinase regulates centriole duplication and is increasingly expressed after DC stimulation. Up to now, we do not know the interacting partners of Plk2 and how they team up to induce the mechanism of generating extra centrosomes. Nevertheless, the results of altered centrosome numbers when altering Plk2 expression can be used to further design studies that address the physiological relevance of extra centrosomes *in vitro* and *in vivo*.

Moreover, we could reveal that extra centrosomes are of great use for DCs as they nucleate more MTs filaments, which correlates with increased cytokine trafficking and secretion as well as accelerated T cell priming.

We could also enhance our understanding on the molecular mechanisms of cytoskeletal dynamics in DCs. Thereby, we showed that centrosomes are centrally located during IS formation and that extra centrosomes cluster during this process. These findings may present one aspect why DCs are the most potent antigen-presenting cell and how multi-conjugated ISs with multicentric conformation can be achieved. Future studies, combining experimental as well as computational approaches will be carried out to understand how centrosome conformation and positioning influences T cell activation in a spatio-temporal manner.

Finally, we conclude, that this inter-disciplinary approach focusing on the IS and the centrosome gained valuable results in the field of immune- and cell biology and will help the scientific community to gain a better understanding of the underlying processes of cell-cell contacts. This might be applicable to various cell types during health and diseases and might allow targeted intervention in case of misregulation.
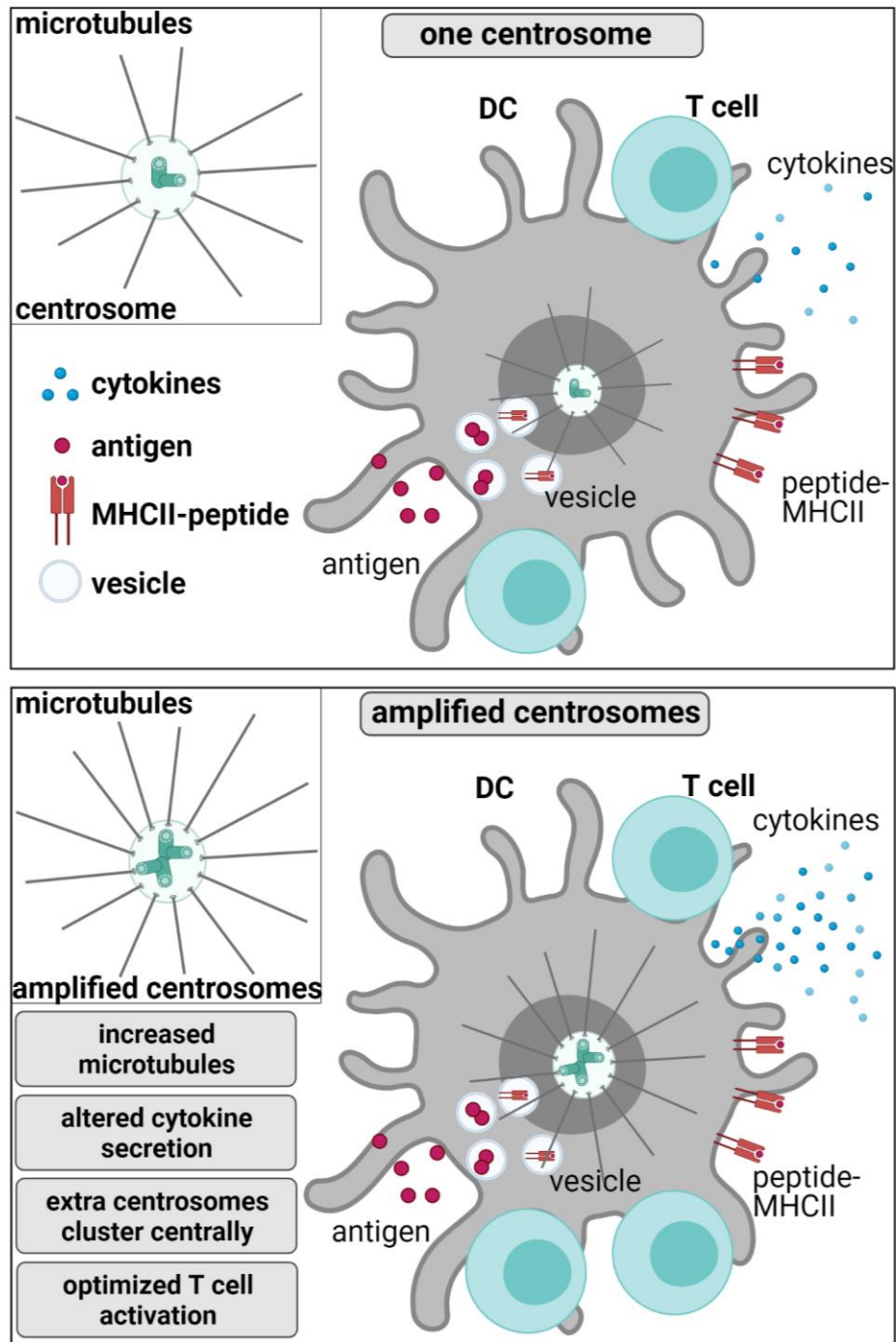
**Figure 4.4** Amplified centrosomes in dendritic cells (DCs) and their beneficial biological functions.
Centrosome in DCs are centrally localized during immune synapse (IS) formation. They function as microtubule organizing center, thereby overtaking important functions during IS formation. Amplified centrosomes in DCs show increased microtubules nucleation capacity, cluster centrally and correlate with altered cytokine secretion and optimized T cell activation.

# References

1. Banchereau, J. & Steinman, R. M. Dendritic cells and the control of immunity. *Nature* **392,** 245–252; 10.1038/32588 (1998).

2. Guilliams, M. *et al.* Dendritic cells, monocytes and macrophages: a unified nomenclature based on ontogeny, 2014 Aug.

3. Anderson, D. A. 3., Dutertre, C.-A., Ginhoux, F. & Murphy, K. M. Genetic models of human and mouse dendritic cell development and function. *Nature Reviews Immunology* **21,** 101–115; 10.1038/s41577-020-00413-x (2021).

4. Reizis, B. Plasmacytoid Dendritic Cells: Development, Regulation, and Function. *Immunity* **50,** 37–50; 10.1016/j.immuni.2018.12.027 (2019).

5. Naik, S. H. *et al.* Intrasplenic steady-state dendritic cell precursors that are distinct from monocytes. *Nature immunology* **7,** 663–671; 10.1038/ni1340 (2006).

6. Naik, S. H. *et al.* Development of plasmacytoid and conventional dendritic cell subtypes from single precursor cells derived in vitro and in vivo. *Nature immunology* **8,** 1217–1226; 10.1038/ni1522 (2007).

7. Sathe, P. *et al.* Lymphoid tissue and plasmacytoid dendritic cells and macrophages do not share a common macrophage-dendritic cell-restricted progenitor. *Immunity* **41,** 104–115; 10.1016/j.immuni.2014.05.020 (2014).

8. Schlitzer, A. *et al.* Identification of cDC1- and cDC2-committed DC progenitors reveals early lineage priming at the common DC progenitor stage in the bone marrow. *Nature immunology* **16,** 718–728; 10.1038/ni.3200 (2015).

9. Schlitzer, A and Zhang, W and Song, M and Ma, X. Recent advances in understanding dendritic cell development, classification, and phenotype [version 1; peer review: 2 approved]. *F1000Research* **7**; 10.12688/f1000research.14793.1 (2018).

10. Onai, N. *et al.* Identification of clonogenic common Flt3+M-CSFR+ plasmacytoid and conventional dendritic cell progenitors in mouse bone marrow. *Nature immunology* **8,** 1207–1216; 10.1038/ni1518 (2007).

11. Sichien, D. *et al.* IRF8 Transcription Factor Controls Survival and Function of Terminally Differentiated Conventional and Plasmacytoid Dendritic Cells, Respectively. *Immunity* **45,** 626–640; 10.1016/j.immuni.2016.08.013 (2016).

12. Tailor, P., Tamura, T., Morse, H. C. 3. & Ozato, K. The BXH2 mutation in IRF8 differentially impairs dendritic cell subset development in the mouse. *Blood* **111,** 1942–1945; 10.1182/blood-2007-07-100750 (2008).

13. Ginhoux, F. *et al.* The origin and development of nonlymphoid tissue CD103+ DCs. *The Journal of experimental medicine* **206,** 3115–3130; 10.1084/jem.20091756 (2009).

14. Hildner, K. *et al.* Batf3 deficiency reveals a critical role for CD8alpha+ dendritic cells in cytotoxic T cell immunity. *Science (New York, N.Y.)* **322,** 1097–1100; 10.1126/science.1164206 (2008).

15. Edelson, B. T. *et al.* Peripheral CD103+ dendritic cells form a unified subset developmentally related to CD8alpha+ conventional dendritic cells. *The Journal of experimental medicine* **207,** 823–836; 10.1084/jem.20091627 (2010).

16. Grajales-Reyes, G. E. *et al.* Batf3 maintains autoactivation of Irf8 for commitment of a CD8α(+) conventional DC clonogenic progenitor. *Nature immunology* **16,** 708–717; 10.1038/ni.3197 (2015).

17. Hacker, C. *et al.* Transcriptional profiling identifies Id2 function in dendritic cell development. *Nature immunology* **4,** 380–386; 10.1038/ni903 (2003).

18. Kashiwada, M., Pham, N.-L. L., Pewe, L. L., Harty, J. T. & Rothman, P. B. NFIL3/E4BP4 is a key transcription factor for CD8α+ dendritic cell development. *Blood* **117,** 6193–6197 (2011).

19. Satpathy, A. T. *et al.* Zbtb46 expression distinguishes classical dendritic cells and their committed progenitors from other immune lineages. *The Journal of experimental medicine* **209,** 1135–1152 (2012).

20. Silva, N. S. de, Simonetti, G., Heise, N. & Klein, U. The diverse roles of IRF4 in late germinal center B‐cell differentiation. *Immunological reviews* **247,** 73–92 (2012).

21. Caton, M. L., Smith-Raska, M. R. & Reizis, B. Notch-RBP-J signaling controls the homeostasis of CD8- dendritic cells in the spleen. *The Journal of experimental medicine* **204,** 1653–1664; 10.1084/jem.20062648 (2007).

22. Tussiwand, R. *et al.* Klf4 expression in conventional dendritic cells is required for T helper 2 cell responses. *Immunity* **42,** 916–928; 10.1016/j.immuni.2015.04.017 (2015).

23. Brown, C. C. *et al.* Transcriptional basis of mouse and human dendritic cell heterogeneity. *Cell* **179,** 846-863. e24 (2019).

24. Liu, K. *et al.* In vivo analysis of dendritic cell development and homeostasis. *Science (New York, N.Y.)* **324,** 392–397 (2009).

25. Cabeza-Cabrerizo, M. *et al.* Tissue clonality of dendritic cell subsets and emergency DCpoiesis revealed by multicolor fate mapping of DC progenitors. *Science immunology* **4** (2019).

26. Rodrigues, P. F. *et al.* Distinct progenitor lineages contribute to the heterogeneity of plasmacytoid dendritic cells. *Nature immunology* **19,** 711–722 (2018).

27. Dress, R. J. *et al.* Plasmacytoid dendritic cells develop from Ly6D+ lymphoid progenitors distinct from the myeloid lineage. *Nature immunology* **20,** 852–864 (2019).

28. Cisse, B. *et al.* Transcription factor E2-2 is an essential and specific regulator of plasmacytoid dendritic cell development. *Cell* **135,** 37–48 (2008).

29. Scott, C. L. *et al.* The transcription factor Zeb2 regulates development of conventional and plasmacytoid DCs by repressing Id2. *The Journal of experimental medicine* **213,** 897–911 (2016).

30. Wu, X. *et al.* Transcription factor Zeb2 regulates commitment to plasmacytoid dendritic cell and monocyte fate. *Proceedings of the National Academy of Sciences* **113,** 14775–14780 (2016).

31. Grajkowska, L. T. *et al.* Isoform-specific expression and feedback regulation of E protein TCF4 control dendritic cell lineage specification. *Immunity* **46,** 65–77 (2017).

32. Diao, J. *et al.* In situ replication of immediate dendritic cell (DC) precursors contributes to conventional DC homeostasis in lymphoid tissue. *Journal of immunology (Baltimore, Md. : 1950)* **176,** 7196–7206; 10.4049/jimmunol.176.12.7196 (2006).

33. Sichien, D., Lambrecht, B. N., Guilliams, M. & Scott, C. L. Development of conventional dendritic cells: from common bone marrow progenitors to multiple subsets in peripheral tissues. *Mucosal Immunology* **10,** 831–844; 10.1038/mi.2017.8 (2017).

34. Eisenbarth, S. C. Dendritic cell subsets in T cell programming: location dictates function. *Nature Reviews Immunology* **19,** 89–103; 10.1038/s41577-018-0088-1 (2019).

35. Granot, T. *et al.* Dendritic Cells Display Subset and Tissue-Specific Maturation Dynamics over Human Life. *Immunity* **46,** 504–515; 10.1016/j.immuni.2017.02.019 (2017).

36. Inaba, K. *et al.* Generation of large numbers of dendritic cells from mouse bone marrow cultures supplemented with granulocyte/macrophage colony-stimulating factor. *The Journal of experimental medicine* **176,** 1693–1702; 10.1084/jem.176.6.1693 (1992).

37. Bruno, L. Differentiation of dendritic cell subsets from mouse bone marrow. *Methods in molecular biology (Clifton, N.J.)* **380,** 47–57; 10.1007/978-1-59745-395-0_3 (2007).

38. Ruhland, M. K. *et al.* Visualizing Synaptic Transfer of Tumor Antigens among Dendritic Cells. *Cancer cell* **37,** 786-799.e5; 10.1016/j.ccell.2020.05.002 (2020).

39. Merad, M., Sathe, P., Helft, J., Miller, J. & Mortha, A. The dendritic cell lineage: ontogeny and function of dendritic cells and their subsets in the steady state and the inflamed setting. *Annual review of immunology* **31,** 563–604; 10.1146/annurev-immunol-020711-074950 (2013).

40. Waithman, J. *et al.* Resident CD8(+) and migratory CD103(+) dendritic cells control CD8 T cell immunity during acute influenza infection. *PloS one* **8,** e66136; 10.1371/journal.pone.0066136 (2013).

41. Mildner, A. & Jung, S. Development and function of dendritic cell subsets. *Immunity* **40,** 642–656 (2014).

42. Murphy, T. L. *et al.* Transcriptional control of dendritic cell development. *Annual review of immunology* **34,** 93–119 (2016).

43. Zhang, J. *et al.* Characterization of Siglec-H as a novel endocytic receptor expressed on murine plasmacytoid dendritic cell precursors. *Blood* **107,** 3600–3608 (2006).

44. Herman, J. S., Sagar & Grün, D. FateID infers cell fate bias in multipotent progenitors from single-cell RNA-seq data. *Nature methods* **15,** 379–386; 10.1038/nmeth.4662 (2018).

45. Haan, J. M. M. den, Lehar, S. M. & Bevan, M. J. CD8+ but not CD8− dendritic cells cross-prime cytotoxic T cells in vivo. *The Journal of experimental medicine* **192,** 1685–1696 (2000).

46. Pooley, J. L., Heath, W. R. & Shortman, K. Cutting edge: intravenous soluble antigen is presented to CD4 T cells by CD8− dendritic cells, but cross-presented to CD8 T cells by CD8+ dendritic cells. *Journal of immunology (Baltimore, Md. : 1950)* **166,** 5327–5330 (2001).

47. Schulz, O. & Reis e Sousa, C. Cross‑presentation of cell‑associated antigens by CD8α+ dendritic cells is attributable to their ability to internalize dead cells. *Immunology* **107,** 183–189 (2002).

48. Schnorrer, P. *et al.* The dominant role of CD8+ dendritic cells in cross-presentation is not dictated by antigen capture. *Proceedings of the National Academy of Sciences* **103,** 10729–10734 (2006).

49. Hildner, K. *et al.* Batf3 deficiency reveals a critical role for CD8α+ dendritic cells in cytotoxic T cell immunity. *Science (New York, N.Y.)* **322,** 1097–1100 (2008).

50. Martínez‑López, M., Iborra, S., Conde‑Garrosa, R. & Sancho, D. Batf3‑dependent CD103+ dendritic cells are major producers of IL‑12 that drive local Th1 immunity against Leishmania major infection in mice. *European journal of immunology* **45,** 119–129 (2015).

51. Schulz, O. *et al.* Toll-like receptor 3 promotes cross-priming to virus-infected cells. *Nature* **433,** 887–892 (2005).

52. Desch, A. N. *et al.* CD103+ pulmonary dendritic cells preferentially acquire and present apoptotic cell-associated antigen. *The Journal of experimental medicine* **208,** 1789–1797; 10.1084/jem.20110538 (2011).

53. Miller, J. C. *et al.* Deciphering the transcriptional network of the dendritic cell lineage. *Nature immunology* **13,** 888 (2012).

54. Durai, V. & Murphy, K. M. Functions of Murine Dendritic Cells. *Immunity* **45,** 719–736; 10.1016/j.immuni.2016.10.010 (2016).

55. Janela, B. *et al.* A Subset of Type I Conventional Dendritic Cells Controls Cutaneous Bacterial Infections through VEGFα-Mediated Recruitment of Neutrophils. *Immunity* **50,** 1069-1083.e8; 10.1016/j.immuni.2019.03.001 (2019).

56. Dudziak, D. *et al.* Differential antigen processing by dendritic cell subsets in vivo. *Science (New York, N.Y.)* **315,** 107–111; 10.1126/science.1136080 (2007).

57. Lewis, K. L. *et al.* Notch2 receptor signaling controls functional differentiation of dendritic cells in the spleen and intestine. *Immunity* **35,** 780–791; 10.1016/j.immuni.2011.08.013 (2011).

58. Satpathy, A. T. *et al.* Notch2-dependent classical dendritic cells orchestrate intestinal immunity to attaching-and-effacing bacterial pathogens. *Nature immunology* **14,** 937–948; 10.1038/ni.2679 (2013).

59. Alferink, J. *et al.* Compartmentalized production of CCL17 in vivo: strong inducibility in peripheral dendritic cells contrasts selective absence from the spleen. *The Journal of experimental medicine* **197,** 585–599 (2003).

60. Proietto, A. I. *et al.* Dendritic cells in the thymus contribute to T-regulatory cell induction. *Proceedings of the National Academy of Sciences* **105,** 19869–19874; 10.1073/pnas.0810268105 (2008).

61. Stutte, S. *et al.* Requirement of CCL17 for CCR7-and CXCR4-dependent migration of cutaneous dendritic cells. *Proceedings of the National Academy of Sciences* **107,** 8736–8741 (2010).

62. Weber, C. *et al.* CCL17-expressing dendritic cells drive atherosclerosis by restraining regulatory T cell homeostasis in mice. *The Journal of clinical investigation* **121,** 2898–2910 (2011).

63. Fülle, L. *et al.* RNA aptamers recognizing murine CCL17 inhibit T cell chemotaxis and reduce contact hypersensitivity in vivo. *Molecular Therapy* **26,** 95–104 (2018).

64. Schlitzer, A., McGovern, N. & Ginhoux, F. Dendritic cells and monocyte-derived cells: Two complementary and integrated functional systems. *Seminars in cell & developmental biology* **41,** 9–22; 10.1016/j.semcdb.2015.03.011 (2015).

65. Gao, Y. *et al.* Control of T helper 2 responses by transcription factor IRF4-dependent dendritic cells. *Immunity* **39,** 722–732 (2013).

66. Kumamoto, Y. *et al.* CD301b+ dermal dendritic cells drive T helper 2 cell-mediated immunity. *Immunity* **39,** 733–743 (2013).

67. Persson, E. K. *et al.* IRF4 transcription-factor-dependent CD103+ CD11b+ dendritic cells drive mucosal T helper 17 cell differentiation. *Immunity* **38,** 958–969 (2013).

68. Vu Manh, T.-P., Bertho, N., Hosmalin, A., Schwartz-Cornil, I. & Dalod, M. Investigating evolutionary conservation of dendritic cell subset identity and functions. *Frontiers in immunology* **6,** 260 (2015).

69. Kotsias, F., Cebrian, I. & Alloatti, A. Antigen processing and presentation. *International review of cell and molecular biology* **348,** 69–121; 10.1016/bs.ircmb.2019.07.005 (2019).

70. Santambrogio, L., Berendam, S. J. & Engelhard, V. H. The Antigen Processing and Presentation Machinery in Lymphatic Endothelial Cells. *Frontiers in immunology* **10,** 1033; 10.3389/fimmu.2019.01033 (2019).

71. Inaba, K. *et al.* High levels of a major histocompatibility complex II-self peptide complex on dendritic cells from the T cell areas of lymph nodes. *The Journal of experimental medicine* **186,** 665–672; 10.1084/jem.186.5.665 (1997).

72. Jacques  Banchereau *et al.* Immunobiology of Dendritic Cells. *Annual review of immunology* **18,** 767–811; 10.1146/annurev.immunol.18.1.767 (2000).

73. Huang, A. Y. *et al.* Role of bone marrow-derived cells in presenting MHC class I-restricted tumor antigens. *Science (New York, N.Y.)* **264,** 961–965 (1994).

74. Kovacsovics-Bankowski, M. & Rock, K. L. A phagosome-to-cytosol pathway for exogenous antigens presented on MHC class I molecules. *Science (New York, N.Y.)* **267,** 243–246; 10.1126/science.7809629 (1995).

75. Turley, S. J. *et al.* Transport of peptide-MHC class II complexes in developing dendritic cells. *Science (New York, N.Y.)* **288,** 522–527 (2000).

76. Haan, J. M. M. den & Bevan, M. J. Antigen presentation to CD8+ T cells: cross-priming in infectious diseases. *Current opinion in immunology* **13,** 437–441 (2001).

77. Heath, W. R. & Carbone, F. R. Cross-presentation in viral immunity and self-tolerance. *Nature Reviews Immunology* **1,** 126–134 (2001).

78. Medzhitov, R. Toll-like receptors and innate immunity. *Nature Reviews Immunology* **1,** 135–145 (2001).

79. Akira, S., Uematsu, S. & Takeuchi, O. Pathogen recognition and innate immunity. *Cell* **124,** 783–801; 10.1016/j.cell.2006.02.015 (2006).

80. Kawai, T. & Akira, S. The roles of TLRs, RLRs and NLRs in pathogen recognition. *International immunology* **21,** 317–337; 10.1093/intimm/dxp017 (2009).

81. Takeuchi, O. & Akira, S. Pattern recognition receptors and inflammation. *Cell* **140,** 805–820; 10.1016/j.cell.2010.01.022 (2010).

82. Lenschow, D. J., Walunas, T. L. & Bluestone, J. A. CD28/B7 system of T cell costimulation. *Annual review of immunology* **14,** 233–258; 10.1146/annurev.immunol.14.1.233 (1996).

83. Jonuleit, H. *et al.* Pro‑inflammatory cytokines and prostaglandins induce maturation of potent immunostimulatory dendritic cells under fetal calf serum‑free conditions. *European journal of immunology* **27,** 3135–3142 (1997).

84. Dieu, M. C. *et al.* Selective recruitment of immature and mature dendritic cells by distinct chemokines expressed in different anatomic sites. *The Journal of experimental medicine* **188,** 373–386; 10.1084/jem.188.2.373 (1998).

85. Curtsinger, J. M. *et al.* Inflammatory cytokines provide a third signal for activation of naive CD4+ and CD8+ T cells. *Journal of immunology (Baltimore, Md. : 1950)* **162,** 3256–3262 (1999).

86. Sallusto, F. & Lanzavecchia, A. Understanding dendritic cell and T-lymphocyte traffic through the analysis of chemokine receptor expression. *Immunological reviews* **177,** 134–140; 10.1034/j.1600-065x.2000.17717.x (2000).

87. Hubo, M. *et al.* Costimulatory molecules on immunogenic versus tolerogenic human dendritic cells. *Frontiers in immunology* **4,** 82; 10.3389/fimmu.2013.00082 (2013).

88. Denzin, L. K., Fallas, J. L., Prendes, M. & Yi, W. Right place, right time, right peptide: DO keeps DM focused. *Immunological reviews* **207,** 279–292 (2005).

89. Mellins, E. D. & Stern, L. J. HLA-DM and HLA-DO, key regulators of MHC-II processing and presentation. *Current opinion in immunology* **26,** 115–122; 10.1016/j.coi.2013.11.005 (2014).

90. Garrett, W. S. *et al.* Developmental control of endocytosis in dendritic cells by Cdc42. *Cell* **102,** 325–334 (2000).

91. Sallusto, F., Cella, M., Danieli, C. & Lanzavecchia, A. Dendritic cells use macropinocytosis and the mannose receptor to concentrate macromolecules in the major histocompatibility complex class II compartment: downregulation by cytokines and bacterial products. *The Journal of experimental medicine* **182,** 389–400 (1995).

92. Norbury, C. C., Chambers, B. J., Prescott, A. R., Ljunggren, H.-G. & Watts, C. Constitutive macropinocytosis allows TAP‑dependent major histocompatibility compex class I presentation of exogenous soluble antigen by bone marrow‑derived dendritic cells. *European journal of immunology* **27,** 280–288 (1997).

93. Reis e Sousa, C., Stahl, P. D. & Austyn, J. M. Phagocytosis of antigens by Langerhans cells in vitro. *The Journal of experimental medicine* **178,** 509–519 (1993).

94. Crotzer, V. L. & Blum, J. S. Autophagy and its role in MHC-mediated antigen presentation. *Journal of immunology (Baltimore, Md. : 1950)* **182,** 3335–3341 (2009).

95. Hilligan, K. L. & Ronchese, F. Antigen presentation by dendritic cells and their instruction of CD4+ T helper cell responses. *Cellular & Molecular Immunology* **17,** 587–599; 10.1038/s41423-020-0465-0 (2020).

96. Roche, P. A. & Furuta, K. The ins and outs of MHC class II-mediated antigen processing and presentation. *Nature Reviews Immunology* **15,** 203–216; 10.1038/nri3818 (2015).

97. Kaksonen, M. & Roux, A. Mechanisms of clathrin-mediated endocytosis. *Nature reviews. Molecular cell biology* **19,** 313–326; 10.1038/nrm.2017.132 (2018).

98. Canton, J. Macropinocytosis: New Insights Into Its Underappreciated Role in Innate Immune Cell Surveillance. *Frontiers in immunology* **9,** 2286; 10.3389/fimmu.2018.02286 (2018).

99. Liu, Z. & Roche, P. A. Macropinocytosis in phagocytes: regulation of MHC class-II-restricted antigen presentation in dendritic cells. *Frontiers in physiology* **6,** 1; 10.3389/fphys.2015.00001 (2015).

100. Klionsky, D. J. Autophagy: from phenomenology to molecular understanding in less than a decade. *Nature reviews. Molecular cell biology* **8,** 931–937; 10.1038/nrm2245 (2007).

101. Watts, C. The exogenous pathway for antigen presentation on major histocompatibility complex class II and CD1 molecules. *Nature immunology* **5,** 685–692; 10.1038/ni1088 (2004).

102. Wubbolts, R. *et al.* Direct vesicular transport of MHC class II molecules from lysosomal structures to the cell surface. *The Journal of cell biology* **135,** 611–622; 10.1083/jcb.135.3.611 (1996).

103. Vyas, J. M. *et al.* Tubulation of class II MHC compartments is microtubule dependent and involves multiple endolysosomal membrane proteins in primary dendritic cells. *Journal of immunology (Baltimore, Md. : 1950)* **178,** 7199–7210; 10.4049/jimmunol.178.11.7199 (2007).

104. Rocha, N. & Neefjes, J. MHC class II molecules on the move for successful antigen presentation. *The EMBO journal* **27,** 1–5; 10.1038/sj.emboj.7601945 (2008).

105. Mitchison, T. & Kirschner, M. Dynamic instability of microtubule growth. *Nature* **312,** 237–242; 10.1038/312237a0 (1984).

106. Eva Nogales. Structural Insights into Microtubule Function. *Annual Review of Biophysics and Biomolecular Structure* **30,** 397–420; 10.1146/annurev.biophys.30.1.397 (2001).

107. Hollenbeck, P. J. & Swanson, J. A. Radial extension of macrophage tubular lysosomes supported by kinesin. *Nature* **346,** 864–866; 10.1038/346864a0 (1990).

108. Wubbolts, R. *et al.* Opposing motor activities of dynein and kinesin determine retention and transport of MHC class II-containing compartments. *Journal of cell science* **112 ( Pt 6),** 785–795 (1999).

109. Jordens, I. *et al.* The Rab7 effector protein RILP controls lysosomal transport by inducing the recruitment of dynein-dynactin motors. *Current Biology* **11,** 1680–1685; 10.1016/S0960-9822(01)00531-0 (2001).

110. Blum, J. S., Wearsch, P. A. & Cresswell, P. Pathways of antigen processing. *Annual review of immunology* **31,** 443–473; 10.1146/annurev-immunol-032712-095910 (2013).

111. Kovacsovics-Bankowski, M. & Rock, K. L. A phagosome-to-cytosol pathway for exogenous antigens presented on MHC class I molecules. *Science (New York, N.Y.)* **267,** 243–246; 10.1126/science.7809629 (1995).

112.    Ackerman, A. L., Kyritsis, C., Tampé, R. & Cresswell, P. Early phagosomes in dendritic cells form a cellular compartment sufficient for cross presentation of exogenous antigens. *Proceedings of the National Academy of Sciences* **100,** 12889–12894; 10.1073/pnas.1735556100 (2003).

113.    Ackerman, A. L., Giodini, A. & Cresswell, P. A role for the endoplasmic reticulum protein retrotranslocation machinery during crosspresentation by dendritic cells. *Immunity* **25,** 607–617; 10.1016/j.immuni.2006.08.017 (2006).

114.    Palmowski, M. J. *et al.* Role of immunoproteasomes in cross-presentation. *Journal of immunology (Baltimore, Md. : 1950)* **177,** 983–990; 10.4049/jimmunol.177.2.983 (2006).

115.    Burgdorf, S., Schölz, C., Kautz, A., Tampé, R. & Kurts, C. Spatial and mechanistic separation of cross-presentation and endogenous antigen presentation. *Nature immunology* **9,** 558–566; 10.1038/ni.1601 (2008).

116.    Firat, E. *et al.* The role of endoplasmic reticulum-associated aminopeptidase 1 in immunity to infection and in cross-presentation. *Journal of immunology (Baltimore, Md. : 1950)* **178,** 2241–2248; 10.4049/jimmunol.178.4.2241 (2007).

117.    Saveanu, L. *et al.* IRAP identifies an endosomal compartment required for MHC class I cross-presentation. *Science (New York, N.Y.)* **325,** 213–217; 10.1126/science.1172845 (2009).

118.    Lizée, G. *et al.* Control of dendritic cell cross-presentation by the major histocompatibility complex class I cytoplasmic domain. *Nature immunology* **4,** 1065–1073; 10.1038/ni989 (2003).

119.    Basha, G. *et al.* A CD74-dependent MHC class I endolysosomal cross-presentation pathway. *Nature immunology* **13,** 237–245; 10.1038/ni.2225 (2012).

120.    Alloatti, A., Kotsias, F., Magalhaes, J. G. & Amigorena, S. Dendritic cell maturation and cross-presentation: timing matters! *Immunological reviews* **272,** 97–108; 10.1111/imr.12432 (2016).

121.    Shen, L., Sigal, L. J., Boes, M. & Rock, K. L. Important Role of Cathepsin S in Generating Peptides for TAP-Independent MHC Class I Crosspresentation In Vivo. *Immunity* **21,** 155–165; 10.1016/j.immuni.2004.07.004 (2004).

122.    Embgenbroich, M. & Burgdorf, S. Current Concepts of Antigen Cross-Presentation. *Frontiers in immunology* **9,** 1643; 10.3389/fimmu.2018.01643 (2018).

123.    Delamarre, L., Pack, M., Chang, H., Mellman, I. & Trombetta, E. S. Differential lysosomal proteolysis in antigen-presenting cells determines antigen fate. *Science (New York, N.Y.)* **307,** 1630–1634; 10.1126/science.1108003 (2005).

124.    Savina, A. *et al.* The small GTPase Rac2 controls phagosomal alkalinization and antigen crosspresentation selectively in CD8(+) dendritic cells. *Immunity* **30,** 544–555; 10.1016/j.immuni.2009.01.013 (2009).

125.    Burgdorf, S., Kautz, A., Böhnert, V., Knolle, P. A. & Kurts, C. Distinct Pathways of Antigen Uptake and Intracellular Routing in CD4 and CD8 T Cell Activation. *Science (New York, N.Y.)* **316,** 612–616; 10.1126/science.1137971 (2007).

126. Trombetta, E. S., Ebersold, M., Garrett, W., Pypaert, M. & Mellman, I. Activation of lysosomal function during dendritic cell maturation. *Science (New York, N.Y.)* **299,** 1400–1403; 10.1126/science.1080106 (2003).

127. Savina, A. *et al.* NOX2 controls phagosomal pH to regulate antigen processing during crosspresentation by dendritic cells. *Cell* **126,** 205–218; 10.1016/j.cell.2006.05.035 (2006).

128. van Montfoort, N. *et al.* Antigen storage compartments in mature dendritic cells facilitate prolonged cytotoxic T lymphocyte cross-priming capacity. *Proceedings of the National Academy of Sciences* **106,** 6730–6735; 10.1073/pnas.0900969106 (2009).

129. Itano, A. A. *et al.* Distinct Dendritic Cell Populations Sequentially Present Antigen to CD4 T Cells and Stimulate Different Aspects of Cell-Mediated Immunity. *Immunity* **19,** 47–57; 10.1016/S1074-7613(03)00175-4 (2003).

130. Worbs, T., Hammerschmidt, S. I. & Förster, R. Dendritic cell migration in health and disease. *Nature Reviews Immunology* **17,** 30–48; 10.1038/nri.2016.116 (2017).

131. Lämmermann, T. *et al.* Rapid leukocyte migration by integrin-independent flowing and squeezing. *Nature* **453,** 51–55; 10.1038/nature06887 (2008).

132. Braun, A. *et al.* Afferent lymph-derived T cells and DCs use different chemokine receptor CCR7-dependent routes for entry into the lymph node and intranodal migration. *Nature immunology* **12,** 879–887; 10.1038/ni.2085 (2011).

133. Sixt, M. *et al.* The conduit system transports soluble antigens from the afferent lymph to resident dendritic cells in the T cell area of the lymph node. *Immunity* **22,** 19–29; 10.1016/j.immuni.2004.11.013 (2005).

134. Bajénoff, M. *et al.* Stromal cell networks regulate lymphocyte entry, migration, and territoriality in lymph nodes. *Immunity* **25,** 989–1001; 10.1016/j.immuni.2006.10.011 (2006).

135. Girard, J.-P., Moussion, C. & Förster, R. HEVs, lymphatics and homeostatic immune cell trafficking in lymph nodes. *Nature Reviews Immunology* **12,** 762–773; 10.1038/nri3298 (2012).

136. Worbs, T., Mempel, T. R., Bölter, J., Andrian, U. H. von & Förster, R. CCR7 ligands stimulate the intranodal motility of T lymphocytes in vivo. *The Journal of experimental medicine* **204,** 489–495; 10.1084/jem.20061706 (2007).

137. Tomura, M. *et al.* Monitoring cellular movement in vivo with photoconvertible fluorescence protein "Kaede" transgenic mice. *Proceedings of the National Academy of Sciences* **105,** 10871–10876; 10.1073/pnas.0802278105 (2008).

138. Mandl, J. N. *et al.* Quantification of lymph node transit times reveals differences in antigen surveillance strategies of naive CD4+ and CD8+ T cells. *Proceedings of the National Academy of Sciences* **109,** 18036–18041; 10.1073/pnas.1211717109 (2012).

139. Förster, R. *et al.* CCR7 coordinates the primary immune response by establishing functional microenvironments in secondary lymphoid organs. *Cell* **99,** 23–33; 10.1016/s0092-8674(00)80059-8 (1999).

140. Ohl, L. *et al.* CCR7 Governs Skin Dendritic Cell Migration under Inflammatory and Steady-State Conditions. *Immunity* **21,** 279–288; 10.1016/j.immuni.2004.06.014 (2004).

141.    Haessler, U., Pisano, M., Wu, M. & Swartz, M. A. Dendritic cell chemotaxis in 3D under defined chemokine gradients reveals differential response to ligands CCL21 and CCL19. *Proceedings of the National Academy of Sciences* **108,** 5614–5619; 10.1073/pnas.1014920108 (2011).

142.    Pflicke, H. & Sixt, M. Preformed portals facilitate dendritic cell entry into afferent lymphatic vessels. *The Journal of experimental medicine* **206,** 2925–2935; 10.1084/jem.20091739 (2009).

143.    Tal, O. *et al.* DC mobilization from the skin requires docking to immobilized CCL21 on lymphatic endothelium and intralymphatic crawling. *The Journal of experimental medicine* **208,** 2141–2153; 10.1084/jem.20102392 (2011).

144.    Weber, M. *et al.* Interstitial dendritic cell guidance by haptotactic chemokine gradients. *Science (New York, N.Y.)* **339,** 328–332; 10.1126/science.1228456 (2013).

145.    Hampton, H. R. & Chtanova, T. Lymphatic Migration of Immune Cells. *Frontiers in immunology* **10,** 1168; 10.3389/fimmu.2019.01168 (2019).

146.    Ulvmar, M. H. *et al.* The atypical chemokine receptor CCRL1 shapes functional CCL21 gradients in lymph nodes. *Nature immunology* **15,** 623–630; 10.1038/ni.2889 (2014).

147.    Kabashima, K. *et al.* CXCL12-CXCR4 engagement is required for migration of cutaneous dendritic cells. *The American journal of pathology* **171,** 1249–1257; 10.2353/ajpath.2007.070225 (2007).

148.    Qu, C. *et al.* Role of CCR8 and other chemokine pathways in the migration of monocyte-derived dendritic cells to lymph nodes. *The Journal of experimental medicine* **200,** 1231–1241; 10.1084/jem.20032152 (2004).

149.    Czeloth, N., Bernhardt, G., Hofmann, F., Genth, H. & Förster, R. Sphingosine-1-phosphate mediates migration of mature dendritic cells. *Journal of immunology (Baltimore, Md. : 1950)* **175,** 2960–2967; 10.4049/jimmunol.175.5.2960 (2005).

150.    Eckert, N., Permanyer, M., Yu, K., Werth, K. & Förster, R. Chemokines and other mediators in the development and functional organization of lymph nodes. *Immunological reviews* **289,** 62–83; 10.1111/imr.12746 (2019).

151.    Pham, T. H. M., Okada, T., Matloubian, M., Lo, C. G. & Cyster, J. G. S1P1 receptor signaling overrides retention mediated by G alpha i-coupled receptors to promote T cell egress. *Immunity* **28,** 122–133; 10.1016/j.immuni.2007.11.017 (2008).

152.    Kamath, A. T. *et al.* The development, maturation, and turnover rate of mouse spleen dendritic cell populations. *Journal of immunology (Baltimore, Md. : 1950)* **165,** 6762–6770; 10.4049/jimmunol.165.12.6762 (2000).

153.    Tomura, M. *et al.* Tracking and quantification of dendritic cell migration and antigen trafficking between the skin and lymph nodes. *Scientific reports* **4,** 6030; 10.1038/srep06030 (2014).

154.    Renkawitz, J. *et al.* Nuclear positioning facilitates amoeboid migration along the path of least resistance. *Nature* **568,** 546–550; 10.1038/s41586-019-1087-5 (2019).

155.	Kopf, A. *et al.* Microtubules control cellular shape and coherence in amoeboid migrating cells. *The Journal of cell biology* **219**; 10.1083/jcb.201907154 (2020).

156.	Kopf, A. & Kiermaier, E. Dynamic Microtubule Arrays in Leukocytes and Their Role in Cell Migration and Immune Synapse Formation. *Frontiers in cell and developmental biology* **9,** 635511; 10.3389/fcell.2021.635511 (2021).

157.	Dustin, M. L. *et al.* A Novel Adaptor Protein Orchestrates Receptor Patterning and Cytoskeletal Polarity in T-Cell Contacts. *Cell* **94,** 667–677; 10.1016/S0092-8674(00)81608-6 (1998).

158.	Monks, C. R. F., Freiberg, B. A., Kupfer, H., Sciaky, N. & Kupfer, A. Three-dimensional segregation of supramolecular activation clusters in T cells. *Nature* **395,** 82–86; 10.1038/25764 (1998).

159.	Friedl, P., Boer, A. T. den & Gunzer, M. Tuning immune responses: diversity and adaptation of the immunological synapse. *Nature reviews. Immunology* **5,** 532–545; 10.1038/nri1647 (2005).

160.	Michael L. Dustin & Kaushik Choudhuri. Signaling and Polarized Communication Across the T Cell Immunological Synapse. *Annual Review of Cell and Developmental Biology* **32,** 303–325; 10.1146/annurev-cellbio-100814-125330 (2016).

161.	Onnis, A. & Baldari, C. T. Orchestration of Immunological Synapse Assembly by Vesicular Trafficking. *Frontiers in cell and developmental biology* **7,** 110; 10.3389/fcell.2019.00110 (2019).

162.	Gérard, A., Beemiller, P., Friedman, R. S., Jacobelli, J. & Krummel, M. F. Evolving immune circuits are generated by flexible, motile, and sequential immunological synapses. *Immunological reviews* **251,** 80–96; 10.1111/imr.12021 (2013).

163.	Verboogen, D. R. J. *et al.* The dendritic cell side of the immunological synapse. *Biomolecular concepts* **7,** 17–28; 10.1515/bmc-2015-0028 (2016).

164.	Grakoui, A. *et al.* The immunological synapse: a molecular machine controlling T cell activation. *Science (New York, N.Y.)* **285,** 221–227; 10.1126/science.285.5425.221 (1999).

165.	Freiberg, B. A. *et al.* Staging and resetting T cell activation in SMACs. *Nature immunology* **3,** 911–917; 10.1038/ni836 (2002).

166.	Stinchcombe, J. C., Majorovits, E., Bossi, G., Fuller, S. & Griffiths, G. M. Centrosome polarization delivers secretory granules to the immunological synapse. *Nature* **443,** 462–465; 10.1038/nature05071 (2006).

167.	Griffiths, G. M., Tsun, A. & Stinchcombe, J. C. The immunological synapse: a focal point for endocytosis and exocytosis. *The Journal of cell biology* **189,** 399–406; 10.1083/jcb.201002027 (2010).

168.	Varma, R., Campi, G., Yokosuka, T., Saito, T. & Dustin, M. L. T cell receptor-proximal signals are sustained in peripheral microclusters and terminated in the central supramolecular activation cluster. *Immunity* **25,** 117–127; 10.1016/j.immuni.2006.04.010 (2006).

169.	Vardhana, S., Choudhuri, K., Varma, R. & Dustin, M. L. Essential role of ubiquitin and TSG101 protein in formation and function of the central supramolecular activation cluster. *Immunity* **32,** 531–540; 10.1016/j.immuni.2010.04.005 (2010).

170.    Bunnell, S. C. *et al.* T cell receptor ligation induces the formation of dynamically regulated signaling assemblies. *The Journal of cell biology* **158,** 1263–1275; 10.1083/jcb.200203043 (2002).

171.    Campi, G., Varma, R. & Dustin, M. L. Actin and agonist MHC-peptide complex-dependent T cell receptor microclusters as scaffolds for signaling. *The Journal of experimental medicine* **202,** 1031–1036; 10.1084/jem.20051182 (2005).

172.    Hashimoto-Tane, A. *et al.* Dynein-driven transport of T cell receptor microclusters regulates immune synapse formation and T cell activation. *Immunity* **34,** 919–931; 10.1016/j.immuni.2011.05.012 (2011).

173.    Benvenuti, F. *et al.* Requirement of Rac1 and Rac2 expression by mature dendritic cells for T cell priming. *Science (New York, N.Y.)* **305,** 1150–1153; 10.1126/science.1099159 (2004).

174.    Mempel, T. R., Henrickson, S. E. & Andrian, U. H. von. T-cell priming by dendritic cells in lymph nodes occurs in three distinct phases. *Nature* **427,** 154–159; 10.1038/nature02238 (2004).

175.    Miller, M. J., Safrina, O., Parker, I. & Cahalan, M. D. Imaging the single cell dynamics of CD4+ T cell activation by dendritic cells in lymph nodes. *The Journal of experimental medicine* **200,** 847–856; 10.1084/jem.20041236 (2004).

176.    Azar, G. A., Lemaître, F., Robey, E. A. & Bousso, P. Subcellular dynamics of T cell immunological synapses and kinapses in lymph nodes. *Proceedings of the National Academy of Sciences* **107,** 3675–3680; 10.1073/pnas.0905901107 (2010).

177.    Henrickson, S. E. *et al.* Antigen availability determines CD8⁺ T cell-dendritic cell interaction kinetics and memory fate decisions. *Immunity* **39,** 496–507; 10.1016/j.immuni.2013.08.034 (2013).

178.    Brossard, C. *et al.* Multifocal structure of the T cell - dendritic cell synapse. *European journal of immunology* **35,** 1741–1753; 10.1002/eji.200425857 (2005).

179.    Tseng, S.-Y., Waite, J. C., Liu, M., Vardhana, S. & Dustin, M. L. T cell-dendritic cell immunological synapses contain TCR-dependent CD28-CD80 clusters that recruit protein kinase C theta. *Journal of immunology (Baltimore, Md. : 1950)* **181,** 4852–4863; 10.4049/jimmunol.181.7.4852 (2008).

180.    Thauland, T. J. & Parker, D. C. Diversity in immunological synapse structure. *Immunology* **131,** 466–472; 10.1111/j.1365-2567.2010.03366.x (2010).

181.    Courtney, A. H., Lo, W.-L. & Weiss, A. TCR Signaling: Mechanisms of Initiation and Propagation. *Trends in biochemical sciences* **43,** 108–123; 10.1016/j.tibs.2017.11.008 (2018).

182.    Iwashima, M., Irving, B. A., van Oers, N. S., Chan, A. C. & Weiss, A. Sequential interactions of the TCR with two distinct cytoplasmic tyrosine kinases. *Science (New York, N.Y.)* **263,** 1136–1139; 10.1126/science.7509083 (1994).

183.    Zhang, W., Sloan-Lancaster, J., Kitchen, J., Trible, R. P. & Samelson, L. E. LAT: the ZAP-70 tyrosine kinase substrate that links T cell receptor to cellular activation. *Cell* **92,** 83–92; 10.1016/s0092-8674(00)80901-0 (1998).

184.    Berg, L. J., Finkelstein, L. D., Lucas, J. A. & Schwartzberg, P. L. Tec family kinases in T lymphocyte development and function. *Annual review of immunology* **23,** 549–600; 10.1146/annurev.immunol.22.012703.104743 (2005).

185.    Beach, D., Gonen, R., Bogin, Y., Reischl, I. G. & Yablonski, D. Dual role of SLP-76 in mediating T cell receptor-induced activation of phospholipase C-gamma1. *The Journal of biological chemistry* **282,** 2937–2946; 10.1074/jbc.M606697200 (2007).

186.    Billadeau, D. D., Nolz, J. C. & Gomez, T. S. Regulation of T-cell activation by the cytoskeleton. *Nature reviews. Immunology* **7,** 131–143; 10.1038/nri2021 (2007).

187.    Lo, W.-L. *et al.* Lck promotes Zap70-dependent LAT phosphorylation by bridging Zap70 to LAT. *Nature immunology* **19,** 733–741; 10.1038/s41590-018-0131-1 (2018).

188.    Garcia, E. & Ismail, S. Spatiotemporal Regulation of Signaling: Focus on T Cell Activation and the Immunological Synapse. *International journal of molecular sciences* **21**; 10.3390/ijms21093283 (2020).

189.    Rhee, S. G. & Choi, K. D. Regulation of inositol phospholipid-specific phospholipase C isozymes. *The Journal of biological chemistry* **267,** 12393–12396 (1992).

190.    Zhang, S. L. *et al.* STIM1 is a Ca2+ sensor that activates CRAC channels and migrates from the Ca2+ store to the plasma membrane. *Nature* **437,** 902–905; 10.1038/nature04147 (2005).

191.    Berridge, M. J. Inositol trisphosphate and calcium signalling mechanisms. *Biochimica et Biophysica Acta (BBA) - Molecular Cell Research* **1793,** 933–940; 10.1016/j.bbamcr.2008.10.005 (2009).

192.    Hwang, J.-R., Byeon, Y., Kim, D. & Park, S.-G. Recent insights of T cell receptor-mediated signaling pathways for T cell activation and development. *Experimental & Molecular Medicine* **52,** 750–761; 10.1038/s12276-020-0435-8 (2020).

193.    Comrie, W. A. & Burkhardt, J. K. Action and Traction: Cytoskeletal Control of Receptor Triggering at the Immunological Synapse. *Frontiers in immunology* **7,** 68; 10.3389/fimmu.2016.00068 (2016).

194.    Zhang, J. *et al.* Antigen receptor-induced activation and cytoskeletal rearrangement are impaired in Wiskott-Aldrich syndrome protein-deficient lymphocytes. *The Journal of experimental medicine* **190,** 1329–1342; 10.1084/jem.190.9.1329 (1999).

195.    Gomez, T. S. *et al.* HS1 functions as an essential actin-regulatory adaptor protein at the immune synapse. *Immunity* **24,** 741–752; 10.1016/j.immuni.2006.03.022 (2006).

196.    Leithner, A. *et al.* Dendritic cell actin dynamics control contact duration and priming efficiency at the immunological synapse. *The Journal of cell biology* **220**; 10.1083/jcb.202006081 (2021).

197.    Kupfer, A., Dennert, G. & Singer, S. J. Polarization of the Golgi apparatus and the microtubule-organizing center within cloned natural killer cells bound to their targets. *Proceedings of the National Academy of Sciences* **80,** 7224–7228; 10.1073/pnas.80.23.7224 (1983).

198. Kupfer, A., Mosmann, T. R. & Kupfer, H. Polarized expression of cytokines in cell conjugates of helper T cells and splenic B cells. *Proceedings of the National Academy of Sciences* **88,** 775–779; 10.1073/pnas.88.3.775 (1991).

199. Kuhn, J. R. & Poenie, M. Dynamic polarization of the microtubule cytoskeleton during CTL-mediated killing. *Immunity* **16,** 111–121; 10.1016/s1074-7613(02)00262-5 (2002).

200. Martín-Cófreces, N. B. *et al.* MTOC translocation modulates IS formation and controls sustained T cell signaling. *The Journal of cell biology* **182,** 951–962; 10.1083/jcb.200801014 (2008).

201. Yi, J. *et al.* Centrosome repositioning in T cells is biphasic and driven by microtubule end-on capture-shrinkage. *The Journal of cell biology* **202,** 779–792; 10.1083/jcb.201301004 (2013).

202. Bustos-Morán, E., Blas-Rus, N., Martin-Cófreces, N. B. & Sánchez-Madrid, F. Microtubule-associated protein-4 controls nanovesicle dynamics and T cell activation. *Journal of cell science* **130,** 1217–1223; 10.1242/jcs.199042 (2017).

203. Serrador, J. M. *et al.* HDAC6 deacetylase activity links the tubulin cytoskeleton with immune synapse organization. *Immunity* **20,** 417–428; 10.1016/s1074-7613(04)00078-0 (2004).

204. Andrés-Delgado, L. *et al.* INF2 promotes the formation of detyrosinated microtubules necessary for centrosome reorientation in T cells. *The Journal of cell biology* **198,** 1025–1037; 10.1083/jcb.201202137 (2012).

205. Zyss, D., Ebrahimi, H. & Gergely, F. Casein kinase I delta controls centrosome positioning during T cell activation. *The Journal of cell biology* **195,** 781–797; 10.1083/jcb.201106025 (2011).

206. Filbert, E. L., Le Borgne, M., Lin, J., Heuser, J. E. & Shaw, A. S. Stathmin Regulates Microtubule Dynamics and Microtubule Organizing Center Polarization in Activated T Cells. *The Journal of Immunology* **188,** 5421–5427; 10.4049/jimmunol.1200242 (2012).

207. Martín-Cófreces, N. B. *et al.* End-binding protein 1 controls signal propagation from the T cell receptor. *The EMBO journal* **31,** 4140–4152; 10.1038/emboj.2012.242 (2012).

208. Ilan-Ber, T. & Ilan, Y. The role of microtubules in the immune system and as potential targets for gut-based immunotherapy. *Molecular Immunology* **111,** 73–82; 10.1016/j.molimm.2019.04.014 (2019).

209. Quann, E. J., Merino, E., Furuta, T. & Huse, M. Localized diacylglycerol drives the polarization of the microtubule-organizing center in T cells. *Nature immunology* **10,** 627–635; 10.1038/ni.1734 (2009).

210. Hill, T. L. Theoretical problems related to the attachment of microtubules to kinetochores. *Proceedings of the National Academy of Sciences* **82,** 4404–4408; 10.1073/pnas.82.13.4404 (1985).

211. Pavin, N. & Tolić-Nørrelykke, I. M. Swinging a sword: how microtubules search for their targets. *Systems and Synthetic Biology* **8,** 179–186; 10.1007/s11693-014-9134-x (2014).

212. Sarkar, A., Rieger, H. & Paul, R. Search and Capture Efficiency of Dynamic Microtubules for Centrosome Relocation during IS Formation. *Biophysical Journal* **116,** 2079–2091; 10.1016/j.bpj.2019.04.008 (2019).

213.   Pulecio, J. *et al.* Cdc42-mediated MTOC polarization in dendritic cells controls targeted delivery of cytokines at the immune synapse. *The Journal of experimental medicine* **207,** 2719–2732; 10.1084/jem.20100007 (2010).

214.   Mittelbrunn, M. *et al.* Imaging of plasmacytoid dendritic cell interactions with T cells. *Blood* **113,** 75–84; 10.1182/blood-2008-02-139865 (2009).

215.   Ueda, H., Morphew, M. K., McIntosh, J. R. & Davis, M. M. CD4+ T-cell synapses involve multiple distinct stages. *Proceedings of the National Academy of Sciences* **108,** 17099–17104; 10.1073/pnas.1113703108 (2011).

216.   Ashley N. Mentlik, Keri B. Sanborn, Erika L. Holzbaur & Jordan S. Orange. Rapid Lytic Granule Convergence to the MTOC in Natural Killer Cells Is Dependent on Dynein But Not Cytolytic Commitment. *Molecular Biology of the Cell* **21,** 2241–2256; 10.1091/mbc.e09-11-0930 (2010).

217.   Burkhardt, J. K., McIlvain, J. M., Sheetz, M. P. & Argon, Y. Lytic granules from cytotoxic T cells exhibit kinesin-dependent motility on microtubules in vitro. *Journal of cell science* **104,** 151–162; 10.1242/jcs.104.1.151 (1993).

218.   Kurowska, M. *et al.* Terminal transport of lytic granules to the immune synapse is mediated by the kinesin-1/Slp3/Rab27a complex. *Blood* **119,** 3879–3889; 10.1182/blood-2011-09-382556 (2012).

219.   Jahn, R. & Fasshauer, D. Molecular machines governing exocytosis of synaptic vesicles. *Nature* **490,** 201–207; 10.1038/nature11320 (2012).

220.   Huse, M., Quann, E. J. & Davis, M. M. Shouts, whispers and the kiss of death: directional secretion in T cells. *Nature immunology* **9,** 1105–1111; 10.1038/ni.f.215 (2008).

221.   Ueda, H., Zhou, J., Xie, J. & Davis, M. M. Distinct Roles of Cytoskeletal Components in Immunological Synapse Formation and Directed Secretion. *The Journal of Immunology* **195,** 4117–4125; 10.4049/jimmunol.1402175 (2015).

222.   Finetti, F. *et al.* The small GTPase Rab8 interacts with VAMP-3 to regulate the delivery of recycling T-cell receptors to the immune synapse. *Journal of cell science* **128,** 2541–2552; 10.1242/jcs.171652 (2015).

223.   Balagopalan, L. *et al.* Plasma membrane LAT activation precedes vesicular recruitment defining two phases of early T-cell activation. *Nature Communications* **9,** 2013; 10.1038/s41467-018-04419-x (2018).

224.   Bouchet, J., McCaffrey, M. W., Graziani, A. & Alcover, A. The functional interplay of Rab11, FIP3 and Rho proteins on the endosomal recycling pathway controls cell shape and symmetry. *Small GTPases* **9,** 310–315; 10.1080/21541248.2016.1224288 (2018).

225.   Piotrowski, J. T., Gomez, T. S., Schoon, R. A., Mangalam, A. K. & Billadeau, D. D. WASH knockout T cells demonstrate defective receptor trafficking, proliferation, and effector function. *Molecular and cellular biology* **33,** 958–973; 10.1128/MCB.01288-12 (2013).

226.   Boes, M. *et al.* T-cell engagement of dendritic cells rapidly rearranges MHC class II transport. *Nature* **418,** 983–988; 10.1038/nature01004 (2002).

227. Bertho, N. *et al.* Requirements for T Cell-Polarized Tubulation of Class II$^+$ Compartments in Dendritic Cells. *The Journal of Immunology* **171,** 5689–5696; 10.4049/jimmunol.171.11.5689 (2003).

228. Compeer, E. B., Flinsenberg, T. W. H., Boon, L., Hoekstra, M. E. & Boes, M. Tubulation of endosomal structures in human dendritic cells by Toll-like receptor ligation and lymphocyte contact accompanies antigen cross-presentation. *The Journal of biological chemistry* **289,** 520–528; 10.1074/jbc.M113.511147 (2014).

229. Keller, A. M. *et al.* Costimulatory ligand CD70 is delivered to the immunological synapse by shared intracellular trafficking with MHC class II molecules. *Proceedings of the National Academy of Sciences* **104,** 5989–5994; 10.1073/pnas.0700946104 (2007).

230. Jo, J.-H. *et al.* Recycling and LFA-1-dependent trafficking of ICAM-1 to the immunological synapse. *Journal of cellular biochemistry* **111,** 1125–1137; 10.1002/jcb.22798 (2010).

231. Smyth, C. M. *et al.* Differential subcellular localization of CD86 in human PBMC-derived macrophages and DCs, and ultrastructural characterization by immuno-electron microscopy. *International immunology* **17,** 123–132; 10.1093/intimm/dxh193 (2004).

232. Efimov, A. *et al.* Asymmetric CLASP-Dependent Nucleation of Noncentrosomal Microtubules at the trans-Golgi Network. *Developmental Cell* **12,** 917–930; 10.1016/j.devcel.2007.04.002 (2007).

233. Oddoux, S. *et al.* Microtubules that form the stationary lattice of muscle fibers are dynamic and nucleated at Golgi elements. *The Journal of cell biology* **203,** 205–213; 10.1083/jcb.201304063 (2013).

234. Zhu, X. *et al.* Microtubules Negatively Regulate Insulin Secretion in Pancreatic β Cells. *Developmental Cell* **34,** 656–668; 10.1016/j.devcel.2015.08.020 (2015).

235. Ori-McKenney, K. M., Jan, L. Y. & Jan, Y.-N. Golgi Outposts Shape Dendrite Morphology by Functioning as Sites of Acentrosomal Microtubule Nucleation in Neurons. *Neuron* **76,** 921–930; 10.1016/j.neuron.2012.10.008 (2012).

236. Nigg, E. A. & Holland, A. J. Once and only once: mechanisms of centriole duplication and their deregulation in disease. *Nature reviews. Molecular cell biology* **19,** 297–312; 10.1038/nrm.2017.127 (2018).

237. Kloc, M., Kubiak, J. Z., Li, X. C. & Ghobrial, R. M. The newly found functions of MTOC in immunological response. *Journal of Leukocyte Biology* **95,** 417–430; 10.1189/jlb.0813468 (2014).

238. Azimzadeh, J. & Marshall, W. F. Building the centriole. *Current Biology* **20,** R816-25; 10.1016/j.cub.2010.08.010 (2010).

239. Gönczy, P. Towards a molecular architecture of centriole assembly. *Nature reviews. Molecular cell biology* **13,** 425–435; 10.1038/nrm3373 (2012).

240. Truelove, S. C. Ulcerative colitis beginning in childhood. *The New England journal of medicine* **285,** 50–52; 10.1056/NEJM197107012850112 (1971).

241. Garcia, G. 3. & Reiter, J. F. A primer on the mouse basal body. *Cilia* **5,** 17; 10.1186/s13630-016-0038-0 (2016).

242. Azimzadeh, J. *et al.* hPOC5 is a centrin-binding protein required for assembly of full-length centrioles. *The Journal of cell biology* **185,** 101–114; 10.1083/jcb.200808082 (2009).

243. Hirono, M. Cartwheel assembly. *Philosophical transactions of the Royal Society of London. Series B, Biological sciences* **369**; 10.1098/rstb.2013.0458 (2014).

244. Hilbert, M. *et al.* SAS-6 engineering reveals interdependence between cartwheel and microtubules in determining centriole architecture. *Nature cell biology* **18,** 393–403; 10.1038/ncb3329 (2016).

245. Mennella, V. *et al.* Subdiffraction-resolution fluorescence microscopy reveals a domain of the centrosome critical for pericentriolar material organization. *Nature cell biology* **14,** 1159–1168; 10.1038/ncb2597 (2012).

246. Sonnen, K. F., Schermelleh, L., Leonhardt, H. & Nigg, E. A. 3D-structured illumination microscopy provides novel insight into architecture of human centrosomes. *Biology open* **1,** 965–976; 10.1242/bio.20122337 (2012).

247. Conduit, P. T. *et al.* A molecular mechanism of mitotic centrosome assembly in Drosophila. *eLife* **3,** e03399; 10.7554/eLife.03399 (2014).

248. Banani, S. F., Lee, H. O., Hyman, A. A. & Rosen, M. K. Biomolecular condensates: organizers of cellular biochemistry. *Nature reviews. Molecular cell biology* **18,** 285–298; 10.1038/nrm.2017.7 (2017).

249. Feng, Z. *et al.* Structural Basis for Mitotic Centrosome Assembly in Flies. *Cell* **169,** 1078-1089.e13; 10.1016/j.cell.2017.05.030 (2017).

250. Woodruff, J. B. *et al.* The Centrosome Is a Selective Condensate that Nucleates Microtubules by Concentrating Tubulin. *Cell* **169,** 1066-1077.e10; 10.1016/j.cell.2017.05.028 (2017).

251. Arquint, C., Gabryjonczyk, A.-M. & Nigg, E. A. Centrosomes as signalling centres. *Philosophical transactions of the Royal Society of London. Series B, Biological sciences* **369**; 10.1098/rstb.2013.0464 (2014).

252. Moritz, M., Braunfeld, M. B., Sedat, J. W., Alberts, B. & Agard, D. A. Microtubule nucleation by γ-tubulin-containing rings in the centrosome. *Nature* **378,** 638–640; 10.1038/378638a0 (1995).

253. Kollman, J. M., Merdes, A., Mourey, L. & Agard, D. A. Microtubule nucleation by γ-tubulin complexes. *Nature reviews. Molecular cell biology* **12,** 709–721; 10.1038/nrm3209 (2011).

254. Paintrand, M., Moudjou, M., Delacroix, H. & Bornens, M. Centrosome organization and centriole architecture: their sensitivity to divalent cations. *Journal of structural biology* **108,** 107–128; 10.1016/1047-8477(92)90011-x (1992).

255. Lacey, K. R., Jackson, P. K. & Stearns, T. Cyclin-dependent kinase control of centrosome duplication. *Proceedings of the National Academy of Sciences* **96,** 2817–2822; 10.1073/pnas.96.6.2817 (1999).

256. Kim, T.-S. *et al.* Hierarchical recruitment of Plk4 and regulation of centriole biogenesis by two centrosomal scaffolds, Cep192 and Cep152. *Proceedings of the National Academy of Sciences* **110,** E4849-57; 10.1073/pnas.1319656110 (2013).

257.   Sonnen, K. F., Gabryjonczyk, A.-M., Anselm, E., Stierhof, Y.-D. & Nigg, E. A. Human Cep192 and Cep152 cooperate in Plk4 recruitment and centriole duplication. *Journal of cell science* **126,** 3223–3233; 10.1242/jcs.129502 (2013).

258.   Tsou, M.-F. B. *et al.* Polo kinase and separase regulate the mitotic licensing of centriole duplication in human cells. *Developmental Cell* **17,** 344–354; 10.1016/j.devcel.2009.07.015 (2009).

259.   Lee, K. & Rhee, K. Separase-dependent cleavage of pericentrin B is necessary and sufficient for centriole disengagement during mitosis. *Cell cycle (Georgetown, Tex.)* **11,** 2476–2485; 10.4161/cc.20878 (2012).

260.   Kim, J., Lee, K. & Rhee, K. PLK1 regulation of PCNT cleavage ensures fidelity of centriole separation during mitotic exit. *Nature Communications* **6,** 10076; 10.1038/ncomms10076 (2015).

261.   Vivier, E. & Malissen, B. Innate and adaptive immunity: specificities and signaling hierarchies revisited. *Nature immunology* **6,** 17–21; 10.1038/ni1153 (2005).

262.   Chvatchko, Y. *et al.* A key role for CC chemokine receptor 4 in lipopolysaccharide-induced endotoxic shock. *The Journal of experimental medicine* **191,** 1755–1764; 10.1084/jem.191.10.1755 (2000).

263.   Higginbotham, H., Bielas, S., Tanaka, T. & Gleeson, J. G. Transgenic Mouse Line with Green-fluorescent Protein-labeled Centrin 2 allows Visualization of the Centrosome in Living Cells. *Transgenic Research* **13,** 155–164; 10.1023/B:TRAG.0000026071.41735.8e (2004).

264.   Barnden, M. J., Allison, J., Heath, W. R. & Carbone, F. R. Defective TCR expression in transgenic mice constructed using cDNA-based alpha- and beta-chain genes under the control of heterologous regulatory elements. *Immunology and cell biology* **76,** 34–40; 10.1046/j.1440-1711.1998.00709.x (1998).

265.   Schindelin, J. *et al.* Fiji: an open-source platform for biological-image analysis. *Nature methods* **9,** 676–682; 10.1038/nmeth.2019 (2012).

266.   Redecke, V. *et al.* Hematopoietic progenitor cell lines with myeloid and lymphoid potential. *Nature methods* **10,** 795–803; 10.1038/nmeth.2510 (2013).

267.   Yong-Chen Lu, Wen-Chen Yeh & Pamela S. Ohashi. LPS/TLR4 signal transduction pathway. *Cytokine* **42,** 145–151; 10.1016/j.cyto.2008.01.006 (2008).

268.   Piperno, G., LeDizet, M. & Chang, X. J. Microtubules containing acetylated alpha-tubulin in mammalian cells in culture. *The Journal of cell biology* **104,** 289–302; 10.1083/jcb.104.2.289 (1987).

269.   Chang, C.-W., Hsu, W.-B., Tsai, J.-J., Tang, C.-J. C. & Tang, T. K. CEP295 interacts with microtubules and is required for centriole elongation. *Journal of cell science* **129,** 2501–2513; 10.1242/jcs.186338 (2016).

270.   Cosenza, M. R. & Krämer, A. Centrosome amplification, chromosomal instability and cancer: mechanistic, clinical and therapeutic issues. *Chromosome research : an international journal on the molecular, supramolecular and evolutionary aspects of chromosome biology* **24,** 105–126; 10.1007/s10577-015-9505-5 (2016).

271.    Ling, H., Peng, L., Wang, J., Rahhal, R. & Seto, E. Histone Deacetylase SIRT1 Targets Plk2 to Regulate Centriole Duplication. *Cell reports* **25,** 2851-2865.e3; 10.1016/j.celrep.2018.11.025 (2018).

272.    Cizmecioglu, O. *et al.* Plk2 regulates centriole duplication through phosphorylation-mediated degradation of Fbxw7 (human Cdc4). *Journal of cell science* **125,** 981–992; 10.1242/jcs.095075 (2012).

273.    Badarudeen, B., Gupta, R., Nair, S. V., Chandrasekharan, A. & Manna, T. K. The ubiquitin ligase FBXW7 targets the centriolar assembly protein HsSAS-6 for degradation and thereby regulates centriole duplication. *The Journal of biological chemistry* **295,** 4428–4437; 10.1074/jbc.AC119.012178 (2020).

274.    Wong, Y. L. *et al.* Cell biology. Reversible centriole depletion with an inhibitor of Polo-like kinase 4. *Science (New York, N.Y.)* **348,** 1155–1160; 10.1126/science.aaa5111 (2015).

275.    Leithner, A. *et al.* Fast and efficient genetic engineering of hematopoietic precursor cells for the study of dendritic cell migration. *European journal of immunology* **48,** 1074–1077; 10.1002/eji.201747358 (2018).

276.    Chan, J. Y. A clinical overview of centrosome amplification in human cancers. *International journal of biological sciences* **7,** 1122–1144; 10.7150/ijbs.7.1122 (2011).

277.    Øvrebø, J. I. & Edgar, B. A. Polyploidy in tissue homeostasis and regeneration. *Development (Cambridge, England)* **145**; 10.1242/dev.156034 (2018).

278.    Quah, B. J. C., Warren, H. S. & Parish, C. R. Monitoring lymphocyte proliferation in vitro and in vivo with the intracellular fluorescent dye carboxyfluorescein diacetate succinimidyl ester. *Nature protocols* **2,** 2049–2056; 10.1038/nprot.2007.296 (2007).

279.    Cabukusta, B. & Neefjes, J. Mechanisms of lysosomal positioning and movement. *Traffic (Copenhagen, Denmark)* **19,** 761–769; 10.1111/tra.12587 (2018).

280.    Lemieux, B., Percival, M. D. & Falgueyret, J.-P. Quantitation of the lysosomotropic character of cationic amphiphilic drugs using the fluorescent basic amine Red DND-99. *Analytical biochemistry* **327,** 247–251; 10.1016/j.ab.2004.01.010 (2004).

281.    Gardella, S. *et al.* CD8+ T lymphocytes induce polarized exocytosis of secretory lysosomes by dendritic cells with release of interleukin-1β and cathepsin D. *Blood* **98,** 2152–2159 (2001).

282.    Semino, C., Angelini, G., Poggi, A. & Rubartelli, A. NK/iDC interaction results in IL-18 secretion by DCs at the synaptic cleft followed by NK cell activation and release of the DC maturation factor HMGB1. *Blood* **106,** 609–616; 10.1182/blood-2004-10-3906 (2005).

283.    Stanley, A. C. & Lacy, P. Pathways for Cytokine Secretion. *Physiology* **25,** 218–229; 10.1152/physiol.00017.2010 (2010).

284.    Vertii, A. *et al.* The Centrosome Undergoes Plk1-Independent Interphase Maturation during Inflammation and Mediates Cytokine Release. *Developmental Cell* **37,** 377–386; 10.1016/j.devcel.2016.04.023 (2016).

285.    Arnandis, T. *et al.* Oxidative Stress in Cells with Extra Centrosomes Drives Non-Cell-Autonomous Invasion. *Developmental Cell* **47,** 409-424.e9; 10.1016/j.devcel.2018.10.026 (2018).

286. Dienz, O. & Rincon, M. The effects of IL-6 on CD4 T cell responses. *Clinical immunology (Orlando, Fla.)* **130,** 27–33; 10.1016/j.clim.2008.08.018 (2009).

287. Jensen, S. S. & Gad, M. Differential induction of inflammatory cytokines by dendritic cells treated with novel TLR-agonist and cytokine based cocktails: targeting dendritic cells in autoimmunity. *Journal of Inflammation* **7,** 37; 10.1186/1476-9255-7-37 (2010).

288. Ritzman Anna M. *et al.* The Chemokine Receptor CXCR2 Ligand KC (CXCL1) Mediates Neutrophil Recruitment and Is Critical for Development of Experimental Lyme Arthritis and Carditis. *Infection and Immunity* **78,** 4593–4600; 10.1128/IAI.00798-10 (2010).

289. Griffith, J. W., Sokol, C. L. & Luster, A. D. Chemokines and Chemokine Receptors: Positioning Cells for Host Defense and Immunity. *Annual review of immunology* **32,** 659–702; 10.1146/annurev-immunol-032713-120145 (2014).

290. Viney, J. M. *et al.* Distinct Conformations of the Chemokine Receptor CCR4 with Implications for Its Targeting in Allergy. *The Journal of Immunology* **192,** 3419–3427; 10.4049/jimmunol.1300232 (2014).

291. Link, A. *et al.* Fibroblastic reticular cells in lymph nodes regulate the homeostasis of naive T cells. *Nature immunology* **8,** 1255–1265; 10.1038/ni1513 (2007).

292. Quintyne, N. J., Reing, J. E., Hoffelder, D. R., Gollin, S. M. & Saunders, W. S. Spindle multipolarity is prevented by centrosomal clustering. *Science (New York, N.Y.)* **307,** 127–129; 10.1126/science.1104905 (2005).

293. Blanchard, N., Di Bartolo, V. & Hivroz, C. In the Immune Synapse, ZAP-70 Controls T Cell Polarization and Recruitment of Signaling Proteins but Not Formation of the Synaptic Pattern. *Immunity* **17,** 389–399; 10.1016/S1074-7613(02)00421-1 (2002).

294. Lee, K.-H. *et al.* T Cell Receptor Signaling Precedes Immunological Synapse Formation. *Science (New York, N.Y.)* **295,** 1539–1542; 10.1126/science.1067710 (2002).

295. Orange, J. S. *et al.* The mature activating natural killer cell immunologic synapse is formed in distinct stages. *Proceedings of the National Academy of Sciences* **100,** 14151–14156 (2003).

296. Yuseff, M.-I. *et al.* Polarized secretion of lysosomes at the B cell synapse couples antigen extraction to processing and presentation. *Immunity* **35,** 361–374; 10.1016/j.immuni.2011.07.008 (2011).

297. Perkins, N. D. & Gilmore, T. D. Good cop, bad cop: the different faces of NF-κB. *Cell Death & Differentiation* **13,** 759–772; 10.1038/sj.cdd.4401838 (2006).

298. Dalod, M., Chelbi, R., Malissen, B. & Lawrence, T. Dendritic cell maturation: functional specialization through signaling specificity and transcriptional programming. *The EMBO journal* **33,** 1104–1116; 10.1002/embj.201488027 (2014).

299. Ching, K. & Stearns, T. Centrioles are amplified in cycling progenitors of olfactory sensory neurons. *PLOS Biology* **18,** 1–17; 10.1371/journal.pbio.3000852 (2020).

300. Vardiman, J. W. The World Health Organization (WHO) classification of tumors of the hematopoietic and lymphoid tissues: an overview with emphasis on the myeloid neoplasms. *Chemico-biological interactions* **184,** 16–20; 10.1016/j.cbi.2009.10.009 (2010).

301.    Sapienza, M. R. *et al.* Blastic plasmacytoid dendritic cell neoplasm: genomics mark epigenetic dysregulation as a primary therapeutic target. *Haematologica* **104,** 729–737; 10.3324/haematol.2018.202093 (2019).

302.    Dalia, S., Shao, H., Sagatys, E., Cualing, H. & Sokol, L. Dendritic Cell and Histiocytic Neoplasms: Biology, Diagnosis, and Treatment. *Cancer Control* **21,** 290–300; 10.1177/107327481402100405 (2014).

303.    Donne, R., Saroul-Aïnama, M., Cordier, P., Celton-Morizur, S. & Desdouets, C. Polyploidy in liver development, homeostasis and disease. *Nature Reviews Gastroenterology & Hepatology* **17,** 391–405; 10.1038/s41575-020-0284-x (2020).

304.    Sun, X. & Kaufman, P. D. Ki-67: more than a proliferation marker. *Chromosoma* **127,** 175–186; 10.1007/s00412-018-0659-8 (2018).

305.    Sakaue-Sawano, A. *et al.* Visualizing Spatiotemporal Dynamics of Multicellular Cell-Cycle Progression. *Cell* **132,** 487–498; 10.1016/j.cell.2007.12.033 (2008).

306.    Habedanck, R., Stierhof, Y.-D., Wilkinson, C. J. & Nigg, E. A. The Polo kinase Plk4 functions in centriole duplication. *Nature cell biology* **7,** 1140–1146 (2005).

307.    Michelle S. Levine *et al.* Centrosome Amplification Is Sufficient to Promote Spontaneous Tumorigenesis in Mammals. *Developmental Cell* **40,** 313-322.e5; 10.1016/j.devcel.2016.12.022 (2017).

308.    Silke Warnke *et al.* Polo-like Kinase-2 Is Required for Centriole Duplication in Mammalian Cells. *Current Biology* **14,** 1200–1207; 10.1016/j.cub.2004.06.059 (2004).

309.    Mussman, J. G. *et al.* Synergistic induction of centrosome hyperamplification by loss of p53 and cyclin E overexpression. *Oncogene* **19,** 1635–1646; 10.1038/sj.onc.1203460 (2000).

310.    Okuda, M. *et al.* Nucleophosmin/B23 is a target of CDK2/cyclin E in centrosome duplication. *Cell* **103,** 127–140; 10.1016/s0092-8674(00)00093-3 (2000).

311.    Tokuyama, Y., Horn, H. F., Kawamura, K., Tarapore, P. & Fukasawa, K. Specific phosphorylation of nucleophosmin on Thr(199) by cyclin-dependent kinase 2-cyclin E and its role in centrosome duplication. *The Journal of biological chemistry* **276,** 21529–21537; 10.1074/jbc.M100014200 (2001).

312.    Bonetti, P. *et al.* Nucleophosmin and its AML-associated mutant regulate c-Myc turnover through Fbw7γ. *The Journal of cell biology* **182,** 19–26; 10.1083/jcb.200711040 (2008).

313.    Krause, A. & Hoffmann, I. Polo-like kinase 2-dependent phosphorylation of NPM/B23 on serine 4 triggers centriole duplication. *PloS one* **5,** e9849; 10.1371/journal.pone.0009849 (2010).

314.    Li, J. *et al.* Polo-like kinase 2 activates an antioxidant pathway to promote the survival of cells with mitochondrial dysfunction. *Free radical biology & medicine* **73,** 270–277; 10.1016/j.freeradbiomed.2014.05.022 (2014).

315.    Lavu, N. *et al.* Oxidative stress-induced downregulation of glycogen synthase kinase 3 beta in fetal membranes promotes cellular senescence†. *Biology of reproduction* **101,** 1018–1030; 10.1093/biolre/ioz119 (2019).

316.    Welcker, M. *et al.* Multisite phosphorylation by Cdk2 and GSK3 controls cyclin E degradation. *Molecular cell* **12,** 381–392; 10.1016/s1097-2765(03)00287-9 (2003).

317.    Matthew, E. M. *et al.* Replication Stress, Defective S-phase Checkpoint and Increased Death in Plk2-Deficient Human Cancer Cells. *Cell cycle (Georgetown, Tex.)* **6,** 2571–2578; 10.4161/cc.6.20.5079 (2007).

318.    Inglis, K. J. *et al.* Polo-like kinase 2 (PLK2) phosphorylates alpha-synuclein at serine 129 in central nervous system. *The Journal of biological chemistry* **284,** 2598–2602; 10.1074/jbc.C800206200 (2009).

319.    Colicino, E. G. & Hehnly, H. Regulating a key mitotic regulator, polo-like kinase 1 (PLK1). *Cytoskeleton* **75,** 481–494; 10.1002/cm.21504 (2018).

320.    Matsumoto, T. *et al.* Polo-like kinases mediate cell survival in mitochondrial dysfunction. *Proceedings of the National Academy of Sciences* **106,** 14542–14546; 10.1073/pnas.0904229106 (2009).

321.    Godinho, S. A. *et al.* Oncogene-like induction of cellular invasion from centrosome amplification. *Nature* **510,** 167–171 (2014).

322.    Dadaglio, G., Nelson, C. A., Deck, M. B., Petzold, S. J. & Unanue, E. R. Characterization and quantitation of peptide-MHC complexes produced from hen egg lysozyme using a monoclonal antibody. *Immunity* **6,** 727–738; 10.1016/s1074-7613(00)80448-3 (1997).

323.    Odoardi, F. *et al.* Instant effect of soluble antigen on effector T cells in peripheral immune organs during immunotherapy of autoimmune encephalomyelitis. *Proceedings of the National Academy of Sciences* **104,** 920–925; 10.1073/pnas.0608383104 (2007).

324.    Fenger, J. M. *et al.* Overexpression of miR-9 in mast cells is associated with invasive behavior and spontaneous metastasis. *BMC Cancer* **14,** 84; 10.1186/1471-2407-14-84 (2014).

325.    Zou, H., Yang, P., Huang, T., Zheng, X. & Xu, G. PLK2 Plays an Essential Role in High D-Glucose-Induced Apoptosis, ROS Generation and Inflammation in Podocytes. *Scientific reports* **7,** 4261; 10.1038/s41598-017-00686-8 (2017).

326.    Ohmori, Y., Fukumoto, S. & Hamilton, T. A. Two structurally distinct kappa B sequence motifs cooperatively control LPS-induced KC gene transcription in mouse macrophages. *Journal of immunology (Baltimore, Md. : 1950)* **155,** 3593–3600 (1995).

327.    Moriuchi, H., Moriuchi, M. & Fauci, A. S. Nuclear factor-kappa B potently up-regulates the promoter activity of RANTES, a chemokine that blocks HIV infection. *Journal of immunology (Baltimore, Md. : 1950)* **158,** 3483–3491 (1997).

328.    Nakayama, T. *et al.* Selective induction of Th2-attracting chemokines CCL17 and CCL22 in human B cells by latent membrane protein 1 of Epstein-Barr virus. *Journal of virology* **78,** 1665–1674; 10.1128/jvi.78.4.1665-1674.2004 (2004).

329.    Wickremasinghe, M. I., Thomas, L. H., O'Kane, C. M., Uddin, J. & Friedland, J. S. Transcriptional mechanisms regulating alveolar epithelial cell-specific CCL5 secretion in pulmonary tuberculosis. *The Journal of biological chemistry* **279,** 27199–27210; 10.1074/jbc.M403107200 (2004).

330.    Son, Y.-H. *et al.* Roles of MAPK and NF-kappaB in interleukin-6 induction by lipopolysaccharide in vascular smooth muscle cells. *Journal of cardiovascular pharmacology* **51,** 71–77; 10.1097/FJC.0b013e31815bd23d (2008).

331.    Mihalas, A. B., Araki, Y., Huganir, R. L. & Meffert, M. K. Opposing Action of Nuclear Factor κB and Polo-like Kinases Determines a Homeostatic End Point for Excitatory Synaptic Adaptation. *Journal of Neuroscience* **33,** 16490–16501; 10.1523/JNEUROSCI.2131-13.2013 (2013).

332.    Shadidi, K. R., Aarvak, T., Henriksen, J. E., Natvig, J. B. & Thompson, K. M. The chemokines CCL5, CCL2 and CXCL12 play significant roles in the migration of Th1 cells into rheumatoid synovial tissue. *Scandinavian journal of immunology* **57,** 192–198 (2003).

333.    Jin, L., Batra, S., Douda, D. N., Palaniyar, N. & Jeyaseelan, S. CXCL1 Contributes to Host Defense in Polymicrobial Sepsis via Modulating T Cell and Neutrophil Functions. *Journal of immunology (Baltimore, Md. : 1950)* **193,** 3549–3558; 10.4049/jimmunol.1401138 (2014).

334.    Lydia L. Sohn *et al.* How Can Microfluidic and Microfabrication Approaches Make Experiments More Physiologically Relevant? *Cell Systems* **11,** 209–211; 10.1016/j.cels.2020.07.003 (2020).

335.    Ogden, A. *et al.* Quantitative multi-parametric evaluation of centrosome declustering drugs: centrosome amplification, mitotic phenotype, cell cycle and death. *Cell Death & Disease* **5,** e1204-e1204; 10.1038/cddis.2014.164 (2014).

336.    Vesperini, D., Montalvo, G., Qu, B. & Lautenschläger, F. Characterization of immune cell migration using microfabrication. *Biophysical Reviews* **13,** 185–202; 10.1007/s12551-021-00787-9 (2021).

# Table of Figures

# Acknowledgements